Particular aspects of myelin-axon interactions in health and disease:

The expression of myelin-associated glycoprotein isoforms in CNS and PNS

Early axonal pathology in the dysmyelinating peripheral neuropathy CMT1A

Inauguraldissertation

zur
Erlangung der Würde eines Doktors der Philosophie
vorgelegt der
Philosophisch-Naturwissenschaftlichen Fakultät
der Universität Basel

von

Bettina Flück

aus Brienz BE

Basel, 2007

Genehmigt von der Philosophisch-Naturwissenschaftlichen Fakultät

auf Antrag von

Prof. Dr. N. Schaeren-Wiemers
Prof. Dr. M. Rüegg
Prof. Dr. J. Kapfhammer

Basel, den 13. Februar 2007

Prof. Dr. H.-P. Hauri
Dekan

Table of contents

Abbreviations

bp	base pair
bl	basal lamina
Cdk5	cyclin-dependent kinase 5
CMT1A	Charcot Marie Tooth disease type 1A
CNS	central nervous system
Cx	connexin
DM20	small isoform of the proteolipid protein
DNA	desoxyribonucleic acic
EAE	experimental autoimmune encephalomyelitis
EM	electron microscopy
ERK1/2	extracellular signal-regulated kinases
GSK-3	glycogen-synthetase kinase 3
GFP	green fluorescent protein
HNPP	hereditary neuropathy with liability to pressure palsies
HMSN	hereditary motor and sensory neuropathy
IPL	intraperiod line
kb	kilo base pairs
kD	kilo Dalton
KSP	lysine-serine-proline
MAG	myelin-associated glycoprotein
MDL	major dense line
MBP	myelin basic protein
MOG	myelin oligodendrocyte protein
NCV	nerve conduction velocity
NF-H	neurofilament heavy chain
NF-L	neurofilament light chain
NF-M	neurofilament medium chain
NND	nearest neighbor distance
mRNA	messenger ribonucleic acid
L-MAG	large myelin-associated glycoprotein isoform
PBS	phosphate buffer saline

PDGFα	patelet derived growth factor alpha
PCR	polymerase chain reaction
PLP	proteolipid protein
PMP22	peripheral myelin protein 22
PNS	peripheral nervous system
P0	myelin protein zero
RT	room temperature
S-MAG	short myelin-associated glycoprotein isoform
YAC	yeast artificial chromosome

Summary

An intact myelin sheath is crucial for the rapid propagation of action potentials along myelinated axons. There are many neurodegenerative diseases associated with defect myelin sheaths resulting in severe clinical symptoms such as multiple sclerosis and a group of hereditary neuropathies called "Charcot Marie Tooth diseases". For the maintenance of both, the integrity of the axon and the myelin sheath, reciprocal signaling between the axon and glia is required. Some molecular components involved in these interactions between glial cells and the axons have been investigated. One of these molecules is MAG, the myelin associated glycoprotein, inserted into the periaxonal glial membrane. MAG is expressed as a large and a small isoform (L-MAG, S-MAG) that display a common extracellular but different intracellular domains that cannot be discriminated by antibody staining. In the first part of the thesis, the question how L- and S-MAG are differentially expressed in the CNS and PNS was addressed. For this study a transgenic mouse that expresses the small MAG isoform tagged with green fluorescent protein (GFP) was previously generated (Erb. et al). In the CNS, L- and S-MAG were differentially expressed in certain brain regions such as the corpus callosum and the perforant pathway. In some myelinated fibers L-MAG was predominantly expressed, in others only S-MAG. In the PNS, S-MAG was the predominant isoform; L-MAG was only weakly detectable very early during development. In the PNS, S-MAG-GFP was localized in the expected compartments such as periaxonal membranes, paranodes and Schmidt-Lanterman incisures. In addition, S-MAG was expressed in ring- or disc-like compartments surrounding axons suggesting that there are incisure-like structures distinct from classical Schmidt-Lanterman incisures. The S-MAG-GFP mouse will be a valuable animal model to study the dynamic processes during the formation of Schmidt-Lanterman incisures or paranodal structures *in vitro.*

"Charcot Marie Tooth" diseases are classified into demyelinating and axonal forms and subdivided into different subtypes according to their genetic backgrounds. CMT1A has been classified as primary demyelinating disease and is caused by a duplication of the DNA region encoding the compact myelin protein PMP22 (peripheral myelin protein 22), which results in an overexpression of PMP22. The effects of PMP22 overexpression on the Schwann cells have been well studied. Overexpression of PMP22 impairs Schwann cell differentiation and myelination, and results in accumulations of PMP22. In the second part of this thesis, the question how abnormal Schwann cells influence the development of axons, especially the axonal cytoskeleton, in an animal model for CMT1A disease was addressed. The analysis was focused on the establishment of the neurofilament system during development. In particular, the neurofilament

subunit composition (content of heavy, medium and light chain) and phosphorylation were investigated. In CMT1A mice, there were early changes in the subunit composition and phosphorylation. The axonal pathology in CMT1A mice is marked by a strong increase of the non-phosphorylated neurofilament heavy chains (NF-H) relative to NF-M and NF-L. As unbalanced neurofilament subunits stoichiometries have been associated with reduced axonal calibers, they may account for the predominance of small caliber myelinated axons observed in CMT1A mice. The precise molecular mechanisms by which Schwann cells influence the neurofilament system are not known. However, it was hypothesized that MAG regulates neurofilament phosphorylation interacting with its axonal receptor that induces the activity of Cdk5 or ERK1/2 kinases in the axons. Therefore, the expression of MAG was investigated CMT1A mice to see whether it may correlate with the neurofilament phosphorylation pattern.

General introduction

The interaction of myelin and axons in health and disease is the general subject of the thesis presented here. The purpose of the following section is to give an introduction in the field of myelin biology and particular aspects of axon biology. First, the functional role of myelin, its architecture and biochemical composition will be described. Then a series of peripheral neuropathies called "Charcot Marie Tooth" diseases will be shortly presented. Finally, the structure of neurofilaments, the major cytoskeletal elements in neurons, will be described as neurofilaments are generally affected by myelin disorders.

1 The myelin sheath and propagation of action potentials

Myelination of axons is an exclusive adaptation of vertebrates and enables rapid propagation of action potentials along axons. The myelin sheath, produced by Schwann cells in the PNS and oligodendrocytes in the CNS, consists of membrane extensions tightly wrapped around axons (Figure 1A). Schwann cells myelinate single axonal segments (internodes; Figure 1B, arrowheads) whereas oligodendrocytes form multiple myelin internodes. Between adjacent internodes are the unmyelinated nodes of Ranvier where voltage-sensitive ion channels are concentrated (Figure 1B, asterisk). The myelin sheath is an electrically insulating sheath that promotes rapid propagation of action potentials along axons preventing current flow across the axonal internodal membranes and thereby focuses depolarization produced by action potentials on nodes of Ranvier. An action potential starts with the depolarization of the nodal membrane due to the influx of sodium ions through voltage sensitive sodium channels and is followed by closing and inactivation of sodium channels and the exit of potassium ions for repolarization. The influx of sodium ions depolarizes downstream nodes enabling the action potential to move from node to node in a saltatory manner (Figure 1C). As sodium channels are inactivated for a short time after activation, the action potential is propagated in a unidirectional manner. The conduction velocity of myelinated axons is up to 100m/sec. To achieve similar velocities, unmyelinated axons would require 100 times larger diameters.

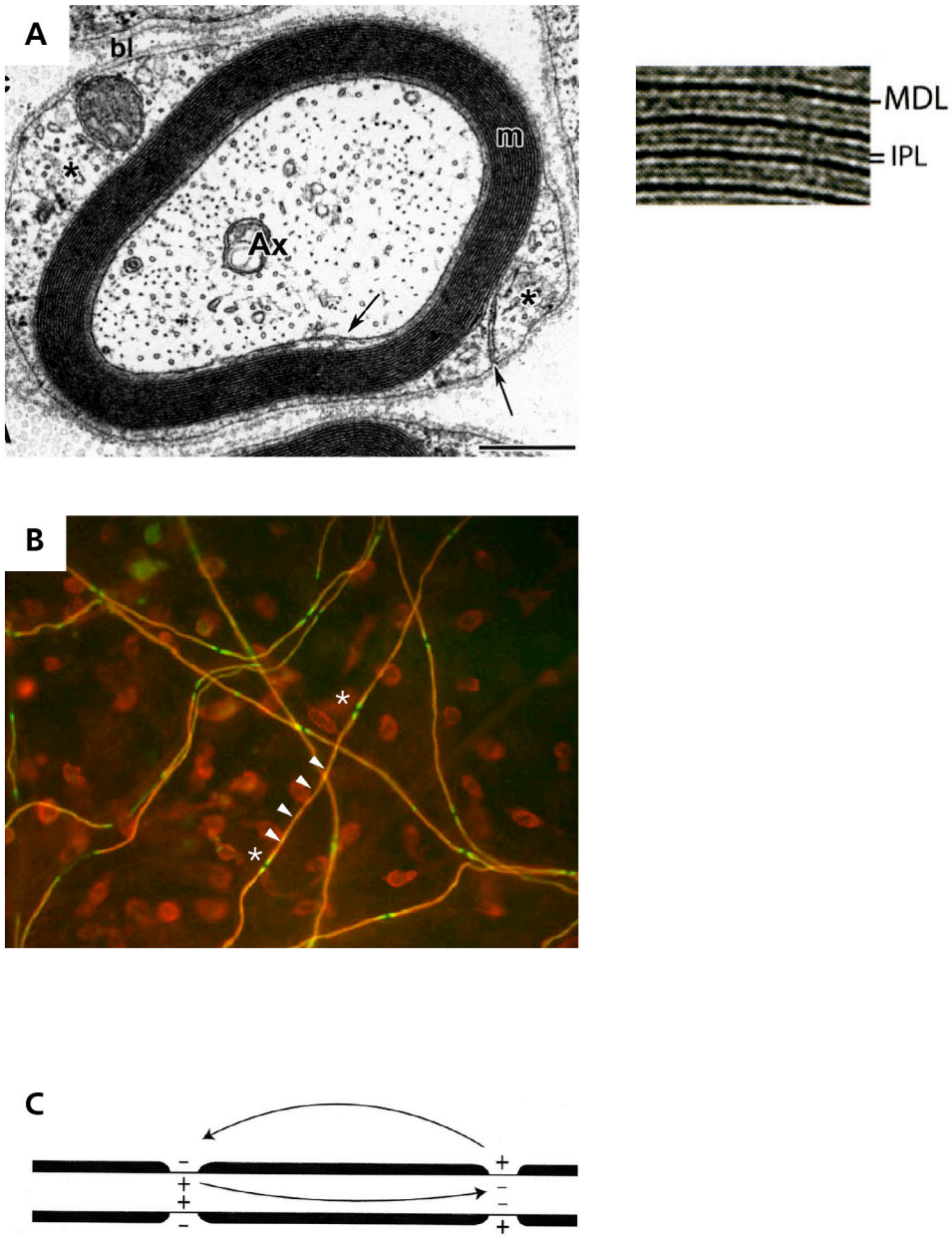

Figure 1 (A) Cross section through a myelinated axon of the peripheral nervous system. Electron microscopy. Axon (Ax), compact myelin (m), basal lamina (bl), extracellular collagen fibrils (c), cytoplasm (asterisk), periaxonal and abaxonal membrane (arrows). Close up: compact myelin membranes. Major dense line (MDL), intraperiod line (IPL). (B) *In vitro* myelinating DRG (dorsal root ganglia) cultures. Nodes of Ranvier (asterisks), myelinated internodes (arrowheads). Staining: (red) myelin basic protein (MBP) (compact myelin); (green) myelin associated glycoprotein (MAG) (periaxonal membranes and paranodal regions). (C) Myelination facilitates rapid propagation of axon potentials, which jump from node to node.

2 The architecture and biochemical composition of the myelin sheath

Myelinated internodes mainly consist of compact myelin that appears electron microscopically as a lamellar structure of alternating dark (major dense line, MDL) and light lines (intraperiod line, IPL) that spiral around the axon. Dark lines represent the condensed intracellular, light lines the extracellular space (Figure 1A, close up, Figure 2A). Membranes of the compact myelin show a unique biochemical composition with about 75% lipids and 25% proteins with mainly adhesive function. Myelin lipids include cholesterols, phospholipids and glycosphingolipids. The protein compositions of myelin sheaths differ in the PNS and CNS. Abundant proteins include P0 (Lemke and Axel, 1985), the myelin basic proteins (MBP) (Staugaitis et al., 1996) and PMP22 in the PNS and proteolipid protein (PLP) and MBP in the CNS myelin (Snipes et al., 1992; Boison et al., 1995). P0, PMP22 and PLP are integral membrane proteins and are important for the maintenance of both, the extracellular and cytoplasmic spacing of myelin membranes (myelin periodicity).

At the lateral ends of the myelin internodes, myelin membranes remain uncompacted and are fixed as loops to the paranodal axonal region. Important molecules for the maintenance of the nodal architecture is for instance neurofascin 155 inserted into the paranodal glial loops acting as binding partner of the axonal paranodin/Caspr-contactin complex (Figure 2A and B; (Charles et al., 2002)).

Other uncompacted myelin compartments exclusively found in the PNS are funnel-shaped incisures spanning through the myelin sheath. The functional role of so called Schmidt-Lanterman incisures has not been defined yet. However, they may provide a shortcut for communication between the outer and inner aspects of the myelin internode (Figure 2C, D).

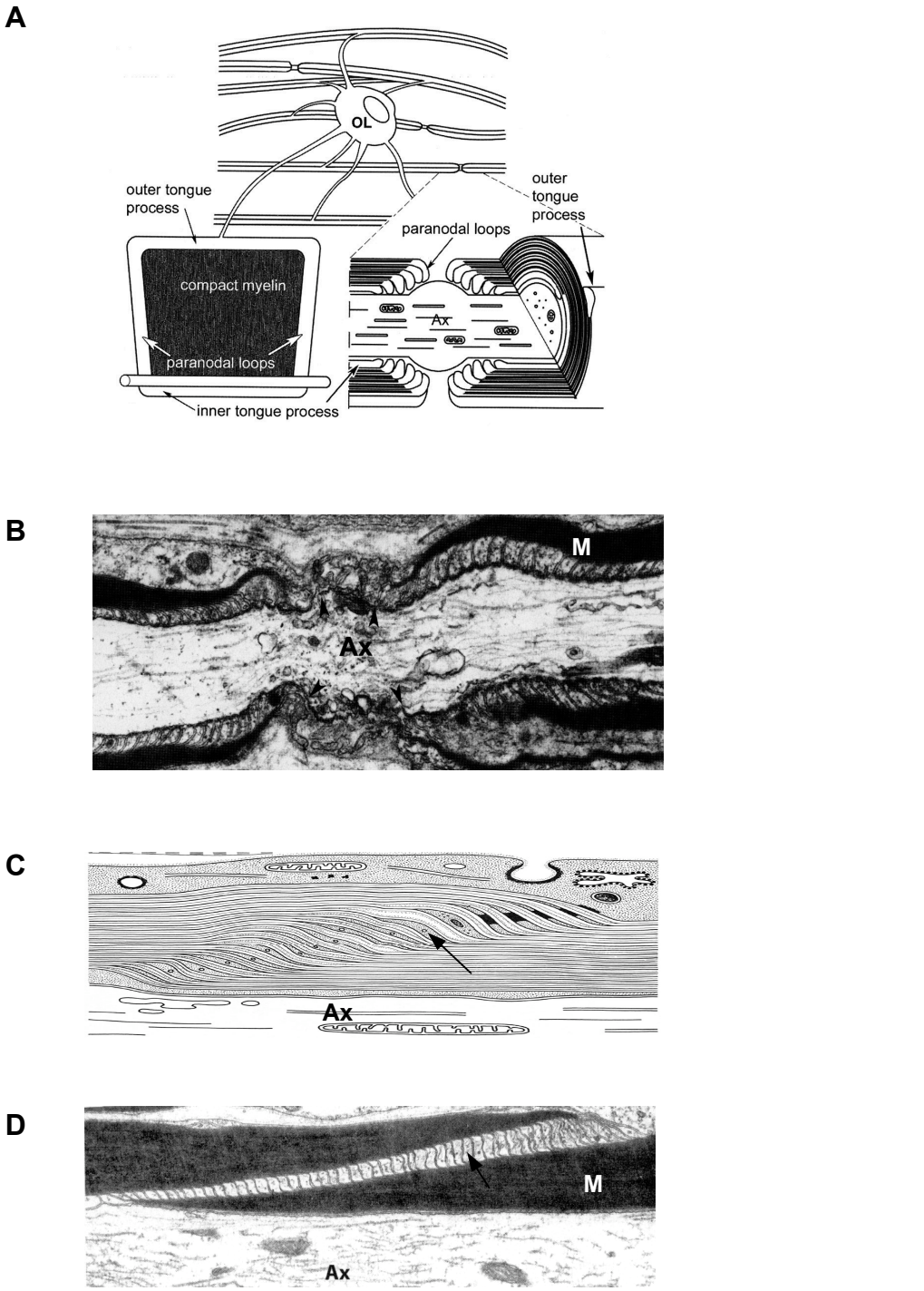

Figure 2 (A) Schematic view of a myelinated internode in the CNS. Unwrapped myelin sheath with compact and uncompact compartments. Paranodal loops are uncompacted and attached to the axons (for instance via caspr/contactin and neurofascin interaction). OL: oligodendrocyte; Ax: axon. (B) Ultrastructure of a node of Ranvier. Ax: axon, M: myelin. (C, D) Schmidt-Lanterman incisure: uncompacted Schwann cell membranes spanning through the myelin sheath (arrow). Ax: axon, M: myelin (Copied from Lazzarini R. A. , 2004).

3 Schwann cell development and myelination

The Schwann cell lineage originates from the neural crest cells. Neural crest cells give rise to Schwann cell precursors that develop into immature Schwann cells that differentiate in two types of mature Schwann cells, the myelinating and non-myelinating Schwann cells (Figure 3). Non-myelinating cells surround multiple axons and form Remak bundles, whereas myelinating Schwann cells form a multilammelar myelin sheath around individual axons. Differentiation of Schwann cells critically depends on signals provided by the associated axons. Whether a particular Schwann cell will differentiate into a myelinating or a non-myelinating Schwann cell depends on the amount of type III neuregulin-1 present on the associated axons; low levels are required for ensheathment by non-myelinating cells whereas high levels induce myelination (Chan et al., 2004; Taveggia et al., 2005). Neuregulin is recognized by the Schwann cells via a receptor tyrosine kinase composed of a ErbB2/ErbB3 heterodimer.

Promyelinating Schwann cells destined to myelinate axons establish a one to one relationship with the axons and cease to proliferate, but remain capable of entering the cell cycle, a property important in adult regeneration (Zorick and Lemke, 1996). The myelination program in Schwann cells is characterized by the expression of specific transcription factor genes like SCIP and Krox-20. SCIP is important for the correct onset of myelination, whereas Krox-20 is required for proper ensheathment and expression of genes encoding myelin proteins (Topilko et al., 1994; Weinstein et al., 1995). Prior the onset of myelination, Schwann cells polarize their surfaces into the abaxonal and periaxonal membranes. The abaxonal membrane directs the production of a basal lamina, a prerequisite for myelination (Bunge et al., 1986). The basal lamina contains laminin 2, type IV collagens, fibronectin, N-syndecan, and glypican. The periaxonal membrane is in direct contact with the axonal membrane via cell adhesion molecules such as N-cadherin, L1 and MAG, the myelin-associated glycoprotein (Seilheimer et al., 1989; Owens et al., 1990b; Wanner and Wood, 2002). The spiral growth of the membrane is initiated by the expansion of membranes at the edges of the Schwann cells. The precise process of the wrapping is not well understood. Once several spiral turns are formed, the cytoplasm between the membranes is extruded and the extracellular space decreased. The conversion of non-compact myelin to compact myelin coincides with the occurrence of P0, the major structural protein of the compact PNS myelin, and disappearance of MAG in the mesaxonal membrane, which is finally exclusively found in periaxonal membranes (Trapp, 1988). The myelin sheath thickness is correlated to axon diameter and is probably regulated by the amount of NRG1-III expressed by

the axons. It is suggested that neurons regulate the expression of NRG1 as a function of their own dimension (Michailov et al., 2004). The cellular mechanisms that regulate the length of myelinated internodes are not known. However, studies have shown that disruption of cytoplasmic bands called Cajal bands impairs Schwann cell elongation. Therefore it has been proposed that internodal growth is permitted by microtubule-based transport along the longitudinal bands of Cajal (Court et al., 2004).

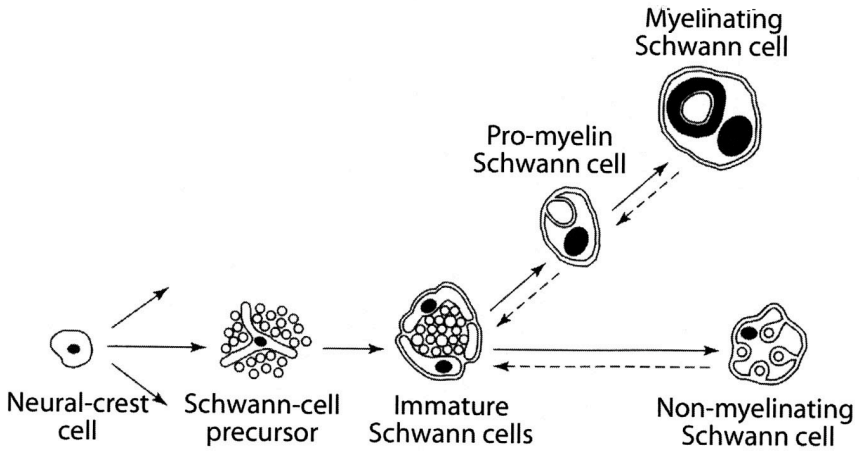

Figure 3 (A) The development of the Schwann cell lineage: neuronal precursor cells give rise to Schwann cell precursor cells that differentiate into immature Schwann cells. From immature Schwann cells two Schwann cell subtypes evolve: the non-myelinating and the myelinating Schwann cells. Differentiation of the Schwann cells is marked by morphological changes and the appearance of characteristic differentiation markers and is reversible (Copied from Lazzarini R. A. , 2004).

4 Oligodendrocyte development and myelination

Oligodendroglial progenitor cells arise from cells of the subventricular zone. The migrating progenitor cells proliferate and populate the nervous system during development. They pass through early and late progenitor stages marked by stellate shapes and develop into premyelinating oligodendrocytes or adult progenitors (Figure 4). All progenitor oligodendrocytes express the patelet derived growth factor receptor α (PDGFαR) and the sulfated proteoglycan, NG2 (Pringle et al., 1992; Nishiyama et al., 1996). Premyelinating oligodendrocytes show radially and symmetrically extended processes and express a subset of myelin proteins such as DM20, MAG, CNPase and MBP. In contrast to Schwann cells, oligodendrocytes do not require axonal contact to initiate myelin protein expression. Premyelinating oligodendrocytes either start

myelination or undergo programmed cell death. It has been estimated that about 50% of oligodendrocytes undergo apoptosis (Barres et al., 1992). Differentiation of premyelinating oligodendrocytes to myelinating oligodendrocytes includes morphological and molecular changes. As myelination begins, oligodendrocytes start to target myelin proteins to specific membrane domains requiring a complex network of microtubules. MAG is confined to the periaxonal membranes, PLP, MBP and MOG to the compact myelin, CNP to non-compact regions of the myelin internodes. MBP RNA is translocated along oligodendrocytes processes and translated into protein (Colman et al., 1982). In contrast to Schwann cells, oligodendrocytes have the potential to myelinate multiple axons.

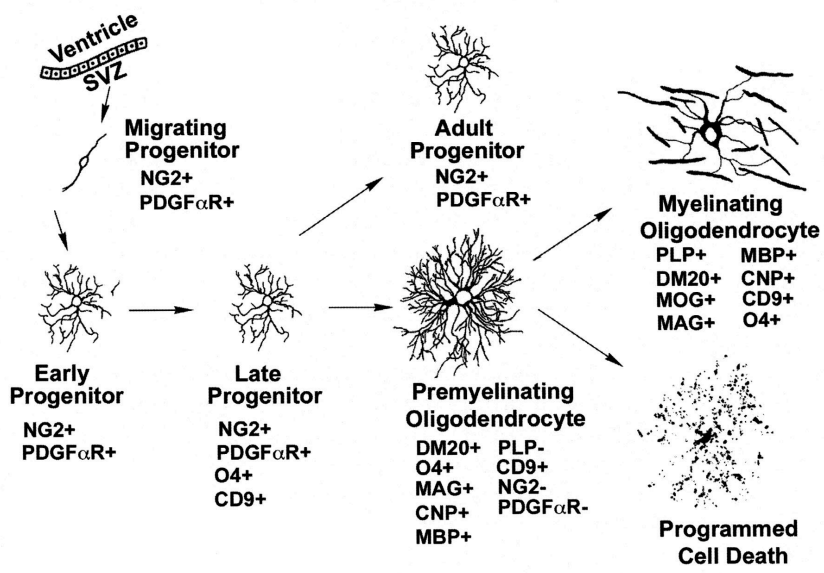

Figure 4 The development of the oligodendrocyte lineage: Oligodendrocyte progenitor cells migrate from the subventricular zone (SVZ) to the developing white and gray matter and They give rise to premyelinating oligodendrocytes and adult progenitor cells. Premyelinating oligodendrocytes either myelinate axons or undergo programmed cell death (Copied from Lazzarini R. A. , 2004).

5 Myelin proteins

The following paragraphs provide background information about a series of myelin proteins. The proteins are described in more detail because they are abundant myelin proteins or because they are of particular importance in this work.

5.1 Myelin basic protein (MBP)

Myelin basic protein is an abundant myelin protein found in the CNS as well as in the PNS. The MBP gene contains three transcription starts that give rise to three different RNAs. The classic MBP isoform expressed by myelinating Schwann cells and oligodendrocytes are generated from the major transcription start site 3. From transcription start site 1, the so-called golli-MBP proteins are generated. Golli-MBP proteins are expressed in the thymus, the spleen and the lymph nodes and only at low levels in the nervous system. At least six alternatively spliced MBP RNAs generated from transcription start site 3 have been documented that encode MBP isoforms that range from 14 to 21kD. The proportions of the different MBP isoforms are developmentally regulated. Early during development, the 17 and 21.5kD isoforms predominate, whereas the proportion of the 14 and 18.5kD isoforms increase later during development.

The main biological function of the classic MBP is to maintain the structure of the myelin sheath. It has been suggested that the highly positively charged MBP interacts with the negatively charged cytoplasmic membrane surface and brings thereby the layers of myelin in a close position (Harauz et al., 2004). The precise roles of the different MBP isoforms are not clear. Mice with mutated MBP protein (*shiverer* mice) caused by a deletion within the MBP gene show a severe phenotype that is marked by a generalized tremor (Roach et al., 1985). In the CNS of *shiverer* mice, there is an almost complete lack of myelin and the oligodendrocyte membranes do not compact to form a major dense line. In the PNS in contrast, compact myelin is formed in *shiverer* mice and myelin periodicity is normal (Rosenbluth, 1980). It is thought that other myelin proteins such as P0 compensate for the loss of MBP in the PNS (Martini et al., 1995).

5.2 Proteolipid protein (PLP)

PLP and its smaller isoform DM20 are the most abundant myelin proteins predominantly expressed in CNS. The PLP gene locus comprises 7 exons and DM20 is produced through alternative splicing of exon 3. DM20 is the predominant isoform early during oligodendrocyte development. PLP is a hydrophobic protein with four α-helical membrane spanning domains with both amino and carboxy termini exposed to the cytoplasm. DM20 has identical amino acid sequences as PLP at the amino and carboxyl termini, but it lacks about 40 amino acids of the cytoplasmic domain. The hydrophobicity of PLP and DM20 is increased by posttranslational covalent linkage of long chain fatty acids (Messier and Bizzozero, 2000). A PLP mutant mouse the so-called *jimpy* mouse shows a myelin deficiency restricted to the CNS due to an aberrant RNA splicing of PLP (Nave et al., 1987).

5.3 Myelin oligodendrocyte protein (MOG)

MOG is a glycoprotein specifically expressed by oligodendrocytes. It is only a minor component of the CNS myelin. It is a transmembrane protein with an extracellular Ig-like domain and the intracellular domain is possibly semi-embedded in the cytosolic side of the membrane. MOG is localized in the abaxonal myelin membrane. Its localization suggests that it could interact with molecules of the extracellular matrix or that it may be involved in adhesion between neighboring myelinated fibers, possibly via homophilic MOG-MOG interaction. The expression of MOG is one of the latest events during CNS myelination. MOG knock out mice develop normally and there are no apparent effects on the myelin morphology (Delarasse et al., 2003). MOG is a major target for autoantibody-mediated demyelination in experimental autoimmune encephalomyelitis (EAE), an animal model for multiple sclerosis (MS).

5.4 Protein zero (P0)

P0 is the most abundant myelin protein of the PNS. It is an integral membrane protein and is important for myelin compaction. P0 belongs to the immunoglobulin gene superfamily and has a disulfide-stabilized V_H domain and a single transmembrane domain. Post-translational modifications of P0 include glycosylation of the extracellular domain with a complex carbohydrate and acylation and phosphorylation of the intracellular domain. It is proposed that P0 form tetramer complexes and that these complexes of opposing membrane layers interact via homophilic interaction. P0 is primarily expressed by Schwann cells and mutations of P0 are

associated with the peripheral neuropathy Charcot Marie Tooth 1B. For the induction and maintenance of P0 expression, Schwann cells require contact with axons.

5.5 Myelin associated glycoprotein (MAG)

Myelin-associated glycoprotein is an immunoglobulin-like cell adhesion molecule. It shows five Ig-like domains and belongs to the sialic acid binding protein family siglec 4a (Arquint et al., 1987; Crocker et al., 1998). MAG is expressed by myelinating Schwann cells and oligodendrocytes. MAG is located in the periaxonal membrane of glial cells and is suggested to play an important role for axon-glia interaction (Figure 5A; (Bartsch et al., 1989)). MAG is also located in compartments of the non-compact myelin such as Schmidt-Lanterman incisures and paranodal loops (Owens and Bunge, 1989). It exists in two isoforms whose expression is regulated spatially and temporally. The isoforms result from alternative splicing and show common extracellular and different intracellular domains (Lai et al., 1987). The MAG gene consists of 13 exons (Figure 5B). Exon 12 can be alternatively spliced in, or skipped, to produce the small isoform (S-MAG, 67kD) or large isoform (L-MAG, 72kD), respectively. L-MAG predominates during CNS development, whereas S-MAG accumulates later. In the PNS, the S-MAG is the predominant isoform (Inuzuka et al., 1991). The alternative splicing of MAG is regulated by the RNA binding protein QKI-5 (Wu et al., 2002). Mice with a naturally occurring mutation within the regulatory region of the QKI gene show a predominant S-MAG expression during development and reduced L-MAG levels.

MAG undergoes a variety of post-translational modifications such as phosphorylation, glycosylation and palmitylation. Potential phosphorylation sites within the cytoplasmic domains are Serine, Threonine and Tyrosine residues (Agrawal et al., 1990). Possible kinases involved in the phosphorylation of MAG are PKA, PKC and Fyn (Jaramillo et al., 1994). Fyn kinase, a member from the Src family of tyrosine kinases, has been shown to interact with the L-MAG cytoplasmic domain. MAG is heavily glycosylated mostly by oligosaccharides of the complex type. Eight N-linked oligosaccharide addition sites have been identified (Burger et al., 1993). A high proportion of the oligosaccharides are sialylated and sulphated. One carbohydrate epitope expressed on MAG as well as other cell adhesion molecules such as N-CAM, L1 and P0 is called HNK-1 (Kruse et al., 1984; Bollensen et al., 1988). Auto-antibodies to MAG commonly react with the HNK-1 epitope and can cause chronic neuropathies involving neuronal degeneration or demyelination (Ilyas et al., 1990).

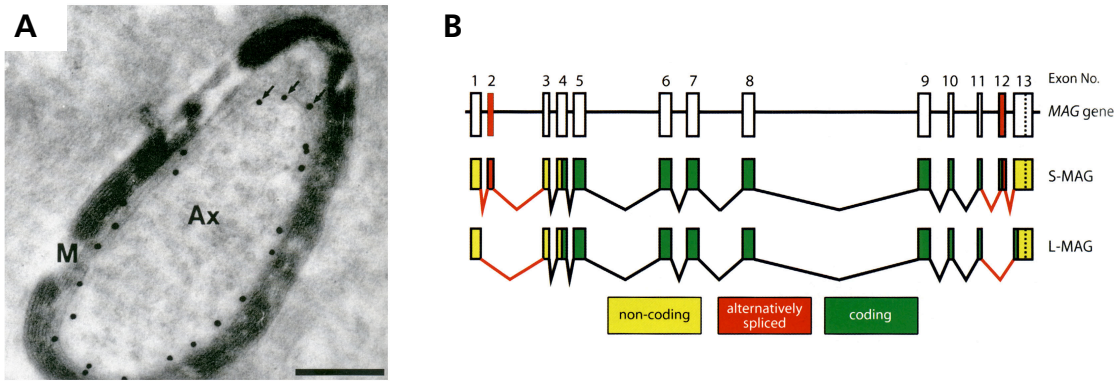

Figure 5 (A) Localization of MAG. MAG is localized in the periaxonal membranes of myelinating oligodendrocytes and Schwann cells. Electron microscopy with postembedding staining technique. (Copied from (Bartsch et al., 1989)). (B) Intron/ exon structure of the MAG gene. The MAG gene consists of 13 exons. Exon 12 is spliced in to produce S-MAG (Copied from Lazzarini R. A. , 2004).

Several axonal MAG binding partners have been described. Among them are gangliosides (sialic acid containing glycosphingolipids) GD1a and GT1b (CNS) (Yang et al., 1996a; Schnaar et al., 1998). Mice lacking the biosynthesis of complex gangliosides show a similar phenotype as MAG knock out mice (Sheikh et al., 1999). MAG/gangliosides signaling pathways possibly regulate neurite outgrowth. MAG may inhibit neurite outgrowth via multivalent clustering of gangliosides on neurons (Vyas et al., 2002). Apart from gangliosides, the Nogo receptor NgR is proposed to bind MAG (Liu et al., 2002). Nogo receptors are thought to mediate the inhibition of axonal outgrowth by binding MAG, OMgp or Nogo in the CNS. As signal transducing coreceptor for gangliosides and NgRs low affinity neurotrophin receptor p75 has been suggested (Wang et al., 2002a; Yamashita et al., 2002b). Microtubule associated protein 1B (MAP1B) is described as an additional MAG binding partner that is expressed at the surface of axonal membranes (Franzen et al., 2001). MAG has also been shown to interact with components of the extracellular matrix such as collagen, tenascin-R and fibronectin (Probstmeier et al., 1992; Yang et al., 1999).

MAG isoforms show different signaling capacities due to their diverse intracellular domains. Cross-linking of L-MAG has been shown to activate Fyn that phosphorylates a tyrosine residue on the L-MAG domain. Phosphorylated L-MAG associates with phospholipase Cγ and may serve as docking site for other signaling molecules (Jaramillo et al., 1994; Umemori et al., 1994). L-MAG also interacts with the cytoplasmic protein S100β, a calcium- and zinc-binding protein (Kursula et al., 1999). S100β interacts with a variety of cytoskeleton associated proteins,

including actin microfilaments, microtubules, and intermediate filaments. The S-MAG specific domain has been shown to bind tubulin and microtubules (Kursula et al., 2001).

The functional role of MAG has been studied *in vitro* as well as *in vivo*. *In vitro* it has been shown that MAG overexpression correlates with accelerated myelination, whereas MAG downregulation correlates with hypomyelination (Owens et al., 1990b; Owens and Bunge, 1991). MAG-deficient mice show only a subtle phenotype with slight defects in myelin formation and maintenance that mainly affects the CNS. In the CNS in contrast to the PNS, myelination is delayed in MAG deficient mice (Montag et al., 1994; Bartsch et al., 1997). In the CNS and less often in the PNS, the periaxonal cytoplasmic collars are collapsed (Montag et al., 1994). In the CNS of MAG-deficient mice, axonal segments are often surrounded by more than one myelin sheath and in old animals oligodendrocyte dystrophy is observed resembling dying-back oligodendrogliopathy (Lassmann et al., 1997). In the PNS of older MAG-deficient mice, alterations such as redundant myelin layers called "onion bulbs" that indicate repeatitive de- and remyelination are observed (Fruttiger et al., 1995). MAG-deficient mice show generally reduced axonal calibers and more densely packed neurofilaments (Yin et al., 1998). Old MAG-deficient mice show reduced nerve conduction velocities.

5.6 Peripheral myelin protein (PMP22)

The peripheral myelin protein PMP22 is an integral membrane protein widely expressed in neural and non-neural tissue (Baechner et al., 1995). The expression of the PMP22-gene is controlled by two different promoters P1 and P2 (Suter et al., 1994). P1 regulates PMP22 expression in Schwann cells and is activated specifically by progesterone (Desarnaud et al., 1998). P2 is more ubiquitously active. PMP22 is strongly expressed in Schwann cells at the beginning of myelination. It is localized in the plasma membranes of non-myelinating and myelinating Schwann cells and the compact myelin (Haney et al., 1996). There is a rapid turnover of PMP22, only a minor proportion of the newly synthesized PMP22 gets glycosylated, accumulates in the Golgi apparatus and is integrated into myelin (Pareek et al., 1993). PMP22 is a tetraspan transmembrane protein with a predicted molecular weight of 18kD. PMP22 runs as 22kD protein on denaturating SDS gels due to glycosylation. It has been proposed to be associated with the tetrameric complex of the compact myelin protein P0 (D'Urso et al., 1999). Changes of the stoichiometry of P0 and PMP22 are likely to affect the ordered structure of myelin and are associated with peripheral neuropathies. Duplication of the PMP22 gene leads to an overexpression of PMP22 causing the peripheral neuropathy CMT1A (Charcot Marie Tooth

disease type 1A). The reciprocal intrachromosomal deletion of PMP22 is associated with the hereditary neuropathy with liability to pressure palsies (HNPP). The functional role of PMP22 has been studied in cells *in vitro* as well as *in vivo*. *In vitro* studies have shown that PMP22 is induced by growth arrest of NIH3T3 cells after serum deprivation (Ciccarelli et al., 1990). Functional experiments have also shown that PMP22 overexpression in NIH3T3 induces apoptosis (Fabbretti et al., 1995). PMP22-deficient mice show a retardation in the onset of myelination and develop abundant sausage-like hypermyelination structures (tomacula) at a young age followed by severe demyelination, axonal loss and functional impairment (Adlkofer et al., 1995). Mice carrying a PMP22 point mutation the so called *trembler* mice display a severe hypomyelination during early development and only few myelinated fibers (Suter et al., 1992).

5.7 Connexin29 and Connexin32 (Cx29, Cx32)

Connexins are a family of highly related proteins and are named according to their predicted molecular weights. Connexins belong to the gap junction proteins that provide direct diffusion pathways of small molecules and are expressed by multiple cell types. In the CNS, Cx29 is localized to the inner membrane of small myelin sheaths, whereas Cx32 is localized on the outer membrane of large myelin sheaths (Kleopa et al., 2004). In the PNS, Cx29 and Cx32 protein have been demonstrated at paranodal loops and Schmidt-Lanterman incisures, and it is widely assumed that Connexins present in these locations provide a direct radial route for transport of ions and metabolites between cytoplasmic myelin layers (Balice-Gordon et al., 1998; Li et al., 2002; Meier et al., 2004). The importance of gap junctions is demonstrated by the fact that mutations in Cx32 are associated with X-linked peripheral neuropathy Charcot-Marie-Tooth disease (CMTX) (Fairweather et al., 1994).

6 Inherited peripheral neuropathies

Originally, hereditary motor and sensory neuropathies (HMSN) also called Charcot-Marie-Tooth diseases (CMT) have been classified according to their clinical, electrophysiological and histological characteristics into primary demyelinating (CMT1) and primary axonal forms (CMT2). Demyelinating forms are usually marked by an early onset (first or second decade of life), segmental demyelination, remyelination and nerve conduction velocities (NCV) below 38 m/s. Axonal forms generally show a later onset (third or fourth decade of life), loss of myelinated axons and NCV above 38 m/s. During the last years molecular and cellular mechanisms underlying the pathologies of CMT diseases have been studied and variety of CMT subclasses

has been formed (Table 1). Known genetic defects causing de- and dysmyelinating subtypes affect structural myelin proteins, transcription factors and proteins for protein synthesis, transport and degradation in Schwann cells. Axonal neuropathies are caused by defects in motor proteins, protein transport or proteins of the axonal cytoskeleton.

Table 1 Classification of peripheral CMT neuropathies and their inheritance (copied from (Berger et al., 2006))

Protein	Synonyms	Disease	Inheritance
Myelin structure			
P0	MPZ	CMT1B	Dominant
PMP22	PASII, SR13, Gas3	CMT1A	Dominant
Cx32	GJP1	X-linked CMT	X-linked
Periaxin	PRX	CMT4F	Recessive
Transcription factors			
EGR2	Krox-20	CMT1D/CMT4E	Dominant/ recessive
Vesicular transport			
MTMR2		CMT4B1	Recessive
MTMR13	SBF2	CMT4B2	Recessive
Dynamin2	DYN2	DI-CMTB	Dominant
SIMPLE	LITAF	CMT1C	Dominant
Others			
KIF1B		CMT2A	Dominant
GDAP1		CMT4A	Recessive
YARS		DI-CMTC	Dominant
NDRG1		CMT4D	Recessive
KIAA1985		CMT4C	Recessive
NF-L		CMT2E	Dominant

6.1 CMT1A is caused by a duplication of the structural protein PMP22

CMT1A is the most common inherited peripheral neuropathy and is caused by the duplication of the gene encoding the structural protein PMP22 (Skre, 1974). Duplication of PMP22 results in an overexpression of PMP22. The precise mechanisms underlying the disease are still not clearly known. It is hypothesized that PMP22 and P0, which are both sensitive to gene-dosage

and physically interact with each other, are required in precise stoichiometric amounts. It has also been shown that overexpression of PMP22 disturbs Schwann cell maturation and causes metabolic disturbances as PMP22 aggregates and blocks protein degradation by the proteasome (Magyar et al., 1996; Notterpek et al., 1999). A variety of animal models has been generated to study the mechanisms of CMT1A disease. There are rat and mouse models for CMT1A disease carrying PMP22 genes from human, rat or murine origin.

The CMT1A rat model

The CMT1A rat model was generated using a 43 kb cosmid containing the mouse PMP22 gene including flanking DNA regions (Sereda et al., 1996). The CMT1A rat carries approximately 3 copies of the PMP22 gene that leads to a 1.6 fold PMP22 overexpression. Many axons have only thin or absent myelin sheaths. Supernumerary Schwann cell processes, so called "onion bulbs" that indicate repetitive demyelination and remyelination are occasionally observed in CMT1A rats. Motor fibers are more severely affected than sensory fibers. Hypomyelination is generally more marked in larger caliber fibers. In CMT1A rats, axonal loss is observed. Many smaller fibers have myelin sheaths of normal or even increased thickness.

The CMT1A mouse models: TgN248 and TgN249

The TgN248 and TgN249 CMT1A animal models were generated using the same 43 kb PMP22 containing cosmid used for the rat model described above (Magyar et al., 1996). The TgN248 mouse carries 16 and the TgN249 30 transgene copies. The expression of PMP22 RNA is approximately 2 fold increased. Both lines display a severe demyelinating phenotype characterized by an almost complete lack of myelin. In both lines, numbers of Schwann cells associated 1:1 with axons as at the promyelination state are increased. Onion bulbs are not observed in TgN248 and TgN249.

The CMT1A mouse model: M41

The M41 mouse line was generated using a YAC construct containing the mouse PMP22 gene with flanking DNA regions (Robertson et al., 2002). Neither the copy number nor the levels of PMP22 RNA have been determined yet in M41 mice. M41 mice have a severe demyelinating phenotype. About 75% of the axons have no or only a thin myelin sheath. Myelinated fibers

show an increased g-ratio (axon diameter/ diameter of myelinated fiber) of 0.74 compared to controls (0.65). In M41 mice, the myelin periodicity is normal and there is no evidence for axonal loss. However, the fiber size distribution shows a lack of large myelinated fibers. The numbers of Schwann cells are increased in M41 mice, which is a general characteristic in demyelinated nerves. Onion bulbs are not observed in M41 mice.

The CMT1A mouse model: C61and C22

The C61and C22 mouse lines were generated using a YAC construct containing the human PMP22 gene with flanking DNA regions (Huxley et al., 1996).

The C61 mouse line carries 4 copies of the human PMP22 gene. C61 mice have a mild demyelinating phenotype. Only about 3.1% of the axons are dysmyelinated. The g-ratios, myelin periodicity and numbers of Schwann cells are normal in C61 mice. In C61 mice, there is no evidence for axonal loss. There is a decreased proportion of large myelinated fibers and an increased proportion of small caliber myelinated fibers.

The C22 mouse line was used in the study presented here. It carries about 7 copies of the PMP22 gene resulting in a 1.7 fold expression of PMP22. The resulting peripheral neuropathy closely resembles the human pathology of CMT1A disease. The characteristics of C22 mice are the progressive weakness of the hind legs and severe hypomyelination (Figure 6A, B). The sciatic nerves display widespread hypomyelination of medium to large axons, but no signs of acute axonal degeneration (Huxley et al., 1996). C22 mice show very slow nerve conduction velocities and prolonged distal motor latencies (MCV 3.7 +/- 2.2m/s in C22; 38.2 +/- 6.3m/s in wild type) (Huxley et al., 1998). C22 have decreased numbers of myelinated fibers during development and in adulthood. Only about 60% of axons are myelinated in adults. Numbers of incompletely surrounded axons during development and in the adult C22 mice are increased. Numbers of Schwann cells per axons are significantly increased in C22 mice at all time points (adult C22 mice: 12.3 Schwann cell nuclei/100 axons; wild type 4.4) (Robertson et al., 1999). The analysis of the fiber size distribution in C22 mice revealed decreased numbers of large myelinated fibers and an increase in the proportion of smaller ones. The average of the g-ratio is significantly increased in C22 indicating inappropriately thin myelin sheaths. The myelin periodicity showed a significant increase in the C22 nerves (Robertson et al., 2002). C22 mice were used in preclinical trials to test the therapeutic efficacy of ascorbic acid that is known to promote Schwann cell differentiation. Ascorbic acid treatment resulted in amelioration of the CMT1A phenotype

improving locomotion and increased the numbers of myelinated axons from 25% (placebo control animals) to 70% (ascorbic acid treated animals). Myelin sheath thickness was returned to normal in ascorbic acid treated animals, which indicates that it may reactivate the myelination process. Measurement of PMP22 RNA levels revealed a 10 fold decreased expression in ascorbic acid treated mice (Passage et al., 2004).

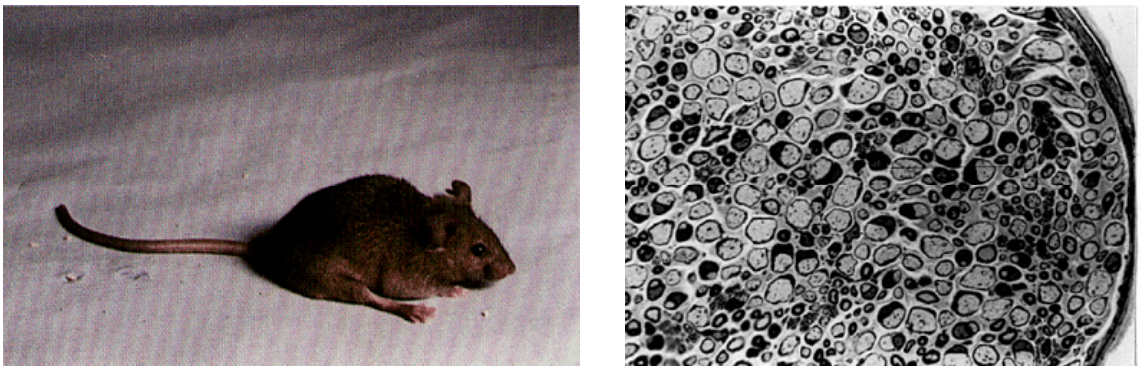

Figure 6 (A) The PMP22 transgenic mouse C22. C22 mice progressively lose control of the hind legs end up with a severe disability. (B) Light microscopic histology of the sciatic nerve (C22) shows a widespread demyelination of axons in C22 animals (Copied from Huxley et al., 1996).

6.2 CMT1D is caused by mutations of the transcription factor EGR2/Krox20

CMT1D is a demyelinating neuropathy caused by mutation of the Schwann cell transcription factor EGR2/Krox20. Mutations are located within the zinc finger domain of EGR2/Krox20 causing a severe form of CMT. It is hypothesized that the expression of compact myelin protein P0 and also lipid synthesis is controlled via EGR2/Krox20 (Nagarajan et al., 2001).

6.3 CMT2A is caused by mutation of the motor protein kinesin

CMT2A is primary axonal neuropathy caused by a mutation within the motor protein kinesin 1B. Kinesins are molecules that transport vesicles along microtubules by hydrolyzing ATP. It is not clear which of the two isoforms of KIF1B is affected in CMT2A patients. The pathology of CMT2A is length dependent reflecting that distal nerves are primarily affected by impaired kinesin dependent transport (Zhao et al., 2001).

6.4 CMT2E is caused by mutation of the neurofilament light chain

CMT2E is another axonal form of CMT. It is caused by mutations within the gene encoding the neurofilament light chain. Neurofilaments are the major components of the axonal cytoskeleton. In animal with mutations in neurofilament light chain, axonal diameters are reduced which probably accounts for slowed nerve conduction velocities (Jordanova et al., 2003).

7 Neurofilaments, the major components of the axonal cytoskeleton

Various neurodegenerative diseases such as Amyotrophic lateral sclerosis, Alzheimer's, Parkinson's and CMT disease are characterized by alterations in the axonal cytoskeleton. Alterations especially affect neurofilaments which are therefore commonly used as surrogate markers for axonal injury (Petzold, 2005). Neurofilaments make up the majority of scaffolding proteins of the axonal cytoskeleton. They are classified as type IV intermediate filaments. Neurofilaments are obligate heteropolymers that are composed of three subunits, a light (NF-L), a medium (NF-M) and a heavy chain (NF-H). During development, NF-L and NF-M are coexpressed initially whereas NF-H appears later (Carden et al., 1987). All neurofilament subunits consist of an amino-terminal head domain, a central conserved rod domain and a carboxy-terminal tail domain. The neurofilament subunits form dimers, which are sorted in an antiparallel fashion to form tetramers. Tetramers combine to protofilaments, which finally assemble into 10nm thick filaments. Assembly of neurofilament subunits in filaments is probably regulated by the phosphorylation of the NF-L head domain as phosphorylation of the NF-L head domain inhibits the formation of protofibrils (Hisanaga et al., 1990). The tail domains of NF-M and especially NF-H can be heavily phosphorylated at lysine-serine-proline (KSP) sites. Phosphorylation of neurofilaments is thought to be controlled by the process of myelination and is regulated by a kinase/phosphatase system. Different kinases are implicated into neurofilament tail phosphorylation such as glycogen synthetase kinase-3, extracellular signal-regulated kinases and cyclin-dependent kinase 5 (Guidato et al., 1996; Veeranna et al., 1998). Neurofilament tail phosphorylation is proposed to increase the distances between neighboring neurofilaments and to be associated with an increase in axonal caliber (Hsieh et al., 1994). However, it seems that NF-M and NF-H stoichiometrics are more important for axonal growth than NF-H phosphorylation (Xu et al., 1996). In addition, phosphorylation of neurofilament tail domains has been suggested to regulate axonal transport. Recent studies suggest that the fast axonal transport motor kinesin participates in neurofilament transport. It has been proposed that phosphorylation of the neurofilaments promotes the dissociation of neurofilaments from the motor protein kinesin and the formation of a macro-structure that cannot readily undergo axonal transport (Jung et al., 2000; Yabe et al., 2000).

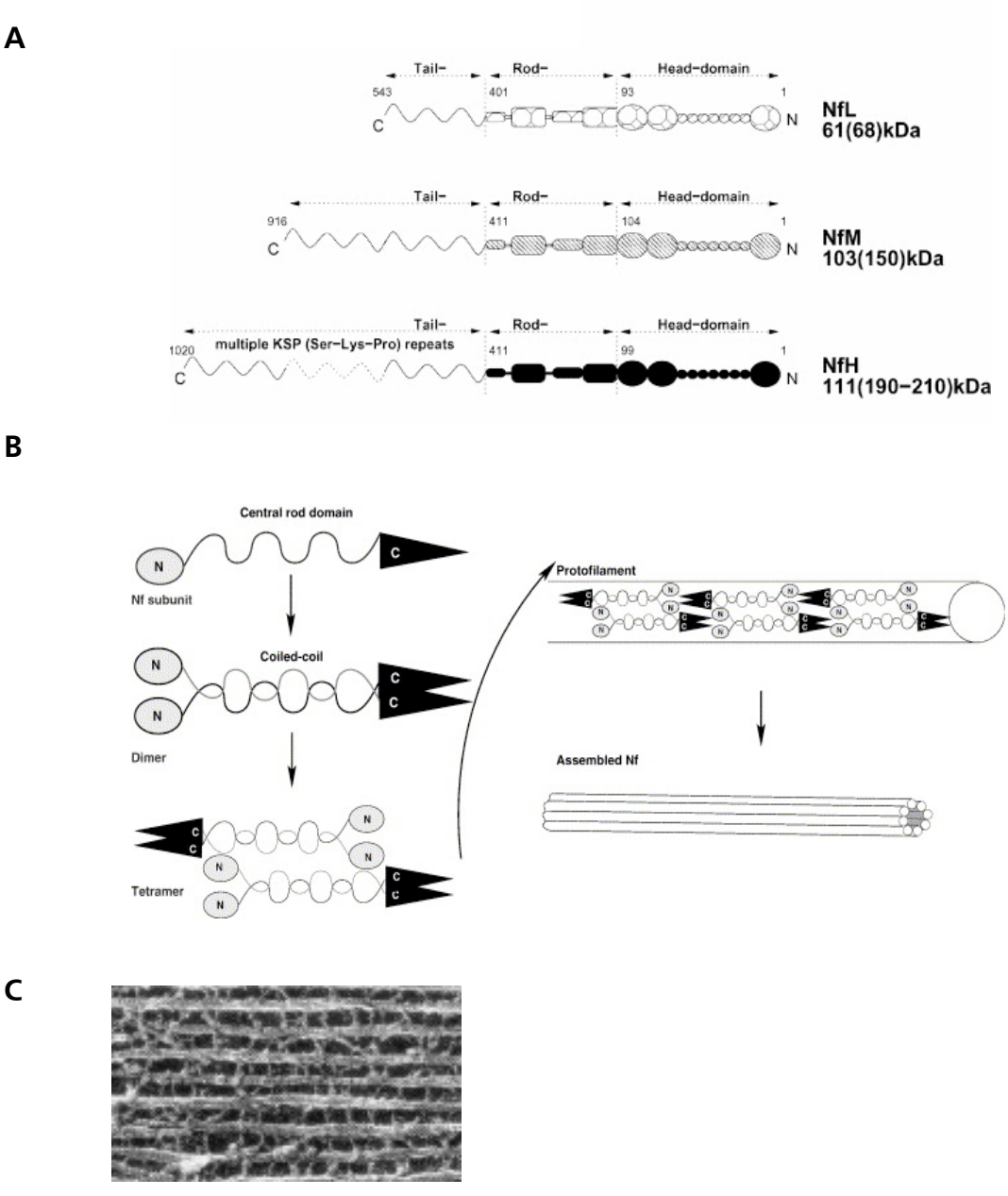

Figure 7 Neurofilament subunits and assembly. (A) Neurofilament light, medium and heavy chains. The subunits share a conserved core and head domain and differ in their tail domains. The tails differ in length and can be phosphorylated at multiple KSP (Lys-Ser-Pro) repeats by proline directed kinases (GSK-3, ERK1/2, Cdk5). (B) Neurofilaments form dimers that are sorted in an antiparallel fashion and arrange to tetramers. Assembled tetramers form protofilaments which finally build 10nm thick neurofilaments. (C) Electron microscopy of assembled neurofilaments (Copied from Petzold, 2005).

7.1 Transgenic and knock out animals generated to study the neurofilament system

Multiple mouse models have been generated to determine the specific roles of the neurofilament subunit composition and the neurofilament phosphorylation in the establishment and maintenance of the neurofilament network. In the following paragraphs the phenotypes of different neurofilament animal models are shortly described.

To study the role of the neurofilament subunit composition, transgenic mice have been generated that overexpress an individual neurofilament subunit (Xu et al., 1996). It has been shown that the increase of the NF-H, NF-M or NF-L subunit alone inhibits radial growth, while increasing both NF-M and NF-H reduces axonal growth even more severely. In contrast, a combined increase of NF-L with either NF-M or NF-H promotes radial growth. Neurofilament subunit composition also determines the number of neurofilaments. Overexpression of NF-L increases neurofilament the numbers, whereas overexpression of NF-M and NF-H reduces the numbers. Neither the inhibition nor the enhancement of axonal growth correlates with changes of the neurofilament neighbor distances in these transgenic mice (Table 2).

The hypothesis that the neurofilament tail phosphorylation of the NF-H specifies axonal growth has been tested by two independent groups using NF-H null mutant mice (Elder et al., 1998b; Rao et al., 1998). The outcome of the two studies is conflicting. The study presented by Rao et al. shows that in the absence of NF-H, levels of NF-M undergo a compensatory increase. In their mouse model, the absence of NF-H shows little effect on the radial axonal growth. The number of neurofilaments is normal and the nearest neighbor distances only slightly reduced. Elder et al. showed that in the absence of NF-H, NF-M levels are not changed and the levels of NF-L only slightly reduced. In their mouse model, the absence of NF-H diminishes axonal calibers. The number of neurofilaments is slightly reduced and the nearest neighbor distances not significantly changed. Both studies do not provide evidence that the nearest neighbor distances of neurofilaments are determined by phosphorylation of the NF-H tail domain.

In further studies, the role of NF-M for axonal growth has been analyzed (Elder et al., 1998a; Rao et al., 2003). According to Elder et al., the absence of NF-M dramatically decreases levels of NF-L and increases levels of NF-H. They have shown that in the absence of NF-M, axon calibers as well as numbers of neurofilaments are diminished. Rao et al. specifically deleted the carboxy-terminal tail domain of the NF-M using a gene knock-in approach. They have shown that mutation of the NF-M tail domain severely inhibits radial axonal growth and reduces the nearest neighbor distances between neurofilaments.

A neurofilament deficient strain of the Japanese quail, named quiver (Quv), has been informative of the functional role of the neurofilament light chain (Yamasaki et al., 1991). In Quiver animals, neurofilaments are electron microscopically and immunohistochemically not detectable in the axons or neuronal cell bodies. In Quiver animals, axons are composed mainly of microtubules, which are increased in number in relation to the axonal size. Molecular biological analyses have shown that the expression of neurofilament-L gene is specifically repressed in neurons of this mutant. The fact that in the absence of NF-L neurofilaments are not produced indicates that the NF-L subunit plays a key role in assembly of the NF subunits. In Quiver animals, the size distribution of the axonal calibers significantly shifted to small size classes.

Table 2 Phenotypes of different neurofilament animal models

Animal model	**Axonal phenotype (PNS, L5 ventral root)**			**Reference**
Overexpression of	*Axon diameter*	*NND*	*Levels of*	(Xu et al., 1996)
NF-L	↓	↓		
NF-M	↓	–		
NF-H	↓	–		
NF-H/M	↓↓	*clustered*		
NF-L/M	↑	↓		
NF-L/H	↑	–		
NF-H knock out	(↓)	–	NF-M ↑ NF-L –	(Rao et al., 1998)
NF-H knock out	↓	(↓)	NF-M – NF-L (↓)	(Elder et al., 1998b)
NF-M knock out	↓	↑	NF-H ↑ NF-L ↓	(Elder et al., 1998a)
NF-MΔtail	↓	↓	NF-H – NF-L –	(Rao et al., 2003)
Quiver (Japanese quail)	↓	Almost depleted		(Yamasaki et al., 1991)

7.2 Modulation of neurofilaments by myelination

Evidence that myelination has an impact on the properties especially the phosphorylation of neurofilaments is given by several studies. Starr et al. have performed experiments *in vitro* with dorsal root ganglion (DRG) Schwann cell co-cultures and have shown that phosphorylation of neurofilaments is regulated by myelination (Starr et al., 1996). They have analyzed the phosphorylation state of neurofilaments in DRG neurons cultured in the presence (myelinated) and absence (unmyelinated) of ascorbic acid and have found that myelination induces an increased immunoreactivity for phosphorylated neurofilament epitopes. In addition, they have detected an increased kinase activity in myelinated cultures compared to unmyelinated ones. The relationship between neurofilament phosphorylation and myelination has also been investigated by Hsieh et al. and Mata et al. (Mata et al., 1992; Hsieh et al., 1994). They have studied the distribution of phosphorylated and non-phosphorylated neurofilaments along the axons of myelinated fibers. Their results have indicated that the degree of phosphorylation of the neurofilament heavy and medium chains is reduced in unmyelinated regions such as the nodes of Ranvier and the stem processes in comparison with internodal neurofilaments.

The impact of myelination on the neurofilament system has also been studied in various mouse models that present a demyelinating phenotype. De Waegh et al. have shown that axon calibers, neurofilament phosphorylation and spacings are locally controlled by myelinating Schwann cells (de Waegh and Brady, 1990; de Waegh et al., 1992). In their experimental set up they grafted nerve segments from Trembler mice (point mutation in PMP22) in control sciatic nerves and compared axon diameters, neurofilament phosphorylation and spacing in grafted segments nerve segments to adjacent regions. They have found reduced axonal calibers, decreased neurofilament phosphorylation and neurofilament spacings in grafted nerve segments.

Cole et al. have studied the consequences of peripheral nerve hypomyelination on the axon diameter, neurofilament phosphorylation and neurofilament density (Cole et al., 1994). For their study they used transgenic mice with a demyelinating phenotype caused by the expression of diphtheria toxin or SV40 controlled by the P0 promoter in Schwann cells. They have found that severe hypomyelination is associated with a decrease in axonal caliber, a dramatic decrease of phosphorylation and an increase in neurofilament density. From their studies they have concluded that signals transmitted by myelinating Schwann cells modulate axon calibers, neurofilament phosphorylation and neurofilament density.

That myelination regulates the neurofilament phosphorylation has been well established and suggests that Schwann cell-axon interactions act to modulate a kinase-phosphatase cycle responsible for maintaining the phosphorylation state of neurofilaments in normal nerve. However, the precise signal transduction pathways have not been determined yet. De Waegh et al. have suggested MAG as logical candidate for the Schwann cell ligand to axonal receptor (de Waegh et al., 1992). They have proposed MAG as signaling molecule on the Schwann cell side of the pathway simply due to its localization at the myelin-axon interface. First experimental evidence that supports a functional role for MAG in the regulation of axonal calibers, neurofilament phosphorylation and spacing has been provided by Yin et al. (Yin et al., 1998). Their study has shown that the absence of MAG correlates with reduced axonal calibers, reduced neurofilament phosphorylation and neurofilament spacing. That these changes are indeed due to the absence of MAG and not a secondary effect of a generally disrupted Schwann cell-axon junction that prevents signaling by other molecules has been demonstrated *in vitro* by Dashiell et al. (Dashiell et al., 2002). They have shown that phosphorylation of neurofilaments is increased in DRG neurons cultured with MAG transfected COS-7 cells as well as in PC12 neurons treated with soluble MAG-Fc. In addition, they have shown that MAG stimulates the activities of Cdk5 and ERK1/2 kinases.

Aim of the project

The formation and maintenance of myelinated nerves requires constant reciprocal signaling between glial cells and axons. However, little is known about the molecules that mediate axon-glial interactions at the onset and during maintenance of the myelin sheath. One molecule implicated in the axon-glial interaction is the myelin-associated glycoprotein (MAG). MAG is expressed early at the onset of myelination when glial cells attach to axons and is still present in the periaxonal membranes after spiral enwrapping and compaction. MAG is expressed as a large (L-MAG) and a small isoform (S-MAG) that display different intracellular domains that cannot be distinguished by antibody staining. The precise functional role of the two MAG isoforms is not known. The purpose of the first part of this thesis was investigation of the temporal and spatial expression pattern of L- and S-MAG isoforms in the CNS and PNS. For this study a transgenic mouse expressing GFP tagged S-MAG controlled by its own promoter was generated by Michael Erb (Erb, 2003) and handed over for detailed characterization. The initial question was whether the introduction of transgene somehow interferes with normal myelination or even with the correct localization of S-MAG in the myelin compartments. Then the isoform specific expression pattern of MAG within different structures of the brain, within different domains of the myelin sheath during development and in adults was investigated.

Charcot-Marie-Tooth disease type 1A is the most frequent hereditary peripheral neuropathy caused by duplication of a DNA region encoding peripheral myelin protein PMP22. The impact of the overexpression of PMP22 on Schwann cells has been well described. The aim of the second part of this thesis was to investigate whether PMP22 overexpression may have an effect on the development of myelinated axons in CMT1A disease as consequence of disrupted Schwann cells/axons signaling. Indications that abnormal Schwann cells have an impact on axons originally came from transplantation experiments, where allografts from Trembler-mice (point-mutation in PMP22) were used as bridges to connect the proximal and distal stumps of transected nerves from normal mice. Regenerating axons penetrating the allograft showed reduced calibers, higher neurofilament density, and a low phosphorylation state, alterations that were restored in the distal host-derived part of the nerve containing wild type Schwann cells (de Waegh et al., 1992). In this work, the developmental effect of PMP22 overexpression on the establishment and maintenance of the axonal cytoskeleton in an animal model for CMT1A disease was investigated with focus on the neurofilament subunit composition and

phosphorylation. A further aim was to investigate the expression of MAG under these conditions.

The expression of myelin-associated glycoprotein isoforms in CNS and PNS (Part I)

Michael Erb*, Bettina Flueck*, Frances Kern, Beat Erne, Andreas J. Steck, and Nicole Schaeren-Wiemers

* Both authors contributed equally to this work

Neurobiology, Department of Research and Neurology, University Hospital Basel, Pharmacenter, Basel, Switzerland

The following section is based on the work published in Molecular and Cellular Neuroscience, "*Unraveling the differential expression of the two isoforms of myelin-associated glycoprotein in a mouse expressing GFP-tagged S-MAG specifically regulated and targeted into the different myelin compartments*" (April 2006, Volume 31, Pages 613-627). The part "Materials and Methods" was extended.

1 Abstract

The two myelin-associated glycoprotein (MAG) isoforms are cell adhesion molecules that differ only in their cytoplasmic domains, but their specific roles are not well understood. In this study, we present a transgenic mouse line that specifically expresses GFP-tagged S-MAG correctly regulated and targeted into the myelin sheath allowing the specific discrimination of L- and S-MAG on the subcellular level. Here, we describe the differential expression pattern and spatial distribution of L-and S-MAG during development as well as in the adult central and peripheral nervous system. In peripheral nerves, where S-MAG is the sole isoform, we observed S-MAG concentrated in different ring-like structures such as periaxonal and abaxonal rings, and discs spanning through the compact myelin sheath perpendicular to the axon. In summary, our data provide new insights in the subcellular distribution of the two isoforms fundamental for the understanding of their specific functions in myelin formation and maintenance.

2 Introduction

For accurate action potential propagation along myelinated axons, the adhesive contacts between the axons and the myelin sheaths and between the myelin lamellae are essential. One adhesion molecule, which is implicated in the interaction between the axon and the myelinating cell during myelinogenesis and maintenance, is the myelin-associated glycoprotein (MAG). MAG is located in the myelin membranes juxtaposed to the axon and on apposing myelin membranes in the non-compact myelin compartments like the Schmidt-Lanterman incisures and the paranodal loops (Sternberger et al., 1979; Trapp and Quarles, 1982; Martini and Schachner, 1988; Trapp et al., 1989). As an axonal binding partner of MAG, MAP1B expressed as plasma membrane glycoprotein on neurons and the NgR2 have been suggested (Franzen et al., 2001; Venkatesh et al., 2005). MAG has also been shown to interact with the sialylated gangliosides GD1a and GT1b (Yang et al., 1996b; Vinson et al., 2001a; Vyas and Schnaar, 2001). Beside its adhesive properties, MAG plays also a role in axon-glia signaling, since the axon caliber of peripheral myelinated fibers of MAG-deficient mice is reduced due to decreased neurofilament phosphorylation, which seems to be mediated in a Cdk5 and Erk-dependent manner (Dashiell et al., 2002). MAG is also known as one of the molecules that impairs axonal regeneration (Venkatesh et al., 2005).

The functional role of MAG is mediated by the two individual intracellular domains of the two MAG isoforms: L-MAG (large) and S-MAG (small). The non-receptor tyrosine kinase Fyn has been identified as a signaling molecule downstream of L-MAG (Umemori et al., 1994). Beside Fyn, the calcium binding protein S100β and the phospholipase Cγ have been shown to be

isoform specific binding partners of L-MAG (Jaramillo et al., 1994; Kursula et al., 1999). These observations point to the functional roles for L-MAG in signal transduction and adhesion in axon-glia and/or glia-glia interactions. The S-MAG specific domain has been reported to bind to tubulin and microtubules, supporting a role for S-MAG as a cell adhesion molecule linking the axonal surface and the myelinating glial cell cytoskeleton (Kursula et al., 2001).

To address the differential expression of L- and S-MAG within the non-compact myelin domains and within individual fiber tracts, we have generated a transgenic mouse line that specifically expresses the S-MAG isoform tagged with green fluorescent protein (GFP) as S-MAG-GFP fusion protein. Here, we report the subcellular compartmentalization of S-MAG-GFP within the myelin sheath; among them are ring- or and disk-like structures in the PNS, and paranodal loops in the CNS and PNS. Furthermore, we describe the differential expression of L- and S-MAG during development and in adult myelinated fibers.

3 Materials and Methods (Part I)

3.1 DNA construct

To generate the *pmag*-MAG-e12GFP genomic expression construct encoding S-MAG-GFP fusion protein, the 19 kb C57Bl mouse MAG gene, including 1.8 kb promoter and all introns/exons was used. Briefly, the GFP sequence was inserted in front of the stop codon within exon 12 (Figure 1A) as described in detail before (Erb et al., 2003). The *pmag*-MAG-e12GFP sequence was excised from pBluescript with SalI and NotI. The insert was separated from the cloning vector by agarose gel electrophoresis using TAE buffer at 4 °C. The DNA was purified from the agarose gel using the GENECLEAN SPIN Kit (Q-BIO gene/Bio 101) and was further purified using the ELUTIP-D-COLUMN-SET (Schleicher&Schuell).

3.2 Generation of transgenic mice

Standard pronuclear injection procedures were used (performed by Dr. C. Goujet-Zalc, CNRS-UPS44, Villejuif-Paris, France). Transgenic animals were identified by PCR genotyping of tail DNA. From the two born founder animals, one transmitted the transgene. This founder animal was further bred with C57BL6. The transgene copy numbers were analyzed by quantitative real-time PCR (Q-PCR). On genomic DNA samples from wild type and transgenic mice, a 140 bp intron sequence of the mag gene (equally present on the endogenous mag gene and the

transgenic mag gene copies) was amplified together with a 200 bp sequence of the neurofascin gene. The mag gene levels obtained from the Q-PCR analysis were normalized to the neurofascin gene levels (internal standard). The normalized mag gene level obtained for wild type samples corresponds to the 2 endogenous mag gene copies. The normalized mag gene levels of transgenic animals were divided by the ones of wild type animals. This ratio corresponds to the x-fold presence of 2 mag gene copies in a transgenic animal. Therefore, this ratio was multiplied by 2 to obtain the single mag gene copy number (endogenous and transgenic), from which the 2 endogenous mag gene copies had to be subtracted to get the transgenic mag gene copy number ((mag-tgnormNF / mag-wtnormNF) x 2 – 2).

The genomic DNA was isolated from a tail specimen using the DNeasy tissue kit (Qiagen) and the Q-PCR was carried out using the Roche LightCycler together with the FastStart DNA Master SybrGreenI (Roche). The 140 bp intron sequence of the mag gene (endogenous and transgenic) was amplified using 5'MAGgen (5'-GCTGGGAATGCTGATGTTGTG-3') and 3'MAGgen (5'-TGGGGAAGGAAGGGAATGGTAG-3'). The 200 bp intron sequence of the neurofascin gene was amplified, using 5'NFgen (5'-AGAGGAAATGAGGCAACGGG-3') and 3'NFgen (5'-GCTGGAATGGGAGGGGAATAAG-3').

3.3 PCR and quantitative real-time PCR

RNA was isolated using guanidine thiocyanate as described before (Chomczynski and Sacchi, 1987). First strand cDNA synthesis was performed with Transcriptor Reverse Transcriptase (Roche) and Oligo (dT)15 Primer (Promega Corporation, Madison, USA). To amplify the MAG mRNA region of exon 10 to 13, the primer pair 5'exon10 (5'-GTCGCCTTTGCCATCCTGATT-3') and 3'exon13 (5'-TCTCAGATCCCAGGCGCTG-3') was used. Q-PCR was carried out using the Roche LightCycler with the FastStart DNA Master SybrGreenI (Roche). Primers were designed by using MacVector (Accelrys GmbH, Germany) and were used as the following:

For total MAG: 5'totalMAG (5'-GTTTGCCCCCATAATCCTTCTG-3') and 3'totalMAG (5'-TCCCTCTCCGTCTCATTCACAGTC-3');

For L-MAG: 5'L/S-MAG (5'-AATCGGTCCTGTGGGTGCTG-3') and 3'L-MAG-exon11/13 (5'-CGCTGCTTCTCACTCTCATAC-3');

For wild-type S-MAG: 5'L/S-MAG and 3'S-MAG-exon12 (5'-GGGGCTCTCAGTGACAATCC-3');

For PLP/DM20: 5'PLP/DM20 (5'-ACTGTTGTATGGCTCCTGGTGTTTG-3') and 3'PLP/DM20 (5'-GCGAAGTTGTAAGTGGCAGCAATC-3');

For MBP: 5'MBP (5'-GGTCCAGGCTTCCTTTGTTTTCTTC-3') and 3'MBP (5'-TGTCCAGCGTGTTCTCCTAAGTCC-3');

For P0: 5'P0 (5'-GGTGACCCTGCACTGCTC-3') and 3'P0 (5'-GCAACAGCACCACCCCGA-3');

For actin: 5'Actin (5'-GGAAATCGTGCGTGACATCAAAG-3') and 3'Actin (5'-CATACCCAAGAAGGAAGGCTGG-3').

cDNA copy numbers for each gene were quantified by using standard curves of known quantities of plasmids containing the corresponding PCR product. The cDNA copy numbers were normalized to actin expression levels. In all analyzed transgenic tissues, no surplus L-MAG mRNA was detected. This is in line with in vitro data of the present MAG transgene, which showed that L-MAG is not transcribed from this transgene (Erb et al., 2003).

Quantification of mRNA levels in brain tissues was performed with three animals from each genotype independently. For quantification of mRNA levels in sciatic nerve tissues, sciatic nerves from 5 animals from each genotype were pooled and three experiments were performed independently.

3.4 Western blotting

Brain and sciatic nerve myelin membrane purification

Myelin was isolated from fresh frozen tissue via a sucrose gradient preparation. One brain was homogenized in 3 ml buffer containing 250 mM sucrose, 10 mM Hepes, 2 mM EGTA pH7.4 and protease inhibitors aprotinin (1 μg/ml), leupeptin (2 μg/ml), pepstatin (1 μg/ml) and PMSF (100 μg/ml) (buffer A). Tissue was homogenized with a 12 mm polytron for 2 times for 10 sec and always kept on ice. The homogenate was centrifuged at 2000 rpm for 3 min at 4 °C in SW rotor. The supernatant was collected and adjusted to a volume of 3.2 ml with buffer A. Then 5.8 ml buffer containing 2 M sucrose, 10 mM Hepes, 2 mM EGTA pH 7.4 (buffer C) were added and mixed by rotation for 5 min (final sucrose concentration in the mixture was 1.4 M). The sucrose gradient was set up in 14 ml Beckman 14x95 mm Polyallomer tube as follows: 1.1 ml buffer C (2 M sucrose), 8.5 ml homogenate (1.4 M sucrose), 2.2 ml buffer B (0.85 M

sucrose), 0.75 ml 0.25 M. The gradient was centrifuged for 20 h at 25000 rpm at 4 °C in a TST-4114 swing out with a Centrikon T-1055 ultracentrifuge. The myelin and plasma membrane phases accumulated in the 250 mM and 850 mM sucrose phases were collected in 15 ml tube using a spatula or a pipette. The collected samples were homogenized ones in 4 ml Hepes, 2 mM EGTA pH 7.4 with a 12 mm polytron and the volume was adjusted to 14 ml. The homogenates were centrifuged at 25000 rpm for 3 h at 4 °C. The supernatant was discarded and the pellet resuspended in 200-500 µl water and stored at –80 °C.

Myelin protein quantification

Protein concentrations were determined by Bradford assay. Myelin samples were diluted 1:10, 1: 20 and 1:40 (duplicates) and a BSA standard dilution series was prepared (100, 200, 400, 600 and 800 ng/µl BSA). 20 µl sample and 200 µl Bradford reagent were mixed, the absorbance at 590 nm was measured and concentrations calculated.

SDS-PAGE/Western blotting

Gels were prepared according to Laemmli protocol (Laemmli, 1970). Resolving gels contained 8 or 15% acrylamide/Bis (Biorad), 375 mM Tris pH8.8 and 0.1% SDS and was polymerized with 50 µl 10% ammonium persulfate (Biorad) and 5 µl TEMED (Biorad) per 10 ml gel. The stacking gels contained 5% Acrylamide/Bis, 125 mM Tris pH6.8 and 0.1% SDS and was polymerized with 50 µl 10% APS and 10 µl TEMED per 10 ml gel. The 4x sample buffer contained 40% glycerol, 8% SDS, 0.5% bromphenol blue, 80 mM Tris pH 6.8 and 20% β-mercaptoethanol (Sigma). Samples were heated for 30 min at 37 °C for denaturation. The running gel buffer contained 25 mM Tris-base (Riedel de Haen) 14.4% glycine (Riedel-de Haen) and 1% SDS. The gels were run overnight at 15 V. Prior protein transfer, gels were washed in running gel buffer and then equilibrated in transfer buffer (25 mM Tris-base, 14,4% glycine). The proteins were transferred to PVDF membranes (Biorad) at 50 V for 1.5 h. Blots were then washed in TBST (500 mM NaCl, 20 mM Tris pH 7.5 and 0.05% Tween20 (Fluka)) and incubated in with either 3% TopBlock (JuroSupply GmBH) in TBST (ECL detection system) or Odyssey blocking reagent (Odyssey detection system) for 3 h at RT. Primary antibodies were incubated overnight at 4 °C in either 1% TopBlock buffer or Odyssey blocking reagent (diluted 1:1 with TBS). Blots were washed 3 times in TBST for 20 min prior incubation with secondary antibodies. Peroxidase coupled secondary antibodies were used for ECL detection, fluorescence coupled ones for the

Odyssey detection. After incubation with secondary antibodies, blots were washed three times in TBST (15 min) and ones in TBS (5 min). Bands were detected with the ECL Western Blotting Detection Reagents (Amersham Pharmacia) and exposed to Hyperfilm ECL (Amersham Pharmacia). Fluorescent bands were detected with Odyssey Infrared Imager from LI-COR Biosciences GmbH, Germany (Hornig and Uhlmann, 2004; Williamson et al., 2004).

To quantify endogenous MAG levels, myelin samples were analyzed simultaneously with MAG and CNPase specific antibodies. We compared the MAG signals normalized to CNPase an internal standard protein in brains from 7 transgenic and 5 wild type animals in 4 independent experiments. Sciatic nerves from 5 animals of each genotype were pooled and quantified in 3 independent experiments.

Primary antibodies: anti-L-MAG (polyclonal, 1:500; (Erb et al., 2003), anti-MAG (polyclonal, 1:5000; kindly provided by Dr. A. Heape, Oulu, Finland), anti-CNPase (monoclonal, 1:1000, SMI91; Sternberger).

Secondary antibodies: goat anti-mouse IgG peroxidase (1:20000) and goat anti-rabbit IgG-peroxidase (1:5000) (Jackson ImmunoResearch), goat anti-mouse Alexa Fluor 680 (1:10000) and goat anti-rabbit IRDye 800 (1:10000) (LI-COR Biosciences GmbH, Germany).

3.5 Immunohistochemistry

Staining of brain and sciatic nerve sections

Brain and sciatic nerves were embedded in Tissue-Tek O. C. T. Compound (Sakura) without prior fixation. Cryostat sections of fresh frozen tissue (10 µm) were mounted on gelatine-chromalaun-coated slides. Sections were fixed in 10% formalin, 0.08 M phosphate buffer pH7.1 for 3 h. For delipidation slides were incubated overnight in 70% ethanol. Slides were washed in PBS (15 min). Before peroxidase staining, endogenous peroxidase activity was prevented with 0.6% H_2O_2 in 80% methanol for 20 min and washed in PBS (15 min). Unspecific binding sites were blocked for at least 1 h in blocking buffer (2.5% normal goat serum (Jackson ImmunoResearch), 0.1% fish skin gelatin (Sigma), 0.05% Saponin (Sigma) in PBS (Frank et al., 1998). Slides were incubated with primary antibodies in blocking buffer at 4 °C for 48 h, washed for 15 min in PBS and detection performed either with the ABC Kit (Vector Laboratories) or fluorochrome labeled secondary antibodies at RT for 30 min. The peroxidase

reaction was performed with AEC substrate as described before (Erne et al., 2002) and cell bodies were counterstained weakly with Mayer's Haemalaun (Merck) for 1 min. Kaisers' glycerol gelatine (Merck) was used for the embedding of the peroxidase stained slides, FluorSaveTM Reagent (Calbiochem/Merck, Germany).

Preparation and staining of sciatic nerve teased fibers

Teased fibers were prepared from Zamboni fixed adult mouse sciatic nerves (De Martino and Zamboni, 1967). Sciatic nerves were fixed for 15 min in Zamboni solution* and washed 2 times in PBS for 15 min. For the preparation a binocular microscope was used. Sciatic nerves were put in a drop of dH_2O for preparation to avoid dehydration and cut into 1-2 mm pieces with razorbills. Connective was removed with sharp needles, bundled axons were separated with forceps and placed on gelatine chromalaun coated slides. The teased fiber samples were dried at 37 °C for 1 h and stored at –20 °C. Teased fibers were postfixed and permeabilized in –20 °C acetone for 10 min, blocked at RT for at least 1 h in PBS containing 4% normal goat serum, 1% Glycine, 3% Triton X-100 and incubated with primary antibodies for 48 h at 4°C. Slides were washed in PBS for 15 min, incubated with fluorochrome labeled antibodies for 30 min, washed with PBS (15 min), rinsed with dH_2O and embedded with FluorSaveTM.

Zamboni solution:* 4 g paraformaldehyde (Fluka) were solved in 30 ml Picric acid (Merck) at 60 °C for 1 h. 3-5 drops of 2.5% NaOH were added until the solution was clear. The solution was cooled on ice, filtered and filled up to 200 ml with Soerenson phosphate buffer. The Zamboni solution can be stored at 4 °C up to 3 days.

***Soerenson phosphate buffer:* 100ml Soerenson phosphate buffer contain 80.4 ml 0.4 M $Na_2HPO_4*2H_2O$, 19.6 ml 0.4M KH_2PO_4 and 138.6 mg glucose pH 7.4.

Culturing and staining of DRG explants

The DRG explant cultures were prepared as described by Kleitman et al. (Kleitman et al., 1998). Embryos were sacrificed at embryonic day 13-13.5 (Time mating procedure is described below). For the dissection and preparation a binocular microscope was used. Embryos were put into L15 medium (pH7.2-7.4, Sigma) for dissection. Embryos were decapitated and the vertebral column and costal arch was laid open. From the ventral side, vertebrae were opened and removed from the spinal cord. The DRGs were collected in an FBS coated 15 ml tube containing 1 ml MEM/10

% FBS (MEM Gibco 31095-029, fetal horse serum Gibco). For dissociation DRGs were centrifuged at 300 g for 5 min, resuspended in 1 ml 0.25% Trypsin-EDTA (Gibco) and incubated at 37 °C, 5% CO_2 for 45 min. Trypsin was inactivated with 3ml MEM/10% FBS. Then the DRGs were centrifuged at 300 g, 5 min and resuspended 600 µl MEM/ 10% FBS/ 10 ng/ml NGF (nerve growth factor Sigma N-1408) and triturated with FBS coated Pasteur pipettes. 150 µl were given on poly-L-lysine/collagen coated glass coverslips (Carenini et al., 1998). The DRGs were cultured at 37 °C, 5% CO_2. After 48 h, 600 µl MEM/ 10% FBS, 10 ng/ml NGF were added. Medium was exchanged every 3-4 days. After one week, 50 µg/ml ascorbic acid (Sigma A-4403) were added to the medium to induce myelination. After 4 to 5 weeks of culturing, DRGs were used for immunohistochemistry. Slides were washed twice in PBS (10 min), fixed with 4% paraformaldehyd for 15 min and washed 3x with PBS (15 min). For permeabilization, slides were incubated with methanol (-20°C) (7 min for Caspr, 15 min for MBP staining). After premeabilization, slides were washed twice (10 min) in PBS and blocked in with 5% bovine serum albumin (Fluka), 1% goat serum and 0.2% Triton-X for 1 hour. Primary antibodies were incubated overnight at 4 °C. After incubation with the primary antibodies, slides were washed 3 times in 0.2% Triton-X PBS (15 min) and incubated with secondary fluorochrome-labeled antibodies. After 3 washing steps in 0.2% Triton-X PBS (15 min), slides were incubated with Hoechst (1:100 in PBS) for 5 min and washed in dH_2O prior embedding with Mowiol.

Mouse breeding: One male and one female mouse were kept in a cage separated by a partition for 48 h. After 48 h the partition was removed for one night. The day after, females were examined for plaques early in the morning. The day of plaque examination corresponded to embryonic day 0 (E0).

Primary antibodies: anti-MBP (polyclonal, 1:2000; kindly provided by Dr. J.-M. Matthieu), anti-L-MAG (polyclonal, 1:500; (Erb et al., 2003)), anti-MAG (monoclonal, recognizing both isoforms, 1:500, Boehringer Mannheim clone 513), anti-MAL (polyclonal, 1:200; (Schaeren-Wiemers et al., 2004)), anti-PMP22 (polyclonal, 1:2000; kindly provided by Dr. U. Suter, ETH-Hönggerberg, Zürich, Switzerland), anti-GFP (polyclonal, 1:2000; kindly provided by Dr. A. Matus, FMI, Basel, Switzerland), anti-Caspr (polyclonal, 1:1000; kindly provided by Dr. E. Peles, Weizmann Institute of Science, Rehovot, Israel), anti-Connexin29 (polyclonal, 1:2000; Zymed), anti-neurofilament medium chain (polyclonal, 1:2000; Biomol Int.).

Secondary antibodies: goat anti-rabbit IgG-Cy3 1:500, Jackson Laboratories; goat anti-mouse IgG-Cy5, 1:250, Jackson Laboratories.

Light microscopy

Confocal fluorescence microscopy was performed on an inverted scanning confocal microscope (LSM 510; Carl Zeiss MicroImaging, Inc.). For 3D reconstructions, data was processed with Imaris software (Bitplane, Zürich, Switzerland). Transmission microscopy was performed on a DMRE Leica microscope.

3.6 Electron microscopy

Buffers and solutions for EM embedding

0.2 M Cacodylate buffer: 42.8 g Sodium cacodylate trihydrate (Fluka) were solved in 800 ml dH_2O. The pH was adjusted to 7.4 with 1N HCl and 200 ml dH_2O were added. The solution can be stored at 4 °C for several of months.

2% Glutaraldehyde in Cacodylate buffer: 8 ml Glutaraldehyde solution (25%) (Fluka), 46 ml 0.2 M Cacodylate buffer pH7.4 and 46 ml dH_2O. Solution can be stored up to 2 months at 4 °C.

Karnovsky solution: 3 g paraformaldyde were solved in 50 ml dH_2O at 60-80 °C for 1 hour and 1-2 drops 1 N NaOH were added. The solution was cooled on ice, filtrated and mixed with 12 ml Glutaraldehyde solution (25%) and 38 ml 0.2 M Cacodylate buffer. Karnovsky solution cannot be stored.

EM wash buffer: 500 ml EM wash buffer contain 2.5 g NaCl, 250 ml 0.2 M Cacodylate buffer and 250 ml dH_2O.

3% Kaliumferrocyanid II: Kaliumhexacyanoferrat (Merck) in 0.2 M Cacodylate buffer. Solution can be stored at 4 °C.

EPON solution: 49 ml glycide-ether 100 (Merck), 16.7 ml DDSA (Dodecenylsuccinic anhydride, Fluka) and 34.3 ml MNA (Methylnorbornene-2, 3-dicarboxylic acid, Fluka) were mixed and 2 ml DMP-30 (2,4,6-Tris(dimethylaminomethyl)phenol, Fluka) were added to catalyze polymerization.

Embedding of sciatic nerves

Tissue was taken from perfused animals (Karnovsky solution at RT for 20 min), incubated for 3 h in Karnovsky solution and transferred in 2% Glutaraldehyde in Cacodylate buffer. Postfixation with osmium tetroxide, dehydration, and EPON embedding were performed as described before (Bartsch et al., 1995). Prior postfixation, tissue was washed 3 times (30, 30, 50 min) in EM wash buffer at 4 °C. For postfixation, tissue was incubated for 3 h in 1% OsO_4, 1.5% KFC, at 4 °C, washed twice (30 and 60 min) in EM wash buffer at 4 °C and stored in EM wash buffer overnight (18 h) at 4 °C. For dehydration tissue was incubated for 20 min (5, 5, 10 min) in 70% ethanol at 4 °C, 15 min (5, 10 min) in 80% at 4°C, 15 min (5, 10 min) in 96% ethanol at RT and 60 min (20, 20, 20 min) in absolute ethanol at RT. Then tissue was incubated in propylenoxid (Fluka) for 60 min (10, 20, 30 min) at RT, in a propylenoxid-Epon solution mixture (1:1) for 90 min at RT (Epon, Fluka) and for 21 h in propylenoxid-Epon solution mixture (1:3) at RT. Then tissue was transferred to Epon solution. For prepolymerization, tissue was incubated at 37 °C for 2 h and for 24 h at 45 °C. For polymerization tissue was incubated 80 h at 65 °C.

Staining ultrathin sections of sciatic nerves

Ultrathin sections (70-80 nm) of the embedded tissue on 150 mesh grids were contrasted by Uranyl-acetate (Fluka) and Pb-citrate (1.33 g $Pb(Na_3)$ (Merck) in 15 ml dH_2O, 1.76 g $Na_3C_6H_5O_2$*$2H_2O$ (Merck) in 15 ml dH_2O , 8 ml 1N NaOH). For this, meshs were incubated for 45 min with Uranyl-acetate kept in the darkness and washed 4 times with water. Then they were incubated with Pb-citrate for 6 min in a N_2 chamber and washed 4 times with water. Sections were imaged with a transmission electron microscope (Morgani 268D; Philips) with a magnification of 7100x.

4 Results

4.1 Generation and validation of the S-MAG-GFP mouse line

To generate transgenic mice expressing the S-MAG isoform tagged as a GFP fusion protein, we used the *pmag*-MAG-e12GFP genomic expression construct (Erb et al., 2003). This construct allows correct regulation of the GFP-tagged S-MAG isoform, since it is driven by the mouse MAG promoter and controlled by alternative splicing of all introns and exons. The GFP-sequence was inserted in front of the stop codon within the S-MAG specific exon 12 (Figure 1A), leading

to a GFP-S-MAG fusion protein with GFP fused to the intracellular and isoform specific C-terminus of S-MAG (Figure 1E). The single founder animal has given spontaneously rise to two separate and stable lines of high (~33) and low (~8) transgene copy numbers. All data presented here are from the high copy number line. We amplified the exon 12 region of the MAG mRNA from wild type and transgenic sciatic nerve and brain by RT-PCR using a single oligonucleotide pair. The S-MAG-GFP mRNA was present in transgenic brain and sciatic nerve samples (Figure 1B). The S-MAG-GFP encoding mRNA runs at the expected position, showing the correct joining of the modified exon 12 to its flanking exons 11 and 13. The endogenous L- and S-MAG mRNAs levels in transgenic samples are unaltered when compared to the ones from wild type samples.

On the protein level, the fusion of GFP (27 kDa) to the glycosylated S-MAG (105 kDa) leads to a molecular weight of about 130 kDa. This is visualized as a second band running above wild type L- and S-MAG in the Western blot analysis of adult brain and sciatic nerve myelin (Figure 1C). Analysis of these myelin samples on a high percentage SDS-Page revealed low molecular MAG bands of about 12, 15 and 40 kDa (Figure 1D). The 12 and 15 kDa bands correspond to the endogenous membrane-associated-intracellular C-terminal domain of S- and L-MAG (S-MAG^{CT} and L-MAG^{CT}), respectively, that result after cleavage of the extracellular domain of MAG (soluble MAG also called dMAG, Figure 1E; (Moller, 1996; Stebbins et al., 1998; Paivalainen et al., 2003). In the brain, both fragments of 12 and 15 kDa corresponding to both isoforms could be detected with the anti-MAG antibody, whereas in sciatic nerve samples only the 12kDa fragment of S-MAG could be detected (Figure 1D). Analysis with the anti-L-MAG specific antiserum did only detect the 15 kDa fragment in the CNS, but not in the PNS (Figure 1D), indicating that L-MAG is not expressed in adult peripheral myelin of mice. The 40 kDa fragment was only detected in the transgenic brain and sciatic nerve myelin samples, representing the cleaved S-MAG-GFP fragment, which consists of the 12k Da of wild type S-MAG and the 27 kDa GFP (Figure 1E). This 40 kDa product was also recognized by the anti-GFP antibody (data not shown). From our data, we conclude that the proteolytic formation of intracellular MAG fragments may be a regular process *in vivo* as myelin was isolated in the presence of protease inhibitors, always kept at 4 °C and loaded without prior incubation. The proteolytic cleavage of S-MAG seems to be more pronounced in the PNS, since the relative amount of S-MAG^{CT} is much higher compared to CNS (Figure 1D).

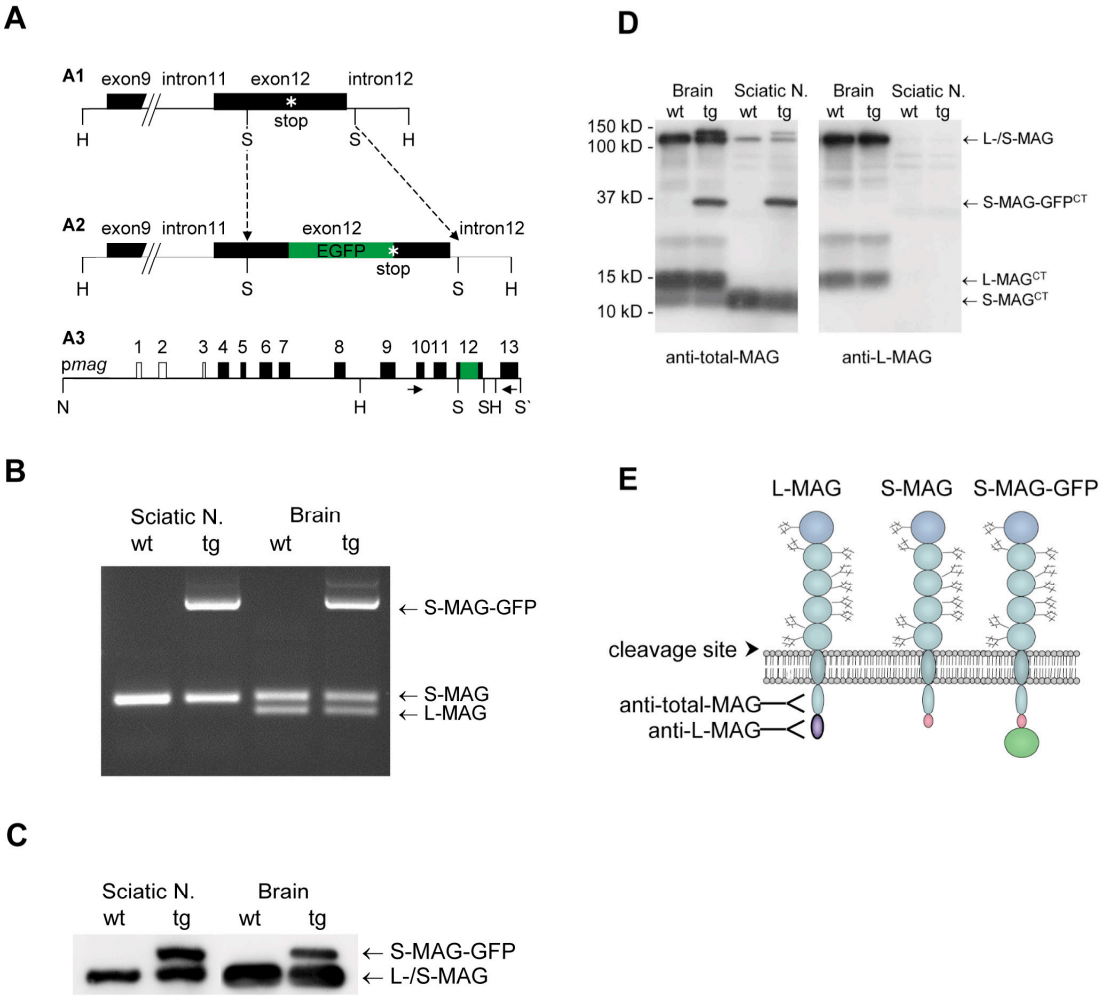

Figure 1 Gene targeting and validation of the S-MAG-GFP mouse line. (A) Cloning strategy: the EGFP sequence was inserted in front of the stop codon within the S-MAG C-terminus encoding exon 12. The exon 12/intron 12 junction is flanked by two SmaI sites (A1). This fragment was replaced by an identical sequence containing the EGFP in front of the exon 12 stop codon (A2). The resulting mouse MAG gene clone (20 kb) contains all exons and introns and 1.8 kb of the MAG promoter (p*mag*; A3). (B) The PCR amplification of the mouse MAG mRNA region spanning exon 10 to 13 from 1-month-old wild type and transgenic brain and sciatic nerve, produces a 184 bp product for L-MAG and a 229 bp for S-MAG, beside the 949 bp product for S-MAG-GFP mRNA (229 bp of S-MAG + 720 bp of EGFP = 949 bp). The insertion of the GFP encoding DNA seems not to affect the splicing process since no unexpected PCR product can be detected. (C) Western blot analysis of 1-month-old brain and sciatic nerve myelin membranes using a 8% SDS-PAGE revealed the S-MAG-GFP fusion protein of around 130-140 kDa above the endogenous L-/S-MAG of around 110kDa. (D) Western blot analysis of myelin preparations of 1-month-old brain and sciatic nerve wild type and transgenic animals using a 15% SDS-PAGE revealed the presence of the 12 and 15 kDa endogenous and 40 kDa transgenic C-terminal MAG fragments. In C and D, 1 µg of CNS and 5 µg of PNS myelin protein were analyzed. Note: In C, the exposure time for PNS myelin was longer than for CNS. (E) A schematic representation of the MAG isoforms, their putative cleavage products and the corresponding antibodies.
White boxes: non-coding exons; black boxes: coding exons; green boxes: EGFP DNA sequence; pmag: MAG promoter H: HindIII; N: NotI; S: SmaI and S': SalI.

4.2 Expression of S-MAG-GFP does not interfere with endogenous L- and S-MAG mRNA expression levels

To determine, if the expression of the S-MAG-GFP transgene has an impact on the endogenous L- and S-MAG transcription and alternative splicing, we have analyzed the L-, S-MAG and S-MAG-GFP mRNA levels by quantitative RT-PCR. These three different MAG transcripts were amplified specifically from brain and sciatic nerve of wild type and transgenic mice at postnatal day four (P4) and at one month (1mo). At postnatal day 4, L-MAG was the predominant isoform in wild type and transgenic mice (Figure 2A). In the adult brain, S-MAG was expressed at comparable levels as L-MAG (Figure 2C). The S-MAG-GFP and the endogenous S-MAG mRNA showed an analogous expression pattern during development (Figure 2A) and in the adult (Figure 2C). In sciatic nerves of wild type and transgenic mice, S-MAG and S-MAG-GFP were the dominant isoform already at postnatal day 4 (Figure 2B), whereas only very low L-MAG expression levels were detected at that stage. In the adult, endogenous S-MAG expression was comparable in wild type and transgenic animals (Figure 2D), whereas the transgenic expression of S-MAG-GFP was twice as much as the endogenous one. In contrast, L-MAG expression was not detectable in the adult mouse sciatic nerve (Figure 2D). In summary, the "additional" S-MAG-GFP mRNA expression did not affect the endogenous L- and S-MAG mRNA expression levels in the CNS and PNS during development and in the adult. In addition, we investigated the expression levels of the major myelin genes MBP, PLP/DM20 and P0 in parallel. None of them showed any alterations in transgenic CNS and PNS tissues (data not shown), demonstrating that transgenic S-MAG-GFP expression did not influence the expression pattern of the major myelin genes.

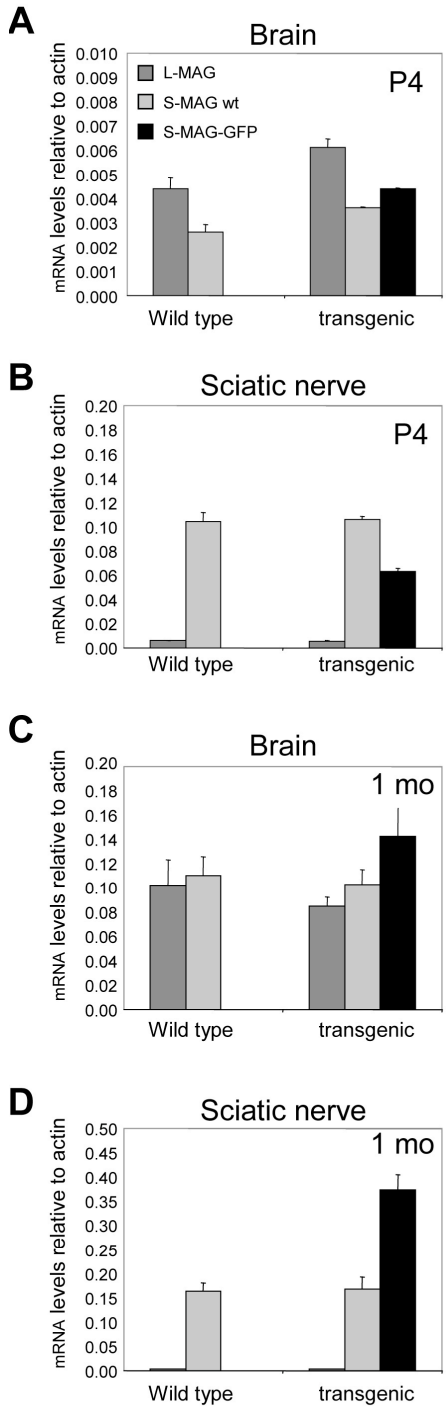

Figure 2 Quantitative analysis of the L- and S-MAG and S-MAG-GFP mRNA levels in CNS and PNS. RT-PCR analysis of the endogenous L-, S-MAG and S-MAG-GFP mRNA levels was performed at postnatal day 4 (A and B, P4) and at 1-month-old (C and D, 1mo) for brain (A and C) and sciatic nerve tissues (B and D). The mRNA levels were normalized to the actin mRNA levels. In the CNS, the levels of the S-MAG-GFP mRNA are comparable to the wild type S-MAG mRNA levels, at P4 and 1mo. In the PNS, the S-MAG mRNA levels are increased by the presence of the transgene to about 60% at P4 and 200% at 1-mo.

4.3 Comparable expression levels of endogenous L- and S-MAG protein in the CNS and PNS of transgenic and wild type animals

To determine whether the expression of additional S-MAG-GFP fusion protein influenced the endogenous expression of L- and S-MAG, we quantified L-, S-MAG and S-MAG-GFP protein levels by quantitative Western blot analysis, using an advanced infrared imaging system. Equal amounts of brain myelin from 1-month-old mice were analyzed in parallel using the anti-MAG antibody recognizing both isoforms (Figure 3A), or the anti-L-MAG specific antibody (Figure 3B). The signal intensities of both endogenous MAG isoforms did not reveal any significant difference between wild type and transgenic animals also when normalized with the one for CNPase. Similarly, quantitative analysis of endogenous S-MAG levels in PNS myelin membrane preparations showed that they were unaltered in transgenic compared to wild type mice (Figure 1D depicts one sample as an example). In parallel, we measured the relative amount of S-MAG-GFP compared to endogenous L- and S-MAG, which was 0.28 (± 0.03), indicating a surplus expression of about 30% S-MAG-GFP in brains of transgenic mice. In the PNS, the additional S-MAG-GFP expression in transgenic mice led to an overall surplus S-MAG synthesis of about 100% (1.10 ± 0.08).

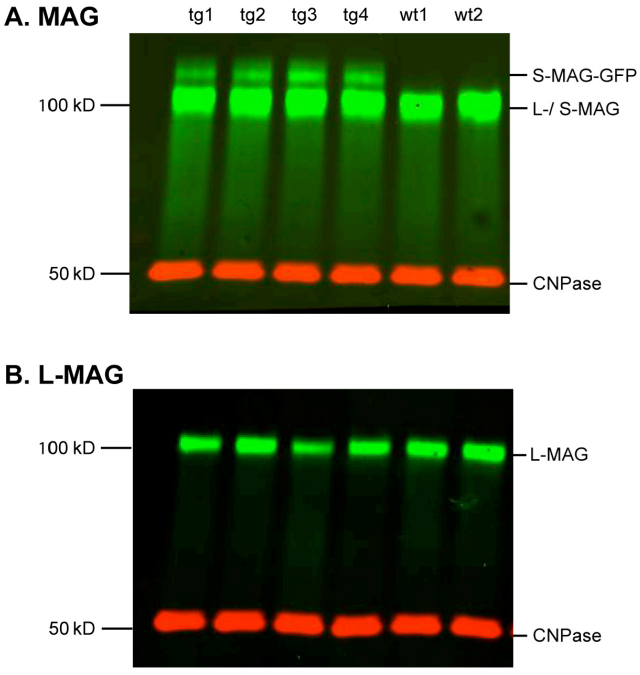

Figure 3 Quantification of L- and S-MAG protein levels in the CNS of wild type versus transgenic mice by infrared imaging system. The amounts of endogenous L-/S-MAG and S-MAG-GFP in brain myelin fractions of 1-month-old animals were measured. A/B Western blot analysis with an antibody recognizing both MAG isoforms (specific to a common intracellular domain) (A) and only L-MAG (B) was performed with myelin membrane preparations of brains from transgenic (4 are depicted as example) and wild type animals (2 are depicted as an example). The amount of CNPase protein served as equal loading control. The endogenous MAG expression in transgenic and wild type mice did not show any difference.

4.4 Differential expression pattern of L-and S-MAG during development

To investigate the developmental expression of the two MAG isoforms on a cellular level, we performed an immunohistochemical analysis on transversal spinal cord sections at different postnatal time points. The anti-MBP immunostaining indicated that the extent of myelination in transgenic and wild type mice (Figure 4A, inset) was comparable. In the CNS, at postnatal day 4 (P4), L-MAG is already strongly expressed, both in the ventral and the dorsal funiculi (Fig 4B, arrowheads), whereas S-MAG is only detectable in a small number of fibers in the ventral funiculus (Figure 4C, arrowhead). The L-MAG expression followed by the expression of S-MAG is also visualized on sagittal brainstem sections, where L-MAG is detected in oligodendrocyte cell bodies at P4 (Figure 4H, arrows), and in their processes at P8 (Fig 4I, arrowheads), whereas S-MAG was detected around P8 mainly in cell bodies (Fig 4J, arrow). In the PNS, S-MAG is the predominant isoform and is already strongly expressed around birth. Figure 4G (arrow) depicts S-MAG in ventral roots at P4. L-MAG, in contrast, is only detectable in distal nerves such as whisker innervations and intercostal nerves (Figure 4F, lower panel, arrow) and could not be detected in spinal roots (Figure 4E, arrow) at any time point during development (P0, P2, P4, P10, data not shown). In a comparative study, we further analyzed the expression pattern of several myelin proteins in transgenic and wild type mice by immunohistochemistry. We found a comparable MBP (Figure 4A), MAL, MOG, PO and Periaxin expression pattern in transgenic and wild type mice suggesting that the elevated S-MAG (S-MAG and S-MAG-GFP) levels did not lead to alterations in myelin protein expression pattern (data not shown).

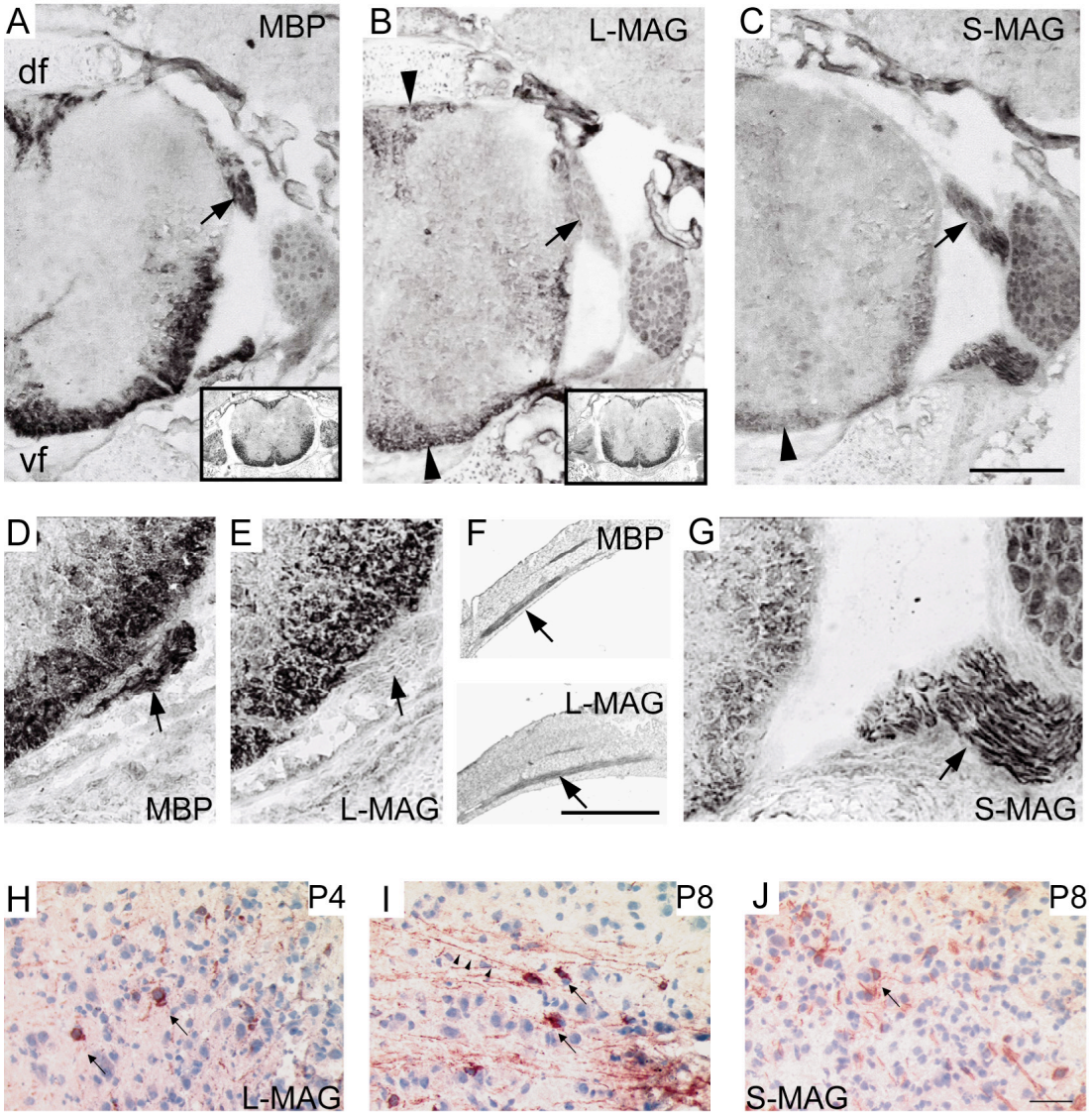

Figure 4 Developmental expression pattern of L- and S-MAG
Immunohistochemical analysis was performed on transversal spinal cord sections of transgenic animals at postnatal day 4 (A-H) and 8 (I, J) for MBP (A, D, F upper panel), L-MAG (B, E, F lower panel, H and I) and for S-MAG-GFP (C, G, J). Insets in A and B show the expression pattern in littermate wild type animals. In the spinal cord at P4 myelination is seen in dorsal and ventral funiculus as detected by MBP (A) and shows a comparable pattern for L-MAG (B, arrowheads). However, S-MAG-GFP expression is only detected in the ventral funiculus (C, arrowhead). In the spinal roots myelination is also depicted by the strong expression of MBP (A and D, arrows) and S-MAG-GFP (C and G, arrows), but L-MAG was absent (E, arrow). Still, some L-MAG positive fibers could be detected in the intercostal nerves (F, upper panel), which were also MBP positive (F, lower panel). H-J: Immunohistochemical analysis of sagittal brainstem section of a transgenic mouse for L-MAG at P4 (H) and P8 (I) and for S-MAG-GFP at P8 (J), which were counter, stained with Haemalaun (blue). Note, at P4 L-MAG is mainly expressed in oligodendrocyte cell bodies (H, arrows), whereas at P8 strong expression in oligodendrocyte processes could be detected (I, arrowheads). In contrast, S-MAG-GFP expression could be detected around P8, where it is mainly localized in the oligodendrocyte cell bodies (arrow). Abbreviation: df, dorsal funiculus; vf, ventral funiculus; DRG, dorsal root ganglion. Bars: A, B, C: 250 μm; F: 500 μm; H, I, J: 50 μm.

4.5 Subcellular distribution of S-MAG in teased sciatic nerve fibers

S-MAG-GFP is localized in Schmidt-Lanterman incisures (Figure 5A and B, arrow) and periaxonal membranes (Figure 5A and B, arrowheads) indicating a correct subcellular distribution of the GFP-tagged MAG fusion protein. The S-MAG-GFP-autofluorescence signal is bright and clear (Figure 5A, left panel) and is indistinguishable from an anti-GFP staining (Figure 5B, middle panel). It was striking that the signal intensity of the periaxonal S-MAG-GFP in different fibers varied strongly. Indeed, sciatic nerve cross sections revealed strong autofluorescence predominantly in small caliber fibers (Figure 5C, arrowhead), whereas the autofluorescent signal in large caliber fibers was weaker, in some cases not even detectable (Figure 5C, arrow). Immunohistochemical analysis revealed an analogous expression pattern of endogenous MAG in wild type mice (Figure 5 D).

In teased fibers, we observed frequently different ring- or disc-like structures where S-MAG-GFP was accumulated. We observed periaxonal rings (Figure 6A, arrows), and rings surrounding myelin sheath lamellae, probably within the abaxonal membrane (Figure 6A, arrowhead). Another abundant ring-like structure appears as disc spanning perpendicular the whole compact myelin sheath (Figure 6B, left panel, arrow; right panel 3D reconstruction). In search of an ultrastructural correlate, we encountered zigzag shaped uncompacted incisures that might reflect the discs seen at light microscopy (Figure 6C1, 6C2). Figure 6C3 depicts a "classical" Schmidt-Lanterman incisure transversely through the myelin sheath in a funnel like fashion.

A colocalization study of MAG and the gap junction protein connexin 29 (Cx29), revealed a nearly congruent expression pattern of both molecules not only in Schmidt-Lanterman incisures, but also in the adaxonal membranes, and paranodal loops (Figure 6D, arrowheads). However, while connexin 29 was strongly accumulated in both, the para- and juxtaparanodal region, S-MAG-GFP was clearly concentrated at the paranodal and much less abundant in the juxtaparanodal region of adult peripheral nerve fibers (Figure 6E, arrow).

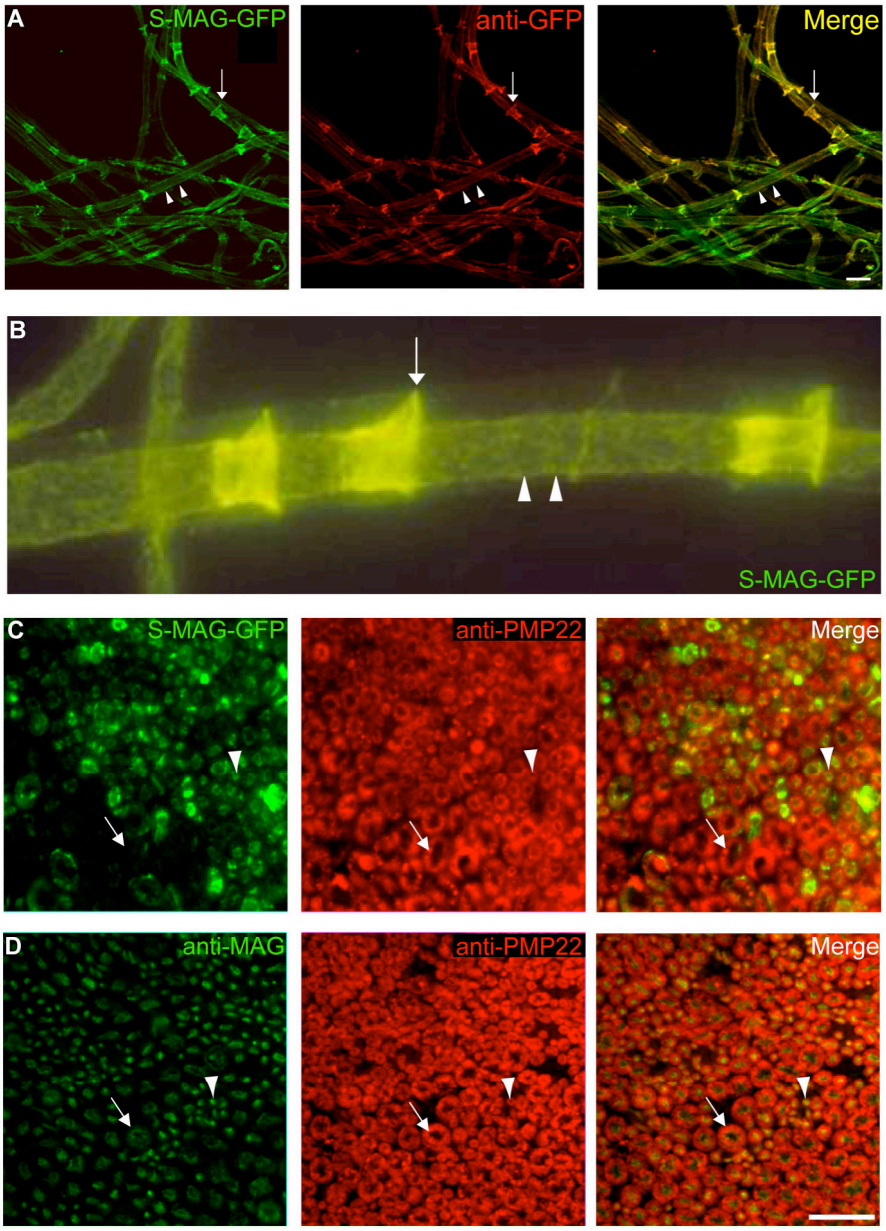

Figure 5 Localization of S-MAG-GFP autofluorescence peripheral nerve fibers
Colocalization study was performed on teased sciatic nerve fiber preparations (A) of 3-months-old transgenic animals. S-MAG-GFP autofluorescence is shown in the left panels (green) and the anti-GFP immunofluorescence in the middle panels (blue). The merged images (right panels) indicate the overlapping expression. Note, that the distribution of the immunofluorescent signal of the GFP-autofluorescence is comparable with the one of the anti-GFP-immunofluorescence. Schmidt-Lanterman incisures (arrow), periaxonal membranes (arrowheads) B: High magnification of S-MAG-GFP autofluorescence in Schmidt-Lanterman incisures (arrow) and in periaxonal membranes (arrowheads). C: S-MAG-GFP autofluorescence (green) and anti-MAL immunofluorescence (red, compact myelin) on sciatic nerve cross section of a transgenic animal. D: anti-MAG (green) and anti-PMP22 (red, compact myelin) immunofluorescence on sciatic nerve cross sections from a wild type mouse. Note, that MAG is mainly present in the small myelinated fibers (arrowhead) and weakly expressed in the large caliber fibers (arrow). Bars: (A) 20 μm, (C, D) 25 μm.

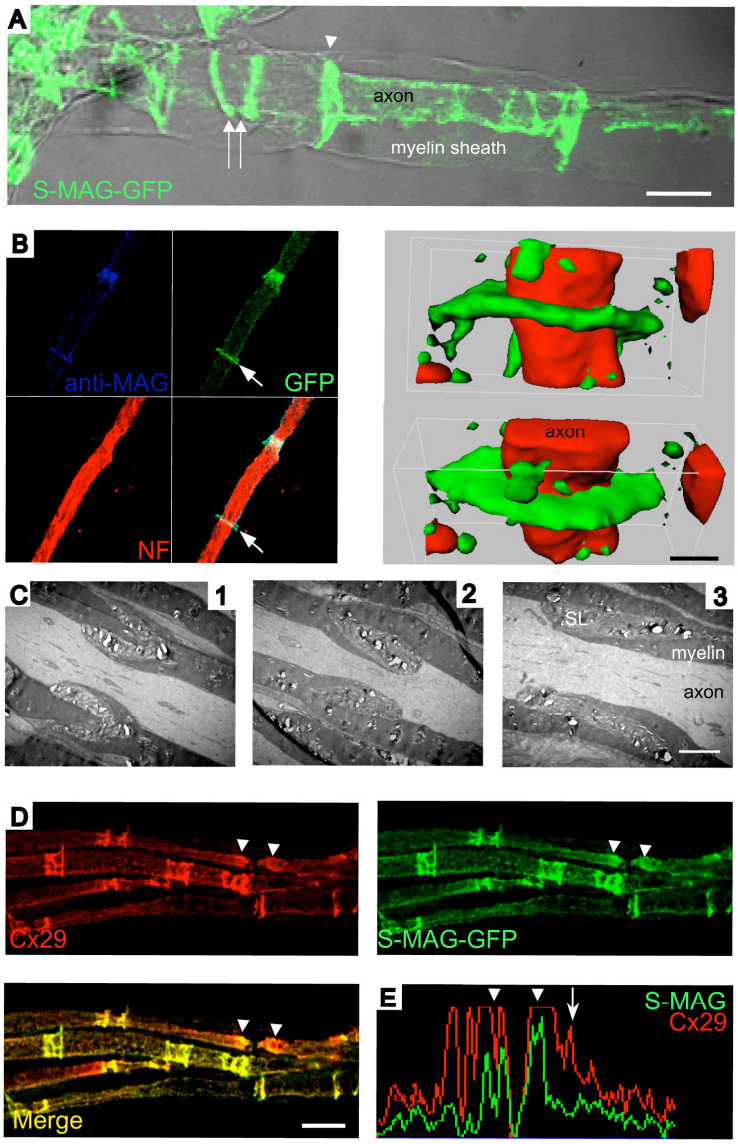

Figure 6 S-MAG-GFP localization in peripheral nerves
Confocal microscopy was performed on teased sciatic nerve fiber preparations of adult animals. (A) S-MAG was detected in ring-like structures adjacent to the axon (arrows) and in discs perpendicular to the axon (arrowhead). (B) An example for a disc-like structure spanning through the myelin sheath (arrow) and "classical" Schmidt-Lanterman incisures is shown (red, neurofilament, axon; green, S-MAG-GFP autofluorescence; blue, anti-MAG). Right panel: 3D reconstruction of the disc (B, arrow) together with the neurofilament staining. The upper panel shows a projection parallel to the axon and perpendicular to the disc, whereas the lower panel shows the same some degrees turned to the front revealing that the disc spans the whole myelin sheath. (C) EM analysis of longitudinal sciatic nerves of 6-month-old mice. Note, the occurrence of zigzag shaped incisures (C1) and incisures spanning half of the myelin sheath (C2). C3: classical Schmidt-Lanterman incisure with its funnel-shaped structure. (D) Immunofluorescent colocalization study for connexin 29 (Cx29) and S-MAG-GFP autofluorescence demonstrating the strong overlapping expression pattern (merge). (E) Intensity profile through the node of Ranvier (D, arrowhead) showing the strong accumulation of Cx29 and S-MAG-GFP in the paranodes (arrowhead). In contrast, in the juxtaparanodal region (arrow) only Cx29 could be detected. Bars: A: 10 µm; B: 3 µm; C: 2 µm; D: 20 µm.

4.6 Differential L- and S-MAG expression in the brain

We analyzed the differential expression of L-and S-MAG in the adult brain. Overall analysis of brainstem, cerebellum, midbrain and optic nerve showed an overlapping expression pattern of both isoforms (data not shown). In certain forebrain regions, however, we found a differential expression of L- and S-MAG. For instance, we detected strong S-MAG and MBP positive fibers in the dorsal fornix (Figure 7A, arrow), which showed very low L-MAG expression (Figure 7B, arrow). Also within the radiatum area of the corpus callosum, we detected strong S-MAG positive fiber tracts that were also MBP positive (Figure 7C, arrow), but the L-MAG signal in those fibers was only weak or even absent (Figure 7D, arrow). In contrast, fibers within the truncus of the corpus callosum showed relative high levels of L-MAG (Figure 7B, arrowhead), and other fiber tracts showed an even reciprocal L- and S-MAG expression (Figure 7E, arrow points to an S-MAG-GFP positive fiber tract). In areas of the striatum and the hippocampus, it was possible to discriminate fibers, which express both isoforms (Figure 7F, merge, yellow), fibers, which express only S-MAG-GFP (Figure 7F, arrow) or fibers, which express preferentially L-MAG (Figure 7F, arrowhead).

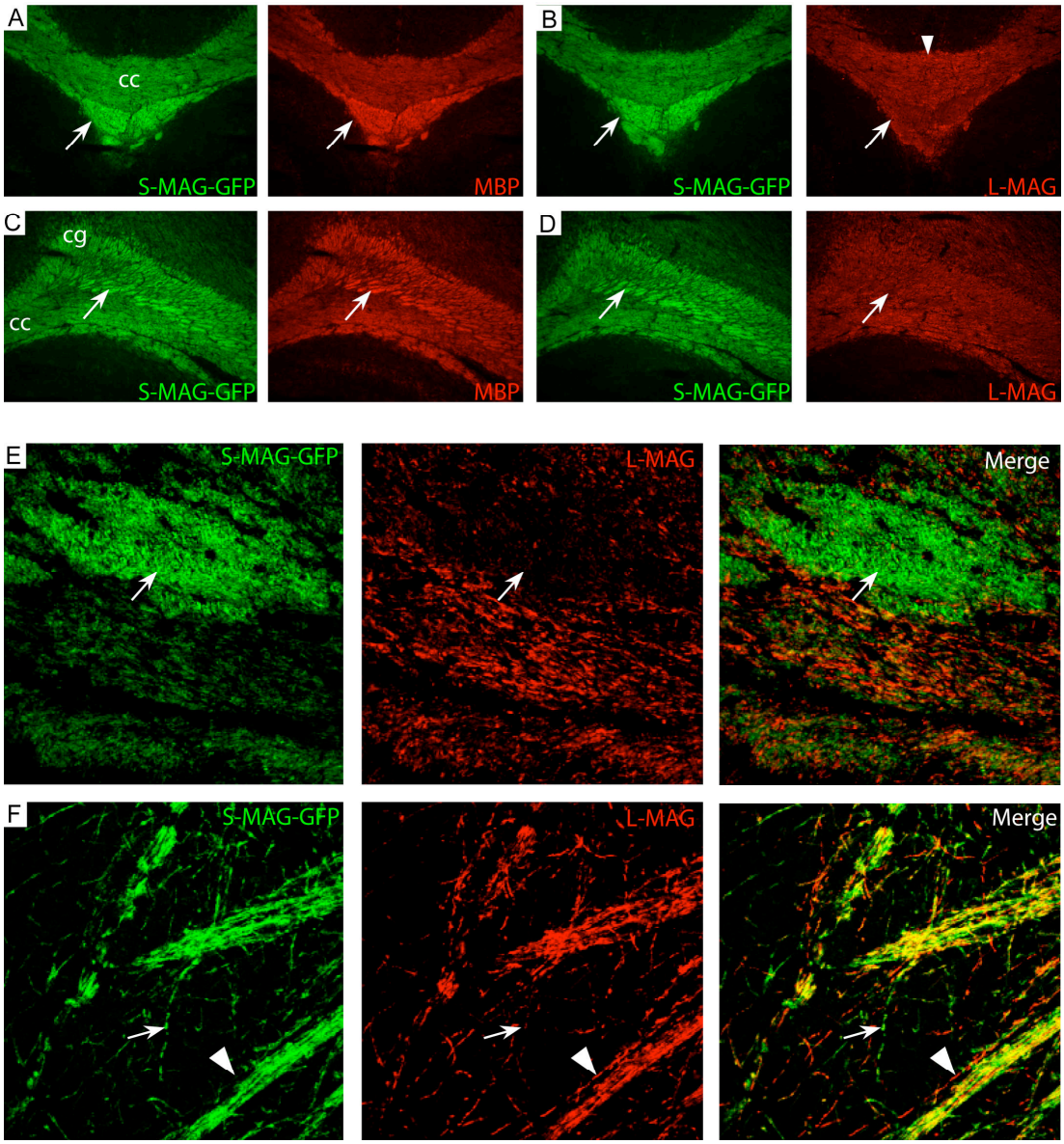

Figure 7 Differential expression of L- and S-MAG in the mouse forebrain
Colocalization studies were performed on horizontal brain sections of 3-months-old transgenic mice for S-MAG-GFP autofluorescence (green), MBP (A and C) and L-MAG (B, D, E and F). A, B: S-MAG-GFP autofluorescence in the area of the contralateral projections of the corpus callosum (cc) with the underlying dorsal fornix of both hemispheres (arrow) colocalized with MBP (A) and L-MAG (B). Note, the strong autofluorescence of S-MAG-GFP and MBP expression in the dorsal fornix, but weak expression of L-MAG. C, D, E: S-MAG-GFP autofluorescence in the adjacent area of the corpus callosum, the radiatum colocalized with MBP (C) and L-MAG (D, E). E: Confocal analysis of distinct fibers within the corpus callosum, which were strongly positive for S-MAG-GFP (arrow), but L-MAG negative, whereas others vice versa. F: Confocal analysis of myelinated fibers of the perforant pathway showing single S-MAG-GFP specific (arrow), L-MAG specific (arrowhead) and fibers expressing both (merge, yellow).

4.7 S-MAG accumulation in CNS paranodes

It is still unresolved whether MAG is localized in the paranodes of the CNS (Bartsch et al., 1989) since its localization by immunofluorescence analysis was difficult due to technical limitation. Therefore, we performed a confocal colocalization study on sagittal brain sections with the paranodal marker Caspr. Generally, we could detect S-MAG-GFP autofluorescent signal regularly in paranodes (Figure 8A1, A2, arrows), but the signal intensity was often relatively moderate. This was confirmed by analyzing intensity profiles through a particular nerve fiber, which revealed a colocalization of S-MAG-GFP autofluorescence and Caspr in the paranodes (Fig 8A1 and A2, lower panels, arrows). Yet, there were also paranodes in which S-MAG-GFP seemed not to be accumulated (Figure 8A3, see also intensity profile in the lower panel).

In contrast, in the PNS S-MAG-GFP accumulation was detected in all paranodes investigated (Figure 8B). Sciatic nerve teased fiber preparations of 6-months-old animals revealed in a 3D reconstruction an extended S-MAG-GFP immunofluorescent signal beyond the periaxonal region (Figure 8B, arrow) supporting the idea that MAG is expressed between the paranodal loops. Interestingly, S-MAG-GFP colocalized with Caspr throughout the paranode except for the edge next to the node (Figure 8B, arrowhead). This feature has also been observed in an early stage of myelination as depicted in *in vitro* myelinating DRG cocultures (Figure 8C, arrowhead). In these cultures it became evident that S-MAG is strongly accumulated in the paranodal loops during myelin formation (Figure 8D, arrow) and went in parallel to Caspr cluster formation (data not shown).

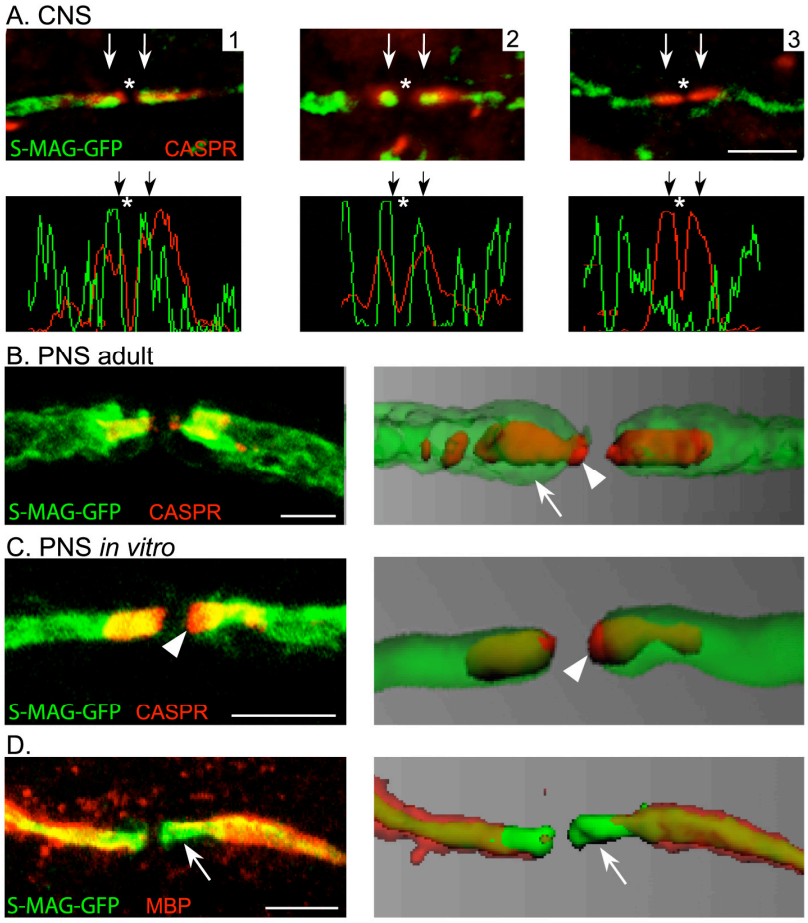

Figure 8 S-MAG expression paranodal loops in the CNS and PNS
A confocal analysis of different Nodes of Ranvier in sagittal brain sections and teased sciatic nerve fiber preparations of 4-months-old transgenic mice with the paranodal marker Caspr was performed. A: A series of Nodes of Ranvier (asterisk) in the hippocampal area are shown as examples (upper panels). Intensity profiles in the lower panels demonstrate colocalization of S-MAG-GFP autofluorescence with Caspr in the paranodes (A1 and A2, arrows). However, there are also paranodes where S-MAG-GFP could not be detected (A3, arrow). B: S-MAG-GFP autofluorescence in teased sciatic nerve fibers. Right panel shows a 3D-reconstruction of the S-MAG-GFP accumulation in the paranodal loops (arrow). C, D: Myelinated axon in DRG explant cocultures from a S-MAG-GFP mouse after 34 days in culture colocalized with Caspr (C, red), and after 48 days with MBP (D, red) delineating the compact myelin sheath from the paranodal region (arrow). Note, that S-MAG-GFP autofluorescence is strongly localized in the paranodes and in periaxonal membranes. Bar: A, B, C, D: 5 µm.

5 Discussion

In this study, we present a transgenic mouse line that expresses GFP-tagged S-MAG as a fusion protein allowing the visualization of particular myelin compartment by autofluorescence. A detailed molecular and cellular characterization during development and adult revealed that this mouse line is comparable to wild type animals in all aspects tested such as gross anatomy and myelinogenesis. This transgenic mouse line enabled us to analyze the differential expression pattern and subcellular distribution of L- and S-MAG using the autofluorescence signal of S-MAG-GFP together with an L-MAG specific antibody.

Almost complete absence of L-MAG in the mouse peripheral nervous system

Our analysis of the differential expression of L- and S-MAG in the mouse PNS revealed that S-MAG is the predominant isoform. Both, on the mRNA levels as well as on the immunohistochemical level, we found only traces of L-MAG during development, and in the adult L-MAG was not detectable at all. Early during development L-MAG was only detected in a subset of distal nerve fibers such as intercostal nerves and nerves innervating whiskers, but not in proximal nerves such as spinal roots. The absence of L-MAG in the mouse PNS is in contrast to the observation in humans (Miescher et al., 1997), and is comparable to studies in the rat, where L-MAG could not be detected as well (Tropak et al., 1988; Noronha et al., 1989). Yet, *in vitro* myelinating co-cultures of rat Schwann cells with purified sensory neurons revealed that L-MAG could be transiently detected in nascent internodes (Owens et al., 1990a), which supports our observation of L-MAG in a subset of internodes during early development. The negligible L-MAG levels in the mouse PNS may explain the missing PNS phenotype of mice expressing truncated L-MAG (Fujita et al., 1998) suggesting that L-MAG may not play a fundamental role in PNS myelin. The functional role and significance of the transient and particular L-MAG expression in mouse PNS myelinogenesis remains still elusive and needs further investigation.

Strong heterogeneity of S-MAG expression in PNS myelin sheaths

In peripheral nerves, we observed that periaxonal expression of S-MAG was predominantly in small caliber fibers. Large myelinated fibers often show little and irregular periaxonal S-MAG expression. This finding might explain that the reduced axon calibers found in MAG-deficient mice did not have an affect on all fibers (Yin et al., 1998).

Beside the well-described localization of S-MAG in the adaxonal membrane, Schmidt-Lanterman incisures and paranodes, we found S-MAG localized in ring- and disk-like structures including the outer- and/or innermost myelin lamellae. We have summarized our observation about the localization of S-MAG in the different compartments of the peripheral myelin sheath in a schematic drawing (Figure 9A and B) and endeavored to associate the known MAG binding partners within the different myelin compartments. The scheme depicts a peripheral myelin sheath made by a Schwann cell but includes also components primarily known from the CNS myelin. Periaxonal MAG possibly interacts with sialylated gangliosides, microtubule-associated protein 1B (MAP1B) and members of the NgR receptor family maintaining a close interaction of the Schwann cell and axon. *In vitro* studies have shown that MAG binds to certain glycan structures prominently expressed on GD1a and GT1b gangliosides (Yang et al., 1996b; Vinson et al., 2001a; Vyas and Schnaar, 2001), and as a signal transducing co-receptor the neurotrophin receptor p75 was implicated (Yamashita et al., 2002a). The MAG-MAP1B interaction has been proposed to be a structural link between the periaxonal membrane of the myelinating cell and the axonal cytoskeleton (Franzen et al., 2001). Nogo-66 receptor (NgR1) and the NgR1 related protein NgR2 possibly in association with p75 have been shown to interact with MAG (Wang et al., 2002b; Wong et al., 2002; Lauren et al., 2003; Venkatesh et al., 2005). Although the proteins of the NgR family are primarily known as an inhibitor of axonal regeneration, it will be interesting to investigate whether it might also interact with MAG under normal conditions stabilizing and maintaining the periaxonal interaction of the myelin sheath with the axon. In the paranodal loops and the Schmidt-Lanterman incisures MAG might stabilize the association of the outer myelin lamellae. The MAG-interacting components are not identified so far, but one possibility could be by homophilic interaction (trans-interaction, Figure 9B), which is supported by its self-adhesive properties (Poltorak et al., 1987; Almazan et al., 1992). We suggest that in the paranodal loops and in Schmidt-Lanterman incisures, the compacted extracellular space may require a parallel orientation of the five Ig-loops between the myelin lamellae (Figure 9B). One can imagine, for example, that two opposing MAG molecules could interact with each other, maybe in a similar fashion as protein zero (P0). Another possibility may be that the outer two Ig-like domains of MAG form a unit that folds back over the rest of the molecule as suggested by Attia and collaborators (Attia et al., 1993). The fact that there is no or only little widening of the extracellular space in uncompacted compartments is clearly illustrated by the EM micrograph (Figure 9C) and also implied by the fact that Connexin 29, a gap junction protein, co-localizes with MAG within these compartments (Figure 9B). Alternatively, one could imagine that gangliosides may be ligands for MAG between paranodal loops and in Schmidt-Lanterman incisures but this has not been

demonstrated yet. Within the uncompacted myelin compartments the intracellular domain of MAG can interact with particular components from the cytoskeleton such as tubulin the core component of the microtubular cytoskeleton (Figure 9B; (Kursula et al., 2001).

The disc or ring-like MAG positive structures observed in the myelin sheaths resemble the ones of E-cadherin and MUPP, two proteins known to be expressed in ring-like structures (Fannon et al., 1995; Poliak et al., 2002). These radial- and disk-like MAG structures could either represent funnel-shaped Schmidt-Lanterman incisures having MAG only expressed in a subdomain or they could represent incisures-related structures such as zigzag-orientated Schmidt-Lanterman incisures. The latter have been observed in our EM study and have been described by Robertson and collaborators as well (Robertson, 1958). The expression of MAG in these ring-like structures that include the outermost myelin lamellae, together with MAG expressed in the outer mesaxon, may represent the link of the myelin sheath with the overlying basal lamina, since MAG has been reported to interact with collagen, tenascin-R and fibronectin that are expressed in the Schwann cell basal lamina (for review see (Quarles, 2002).

L-MAG CNS expression pattern diverges from the pattern of S-MAG and MBP

In adult brain sections we found a differential expression pattern of L- and S-MAG in certain forebrain regions. S-MAG was the predominant isoform in distinct fiber bundles of the cingulum as well as in the dorsal fornix. The strong and comparable expression of S-MAG and MBP in the major myelinated fiber tracts suggests that S-MAG is mainly involved in myelin maintenance. L-MAG, in contrast, stays persistently upregulated in particular myelinated fibers of the corpus callosum, in the striatum as well as in the perforant pathway. The definite identity of these L-MAG positive fibers could not be elucidated yet and needs further investigations.

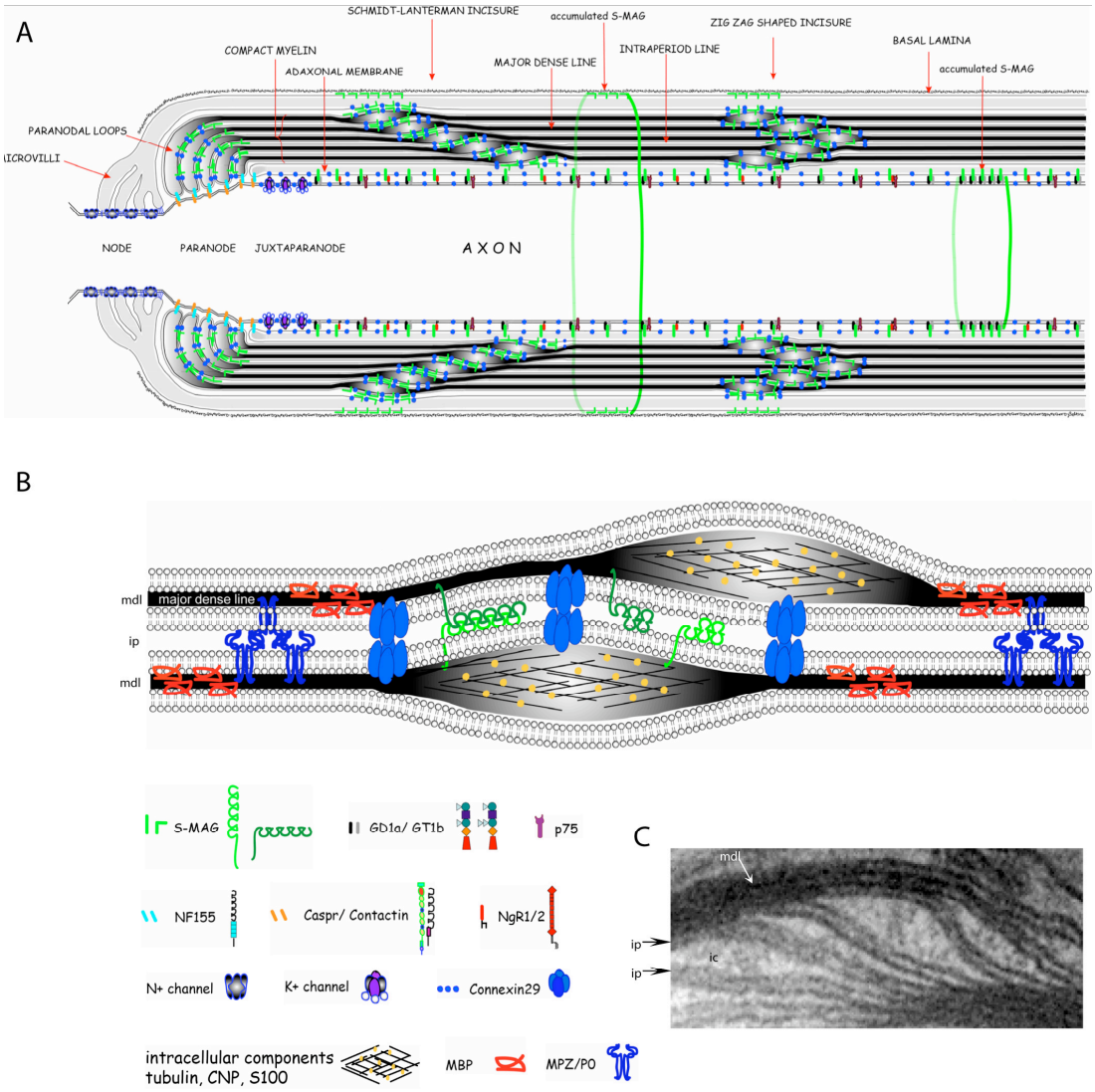

Figure 9 Schematic drawing of a typical peripheral myelin sheath with the described S-MAG-GFP localization in different myelin compartments. (A) S-MAG is localized in the periaxonal plasma membrane possibly interacting with its axonal binding partners GD1a and GT1b, NgR1/2 and p75. S-MAG is also present in non-compact compartments such as Schmidt-Lanterman incisures and paranodal loops where it could interact with itself or other partners on the opposite membrane. (B) Note that the opposing membranes in Schmidt-Lanterman incisures and paranodal loops remain in close contact in a comparable manner as for the intraperiode line in the compact myelin sheath indicated by the EM micrograph in C. Therefore, we suggest that the extracellular domain of MAG with its five Ig-like domains requires to be bent due to this spatial restriction. Zigzag shaped incisures might be a variant of the "classical" Schmidt Lanterman incisures as described by Robertson et al. (1958). The significance of the different ring-like structures around the axon and at the outside of the myelin sheath remains to be defined. Abbreviations: mdl, major dense line; ip, intraperiode line; ic, intracellular compartment of a Schmidt-Lanterman incisures.

S-MAG is expressed in the mouse CNS paranodal loops

There have been controversial statements from earlier Immuno-EM studies about MAG expression in CNS paranodes (Bartsch et al., 1989; Trapp et al., 1989). We found S-MAG-GFP accumulated in the paranodal loops quite frequently, which is in agreement with the study reported by Bartsch and colleagues (Bartsch et al., 1989). A possible functional role of MAG could be the stabilization of the paranodal loops through its self-adhesive properties in a trans-interaction manner (Poltorak et al., 1987; Almazan et al., 1992). This idea is supported by the observation of loosened paranodal loops in the CNS of MAG knock out and MAG/CGT double knockout mice (Marcus et al., 2002; Schaeren-Wiemers et al., 2004), and also in the MAL-deficient mice that showed a strong reduction of MAG (Marcus et al., 2002; Schaeren-Wiemers et al., 2004).

Conclusion

In summary, our data provide new insights in the subcellular distribution of the two MAG isoforms, which is fundamental for the understanding of their specific functions in myelin formation and maintenance. Our observations show that the S-MAG-GFP transgenic mouse is an excellent animal model since it bright autofluorescence allows also the examination of S-MAG expression and myelination per se in *in vitro* myelinating DRG cocultures (Figure 8C and D) as well as in cerebellar slice cultures (data not shown). Further, it will enable us in the future to examine the dynamic processes during the formation of Schmidt-Lanterman incisures or paranodal structures by time-lapse studies. This mouse line can also be bred with other mouse strains to study the functional role of MAG under particular pathophysiological conditions of the myelin sheath.

Early axonal pathology in a mouse model for CMT1A disease (Part II)

Bettina Flueck, Anna K. Stalder, Beat Erne, Jochen Kinter, Roland Lützelschwab, Andreas J. Steck and Nicole Schaeren-Wiemers

Neurobiology, Department of Research and Neurology, University Hospital Basel, Pharmacenter, Basel, Switzerland

The following section is based on the manuscript submitted in December 2006. The part "Materials and Methods" was extended.

1 Abstract

Neurofilaments are implicated in the determination of proper axonal diameter and thereby in the establishment and maintenance of correct nerve conductivity. Mice overexpressing human PMP22 (mouse line C22) have predominantly myelinated fibers with small calibers and a slowed nerve conduction velocity reflecting the pathology of CMT1A disease. Here, we describe the expression of the neurofilament heavy, medium and light chains in sciatic nerves of C22 mice. In these mice, we found a marked increase of neurofilament heavy chain (NF-H) relative to the medium and light chains in developing and adult sciatic nerves. In addition, the analysis of the neurofilament phosphorylation state showed that in C22 mice the majority of NF-H was not phosphorylated in contrast to wild type mice. In wild type animals, most of the phosphorylated NF-H was detected in the stationary pool of neurofilaments representing filamentous subunits, whereas the non-phosphorylated was mainly detected in the mobile pool consisting of monomeric subunits. In C22 mice, however, we detected non-phosphorylated NF-H in both, the stationary and mobile pool of neurofilaments. We suggest that high levels of non-phosphorylated NF-H especially in the stationary pool of neurofilaments might exert a destabilizing effect on the neurofilament network in C22 mice. As both, unbalanced stoichiometries and decreased phosphorylation of neurofilaments are associated with reduced axon calibers, we conclude that in CMT1A disease, they might be the underlying mechanisms that inhibit radial growth and lead ultimately to axonal atrophy.

2 Introduction

Charcot-Marie-Tooth disease (CMT) is the most frequent hereditary peripheral neuropathy. The CMT1A subtype affects about 75% of the patients (Skre, 1974). CMT1A is classified as demyelinating disease and caused by duplication of the DNA region encoding the peripheral myelin protein PMP22 or by a point-mutation within this gene (Roa et al., 1991; Patel et al., 1992; Suter et al., 1992). The overexpression of PMP22 has been described to disturb Schwann cell maturation and to cause metabolic perturbations (Magyar et al., 1996; Notterpek et al., 1999; Niemann et al., 2000; Fortun et al., 2006). Studies have shown that CMT1A leads to distal weakness, atrophy and sensory loss caused by length-dependent degeneration of motor and sensory axons (Krajewski et al., 2000). Demyelination precedes the occurrence of clinical symptoms that correlate with axonal degeneration (Bouche et al., 1983; Berciano et al., 1989; Nicholson, 1991; Garcia et al., 1998). For CMT1A patients, therapeutic approaches reducing PMP22 levels are discussed (Sereda et al., 2003; Passage et al., 2004).

In peripheral demyelinating neuropathies, abnormal Schwann cells are thought to induce axonal dysfunction. Evidence for this comes from transplantation experiments where allografts from Trembler-mice (point-mutation in PMP22) were used as bridges to connect the proximal and distal stumps of transected nerves from normal mice. Regenerating axons penetrating the allograft showed reduced calibers, higher neurofilament density, and a low phosphorylation state, alterations that were restored in the distal host-derived part of the nerve containing wild type Schwann cells (de Waegh et al., 1992).

The precise mechanisms by which abnormal Schwann cells exert adverse effects on axons, especially on neurofilaments, the major components of the axonal cytoskeleton, are not known. Neurofilaments are important for the establishment and maintenance of axonal calibers. They are polymers consisting of three intermediate filament proteins, NF-L, NF-M and NF-H (light, medium and heavy chain). The NF subunits are composed of a conserved helical core region, flanked by the head (N-terminus) and hypervariable tail (C-terminus) domains. The tail domains of NF-M and especially NF-H can be extensively phosphorylated. Neurofilament numbers, subunit stoichiometries and the phosphorylation of their tail domains have been suggested to specify axonal diameter (Ohara et al., 1993; Xu et al., 1996). One hypothesis is that myelination induces neurofilament tail phosphorylation leading to increased neurofilament spacing which is associated with an increase of axonal diameters (Starr et al., 1996). MAG, the myelin-associated-glycoprotein localized in the periaxonal membranes has been suggested to mediate phosphorylation of neurofilaments as in MAG knock out mice neurofilament spacing and phosphorylation state are decreased. (Sternberger et al., 1979; Yin et al., 1998). MAG has been suggested to regulate Cdk5 and ERK1/2 kinases that phosphorylate NF tail domains (Dashiell et al., 2002).

In this work, we investigated the developmental effect of dysmyelination on the axon in CMT1A animal model. For this we used the mouse line C22 that shows a dysmyelinating phenotype and closely reflects the pathology of human CMT1A disease (Huxley et al., 1996; Robaglia-Schlupp et al., 2002). We followed the establishment of the axonal cytoskeleton with focus on the neurofilament subunit composition and phosphorylation in C22 mice. We found early pathological alterations of the neurofilament subunit composition and phosphorylation and suggest that they may be responsible for reduced radial growth leading to the observed axonal atrophy in C22 mice. We also analyzed whether the expression of MAG, a potential regulator of axonal growth, may be altered in C22 mice and CMT1A patients.

3 Material and Methods (Part II)

3.1 Mouse model for CMT1A

The PMP22 overexpressing mice (line C22, kindly provided by Clare Huxley) carry 7 copies of the human PMP22 gene (YAC construct) resulting in a peripheral neuropathy closely reflecting the CMT1A pathology observed in humans (Huxley et al., 1996).

3.2 Electron microscopy

Sciatic nerves were fixed *in situ* with Karnovsky solution (3% paraformaldehyde, 3% glutaraldehyde, 0.1 M Cacodylate buffer) for 5 min (detailed protocol in Material and Methods Part I). For further fixation, tissue was incubated in Karnovsky solution for 3 h and stored in 2% glutaraldehyde. Postfixation with osmium tetroxide, dehydration and EPON embedding were performed as described before (Bartsch et al., 1995). Ultrathin sections of 70-80 nm were contrasted by Uranyl-acetate and Pb-Citrate. Sections were imaged with transmission electron microscope (Morgani 268 D; Philips) with a magnification of 2200x (Figure 1) or 4400x for the analysis of different nerve compartments.

Determination of the proportion of axonal compartment in sciatic nerves

Sampling strategy: Sciatic nerve cross sections on 150 mesh grids were used for analysis. 25 pictures were taken (on 5 random meshs 5 pictures each with 4400x magnification) and overlaid with 2 μm square grids. The compartments on 80 points of intersection were determined (myelin, axonal, extracellular compartments) for analysis.

Axonal diameters and myelin sheath thickness were calculated from the areas of myelinated fibers and axons (C22: n=296; wild type: n=195).

3.3 Western blotting

Tissue preparation for Western blot analysis

The quantification of myelin proteins was done with sciatic nerve myelin membrane preparations purified as described before. For the myelin preparation sciatic nerves of 8 animals were pooled (detailed protocol in Material and Methods Part I) (Schaeren-Wiemers et al., 2004).

For neurofilament Western blot analysis, one sciatic nerve pair was homogenized in 500µl 0.1M Tris-buffer containing the protease inhibitors PMSF (1 mM), Pepstatin A (1 µg/ml), Leupeptin (2 µg/ml), Aprotinin (0.5 µg/ml) and phosphatase inhibitors NaF, NaN_3, pNPP, NaPPi, β-Glycerophosphate (10 mM each). 5 µg protein were loaded for analysis. For the subfractionation and Triton-extraction, one sciatic nerve pair was homogenized in 1200 µl ice-cold 50 mM Tris (pH 7.5) buffer containing 1% Triton X-100, 25 mM KCl, 2 mM $MgCl_2$, 5 mM EGTA, protease and phosphatase inhibitors as described above. Homogenates were centrifuged at 43000 g for 90 min, the supernatant was collected and the pellet resuspended in 1200 µl buffer. 10 µl of supernatant and resuspended pellets were analyzed.

For Cdk5 Western blot analysis, one sciatic nerve pair was homogenized in 300 µl RIPA buffer containing 150 mM NaCl, 2 mM EDTA, 1% Nonidet P-40, 0.1% SDS, 50 mM NaF, protease inhibitors as described above, 20 mM Tris-HCl (pH 7.4), boiled at 95° C for 10 min and centrifuged for 30 min at 10000 g. Supernatants were collected, and 25 µg proteins were analyzed.

Myelin protein quantification

Myelin protein concentrations were determined by Bradford assay (detailed protocol in Material and Methods Part I). Protein concentrations of sciatic nerve homogenates for neurofilament and Cdk5 western blots were measured by BCA assay according to manufacturer protocol (Micro BCA Protein Assay Kit, Pierce). A BSA standard dilution series was prepared (5, 25, 50, 125 and 250 µg/ml). Protein homogenates were diluted 1:10 or 1:100. 20 µl of the diluted samples and 200 µl BCA reagent were mixed and incubated at 37 °C for 1 h. The absorbance at 562 nm was measured and protein concentrations calculated.

SDS-PAGE/ Western blotting

Western blotting of myelin proteins was performed as described before (detailed protocol in Material and Methods Part I; Schaeren-Wiemers et al., 2004). Neurofilaments analysis was performed on 3-8% NuPAGE Novex Tris-acetate gels (Invitrogen) under non-reducing conditions. Samples were mixed with LDS sample buffer (106 mM Tris HCl, 141 mM Tris base, 2% lithium dodecyl sulfate, 10% glycerol, 0.51 mM EDTA, 0.22 mM Comassie G250, 0.175 mM phenol red, pH8.5) heated for 10 min at 70 °C and loaded on the gel. Cdk5 analysis was done on standard 10% SDS-PAGE.

Primary Antibodies: anti-neurofilament heavy chain (specific for phosphorylation independent epitope, monoclonal, clone N52, Sigma), anti-NF-M (polyclonal, Biomol Int.), anti-NF-L (monoclonal, clone DA2, Abcam), anti-MAG (polyclonal, kindly provided by Dr. Anthony Heape, Oulu, Finland), anti-MBP (monoclonal, MAB386, Chemicon), anti-P0 (monoclonal, kindly provided by Dr. Archelos, Karl-Franzens University, Graz, Austria), anti-PMP22 (polyclonal, kindly provided by Dr. U. Suter, ETH-Hönggerberg, Zürich, Switzerland), anti-Cdk5 (Santa Cruz Biotechnology).

Secondary Antibodies: goat anti-mouse Alexa Fluor 680 and goat anti-rabbit IRDye 800 (LI-COR Biosciences GmbH), goat anti-rat IRDye (Rockland).

3.4 Immunohistochemistry

Human tissue (suralis nerves) was obtained either from biopsies or autopsies (kindly provided by Prof. Dr. Taroni (Milan)), mouse tissue (sciatic nerves) from the CMT1A mouse line (C22). Consecutive cryostat sections were mounted on gelatin-chromalaun-coated slides. Fixation, delipidation and staining were performed as described before (detailed protocol in Material and Methods Part I; Gabriel et al., 1996). The blocking buffer for mouse tissues was PBS containing 0.1% fish skin gelatin, 2.5% normal goat serum, 0.05% Saponin. Detection was performed with secondary horseradish peroxidase coupled antibodies (mouse or rabbit, SIGMA). Cell nuclei were counterstained with Mayer's Haemalaun (Merck). For immunofluorescence analysis, slides were incubated with secondary fluorochrome antibodies.

Primary Antibodies: anti-human MAG (specific for extracellular epitope D3A2G5, monoclonal, (Burger et al., 1990), anti-human P0 (monoclonal, D4IE4, (Miller et al., 1984), anti-MAG

(monoclonal, clone 513, Boehringer Mannheim), anti-MAL (Schaeren-Wiemers et al., 2004), anti-PMP22 (kindly provided by Prof. Dr. U. Suter, ETH-Hönggerberg, Zürich, Switzerland).

Secondary antibodies: Goat anti-mouse and goat anti-rabbit peroxidase antibodies (Jackson ImmunoResearch), goat anti-mouse Alexa 555 and goat anti-mouse Alexa 488 (Molecular Probes).

Quantitative image analysis

Mouse sciatic nerve cross sections: For the quantitative analysis of MAG expression, we performed a double staining for MAG and PMP22 or MAL on sciatic nerve cross sections. For quantification we measured the areas of MAG and PMP22 or MAL, positively stained surfaces within single myelinated fibers. We defined two circular areas of different size to analyze large and small caliber fibers separately. We calculated the ratios MAG/PMP22 and MAG/MAL for 50 large and 50 small myelinated fibers in wild type mice and 50 small myelinated fibers in C22 mice. For comparison we used the mean values. For quantitative image analysis "Analysis" (SIS, Münster, Germany) software was used.

Human suralis nerve biopsies/autopsies: Quantifications of MAG expression were performed with biopsies from 3 CMT1A patients and 3 control autopsies. 10 test fields (11011 μm^2 each) per section were analyzed using a Leica Dialux 20 microscope (Leitz, Wetzlar, Germany) and a 40x objective. On consecutive sections, fibers positive for P0 and MAG were counted on test fields. MAG expression was indicated as the percentages of MAG positively stained fibers compared to P0 positively stained nerve fibers. On the same sections, areas stained for MAG and P0 were measured and the ratios of MAG/P0 were calculated. Cameras: JVC KY-F55; F-View, Soft Imaging System.

4 Results

4.1 Morphological characteristics of the myelinated fibers of sciatic nerves in an animal model for CMT1A disease

There are many different animal models for CMT1A disease (Robertson et al., 2002). One animal model, which closely resembles the human pathology of CMT1A disease, is the C22 transgenic mouse overexpressing human PMP22 (Huxley et al., 1996). A morphological characterization of sciatic nerves during development revealed that the onset of myelination is delayed in C22 mice and that only a small percentage of fibers is correctly myelinated (Robaglia-Schlupp et al., 2002). For illustration of these findings, we show in Figure 1A developmental stages of C22 mice (postnatal day 10 and 20). At P10, the number of myelinated fibers is clearly reduced and myelin sheathes are thinner in C22 compared to wild type mice. This reduction in number of myelinated fibers and myelin sheath thickness is also seen at P20. In addition, we analyzed the morphology of the sciatic nerves at P60 (Figure 1A, P60). Until P60, myelinated fibers enlarge their calibers in wild type mice, which is not observed to the same extent in C22 mice. At P60, small caliber myelinated axons still predominate in C22 mice and show a considerable heterogeneity in myelin sheath thickness (Figure 1A and 1B). To closer assess the observed heterogeneity of myelinated fibers, we analyzed a representative number of myelinated fibers in C22 mice and defined different subpopulations of myelinated fibers according to their g-ratios. For this analysis we first defined the range of g-ratios in wild type mice. The g-ratio of 95% of myelinated fibers was between 0.5 and 0.77 in wild type animals; therefore, we considered myelinated fibers with g-ratios above 0.77 as hypomyelinated and those with g-ratios below 0.5 as hypermyelinated. In C22 mice, about 45% of the fibers are normally myelinated (Fig 1B: asterisks). About 20% of the axons are surrounded by Schwann cells, 1:1, but lack myelin (Figure 1B, dots; 1C, open circles). Approximately 30% of the fibers are hypomyelinated (Figure 1B, arrowheads; some fibers have only 2-3 layers of myelin layers). Axons lacking myelin and hypomyelinated axons constitute about 65% of the axonal volume in sciatic nerves of C22 mice. In C22 mice, a minority of about 5% of fibers is hypermyelinated (Figure 1B, arrow). The relative abundance of the different fiber populations is illustrated in Figure 1C.

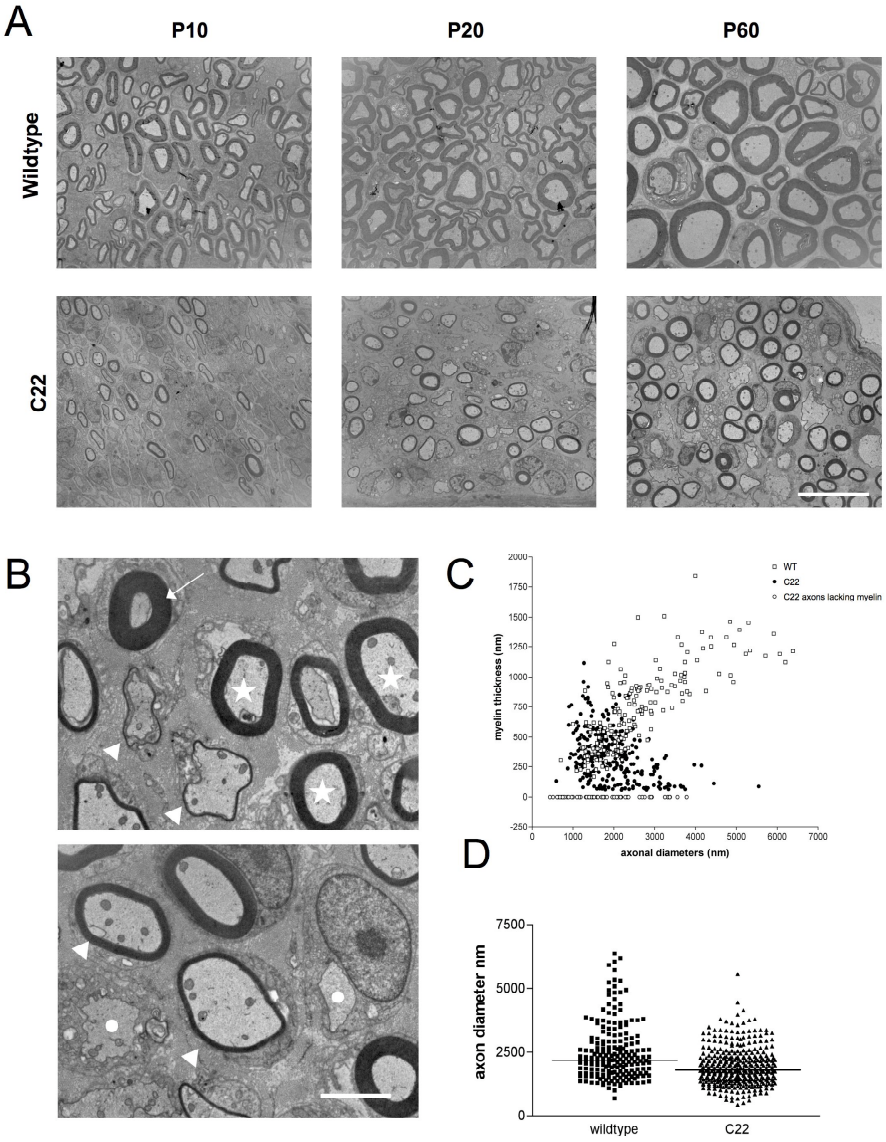

Figure 1 Myelination and axonal growth during development and in adult C22 and wild type mice. (A) Electron micrographs of sciatic nerves cross sections at postnatal day 10, 20 and 60. Most characteristic for C22 mice at P10 and P20 is the reduced number of myelinated fibers, the reduced myelin sheath thickness and the decreased fiber diameters. At P60, small caliber fibers still predominate and the myelin sheath thickness varies considerably. (B) The variability of myelin sheathes in C22 mice at P60: "normal" myelinated axons (asterisks), hypomyelinated axons (arrowheads), hypermyelinated axon (arrow) and axons surrounded by Schwann cells 1:1 without myelin (dots). (C) Scatter plot of myelin sheath thickness versus axon diameter: wild type axons (open squares) and C22 axons (myelinated axons: filled circles; axons lacking myelin: open circles). (D) Distribution of axonal diameters in C22 and wild type mice (median). Note, that large caliber axons with diameters above 4000 nm are almost absent in C22 mice at P60. Scale bars: (A) 10 μm, (B) 2.5 μm.

Apart from the wide heterogeneity of myelinated fibers in C22 mice, the almost complete absence of large caliber myelinated fibers is a particular feature of C22 mice. Figure 1D illustrates the distribution of the axonal diameters in C22 mice and shows that myelinated fibers with diameters above 4000nm are almost absent. In this work, our main interests are the molecular alterations that could contribute to the overall reduced axon diameters of myelinated fibers in C22 mice.

4.2 Alterations in the neurofilament subunit composition and phosphorylation in CMT1A mice

It is generally thought that axon calibers are determined by the content and properties of neurofilaments. Therefore, we investigated whether the axonal cytoskeleton is altered in C22 mice with special focus on neurofilament expression and phosphorylation.

We analyzed the content of the heavy, medium and light chains as well as phosphorylation state of neurofilaments in sciatic nerve homogenates of adult C22 mice (Figure 2A). The electrophoretic mobility of heavy chain depends on the phosphorylation state of the tail domain. Phosphorylated NF-H (NF-HP) runs at 200 kD, whereas the non-phosphorylated NF-H (NF-H) runs at 160-170 kD. In wild type mice, the NF heavy chain is predominantly phosphorylated, whereas in C22 mice the majority is non-phosphorylated. In addition, the levels of non-phosphorylated NF-H relative to NF-M (140-160 kD) and NF-L (70 kD) are strongly increased compared to the wild type, which results in an altered neurofilament subunit composition. Levels of NF-M and NF-L are not significantly altered in C22 mice.

It has been hypothesized that the distances between neurofilaments are determined by the phosphorylation of the tail domains (Yin et al., 1998). Tail phosphorylation was proposed to increase neurofilament nearest neighbor distances (NND) and thereby to enlarge axonal diameters. To see whether increased levels of non-phosphorylated NF-H correlate with decreased NNDs and reduced axonal diameters, we examined NND in C22 mice qualitatively. We observed that the hypomyelinated axons of C22 mice show an irregular neurofilament distribution with varying NNDs (Figure 2C and D: C22, arrows) compared to axons with appropriate myelin sheath thickness (Figure 2B: wild type or 2D: C22, arrowheads). However, a correlation of NNDs with axon diameters was not evident (data not shown).

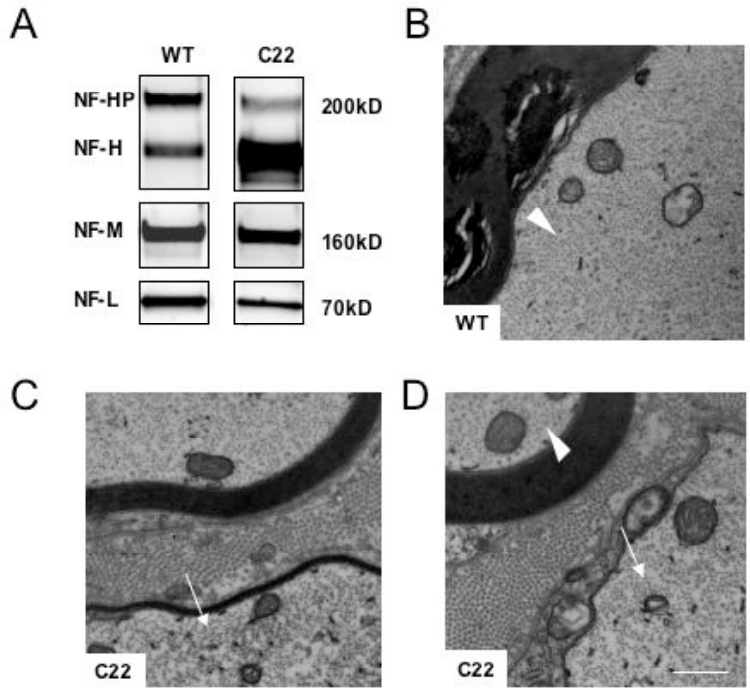

Figure 2 Western blot analysis of the neurofilament subunit composition and phosphorylation in 5 month-old C22 and wild type mice in sciatic nerve homogenates. (A) The Western blot shows phosphorylated NF-H (200 kD), non-phosphorylated NF-H (170 kD), NF-M (160 kD) and NF-L (70 kD) in wild type and C22 mice. Note the predominance of phosphorylated NF-H in wild type mice in contrast to C22 mice with high proportions of non-phosphorylated NF-H. NF-M and NF-L levels correlate in C22 and wild type mice. (B) Neurofilament distribution in a myelinated wild type axon at P60: In wild type axons, neurofilaments are regularly distributed (arrowhead). (C, D) Neurofilament distribution in C22 mice at P60: In hypomyelinated axons and axons lacking myelin neurofilaments are irregularly distributed (C and D, arrows). Note, that axons with appropriate myelin sheath thickness show a regular neurofilament distribution in C22 mice (arrowhead). Scale bar: 0.5 μm.

4.3 Equilibrium of stationary and mobile neurofilaments in CMT1A mice

Neurofilaments are either part of the stationary or mobile neurofilament pool. The cytoskeletal polymers are stationary and in a dynamic equilibrium with transported non-filamentous (monomers or oligomers) subunit proteins. The distribution of neurofilament subunits in the mobile and stationary pool can be determined by Triton-extraction of nervous tissue followed by differential fractionation (Shea et al., 1990; Shea et al., 1997). Triton insoluble neurofilaments in the pellet fractions correspond to the stationary neurofilament pool, whereas Triton-soluble neurofilaments in the supernatants correspond to the mobile neurofilament pool. To clarify whether the non-phosphorylated NF-H, which is substantially increased in C22 mice, is part of the stationary polymers or the mobile pool, we determined the contents of neurofilament subunits in the Triton-insoluble pellets (P) and Triton-soluble supernatants (S) at P10, P20 and P60 (Figure 3A: wild type, 3B: C22).

In wild type animals, one can clearly distinguish the neurofilament composition of the pellet fraction and supernatant fraction at P10. Both fractions differ in their subunit compositions. All subunits (NF-H, NF-M and NF-L) are represented in the pellet, whereas only the non-phosphorylated form of the heavy chain is detectable in the supernatant. At P20, the proportion of phosphorylated NF-H is especially increased in the pellet, while the non-phosphorylated is the predominant form in the supernatant resulting in a reciprocal distribution of NF-HP and NF-H in these fractions. Between P20 and P60, the subunit composition and distribution does not change anymore. Therefore, it seems that maturation of neurofilament subunit composition and distribution is primarily marked by an increase of the phosphorylated NF-H in the stationary neurofilament pool.

In C22 mice at P10, all subunits are only detectable at low levels in the pellet fraction, in contrast to non-phosphorylated NF-H, which is abundant in the supernatant fraction. At P20, all NF subunits are increased in the pellet; however, the increase of phosphorylated NF-H relative to the other subunits is only moderate compared to the wild type at that time point. In C22 mice, the characteristic increase of NF-HP as observed during maturation in wild type mice does not occur, but levels of non-phosphorylated NF-H are further increased. In summary, we see that in C22 mice, neurofilaments never reach a mature subunit composition and distribution as they maintain high levels of non-phosphorylated NF-H in the stationary as well as in the mobile pool.

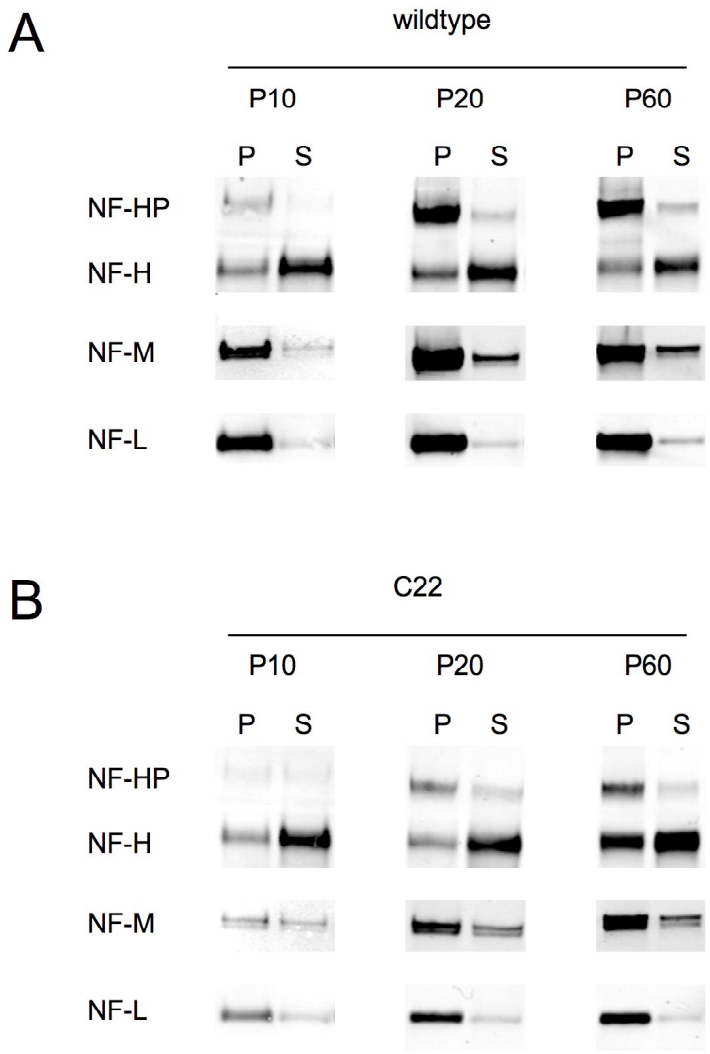

Figure 3 Western blot analysis of neurofilaments in Triton X–insoluble (P) and soluble (S) sciatic nerve fractions at P10, P20 and P60. (A) In wild type mice there is an increase of phosphorylated NF-H in the pellet during development. Phosphorylated and non-phosphorylated NF-H are reciprocally distributed between both fractions, phosphorylated NF-H is almost completely incorporated into the pellet whereas non-phosphorylated NF-H is in the supernatant. NF-M and NF-L are well detected in the pellet fractions already at P10 and levels further increase until P20 and P60. (B) In C22 mice, the increase of phosphorylated NF-H does not occur to the same extent as in the wild type mice. Yet, non-phosphorylated NF-H accumulates in the pellet and even more pronounced in the supernatants. The establishment of a stationary cytoskeleton is delayed; not until P20, subunits can readily be detected in the pellet fraction.

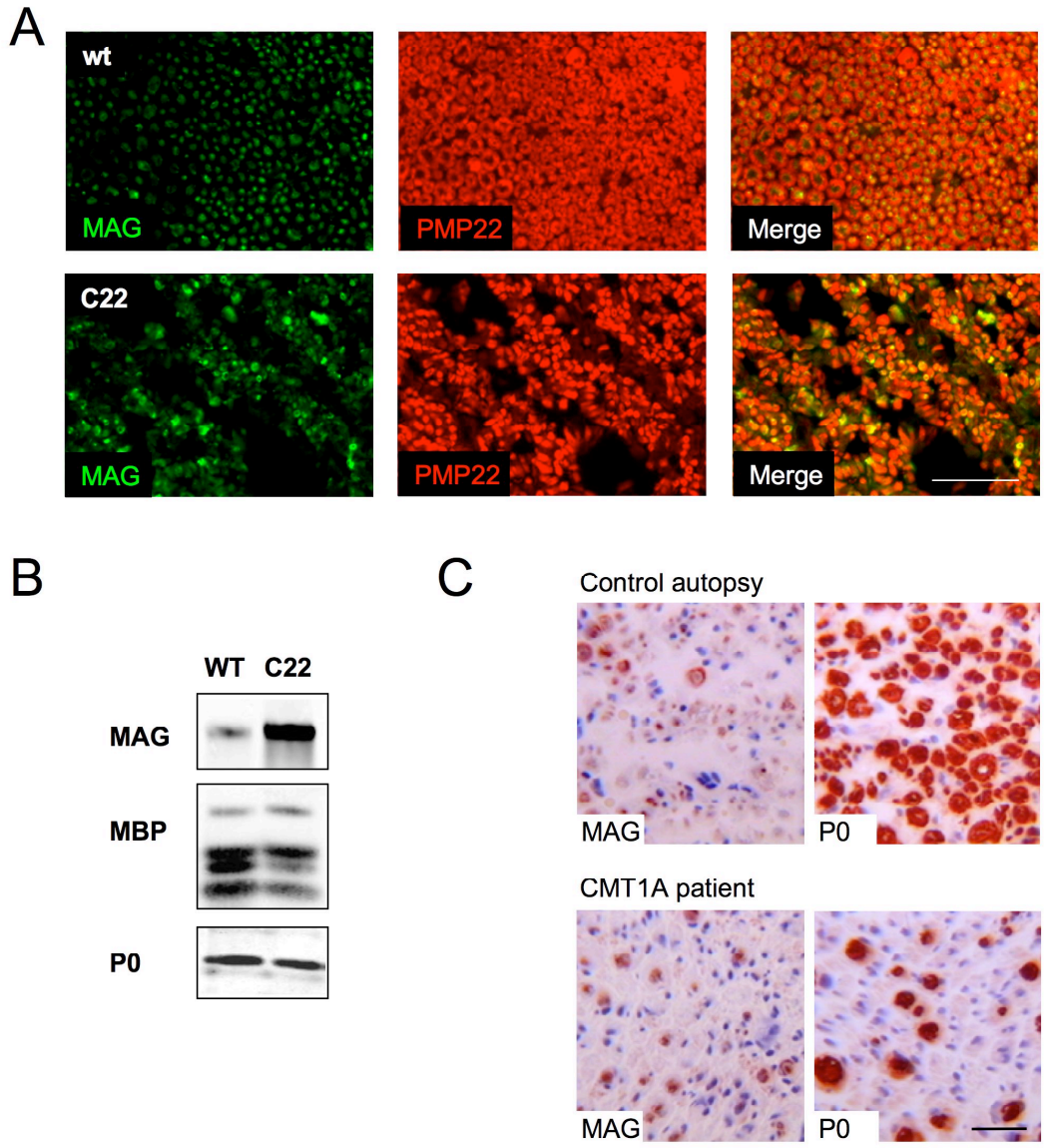

Figure 4 MAG expression under pathological conditions in murine and human CMT1A tissue. (A) Double staining for MAG and PMP22 on cross sections from sciatic nerves of adult wild type and C22 mice. In wild type mice, MAG is predominantly expressed in small caliber myelinated fibers. In C22 mice, MAG expression appears stronger than in wild type mice. (B) Western blot analysis of myelin membranes from sciatic nerves of adult wild type and C22 mice. The MAG signal is stronger in C22 mice than wild type mice relative to the signals of the compact myelin proteins MBP and P0. (C) Transversal sections from sural nerves of control autopsy and CMT1A biopsies stained for MAG and P0. In CMT1A patients, the number of myelinated P0 positive fibers is reduced. However, the number of MAG positive stained fibers relative to P0 positive nerve fibers is higher in the CMT1A patients than in the control autopsy. Scale bar: (A) 50 μm, (C) 20 μm.

Table 1 MAG expression in C22 mice (sciatic nerves)

	Fiber size	ratios MAG/PMP22	ratios MAG/MAL
wt	small	**0.14**	0.19
	large	**0.01**	0.016
C22	small	**0.31**	**0.409**

Table 1: Quantitative analysis of MAG signals in myelinated fibers from wild type and C22 mice. For this analysis we performed a double staining for MAG and PMP22 or MAL on sciatic nerve cross sections. For quantification we measured the areas of MAG and PMP22 or MAL stained surfaces within single myelinated fibers. We calculated the ratios MAG/PMP22 and MAG/MAL for 50 large and 50 small myelinated fibers in wild type mice and 50 small myelinated fibers in C22 mice. Indicated on the table are the mean values. Note, that small caliber myelinated fibers in wild type mice express more MAG than large ones. In C22 small caliber myelinated fibers, MAG expression is higher than in the small fibers of wild type animals.

Table 2 MAG expression in CMT1A biopsies and control autopsies (suralis nerves)

	% MAG positive myelinated fibers	ratios MAG/P0
CMT1A (mi5)	92%	0.1109
CMT1A (mi6)	88%	0.2124
CMT1A (mi7)	87%	0.6105
Control autopsy (S)	50%	0.0774
Control autopsy (U)	79%	0.0454
Control autopsy (X)	64%	0.0212

Table 2: Quantitative analysis of MAG expression in CMT1A patients and control autopsies. Suralis nerve cross sections were stained for MAG and P0. Numbers of positively stained fibers were counted and ratios of the numbers MAG/P0 calculated. In addition, areas positive for MAG and P0 were measured and ratios of the areas MAG/P0 calculated. Both analysis indicate an upregulation of MAG in CMT1A patients.

4.5 Cdk5 kinase levels in sciatic nerves of CMT1A mice

There are several kinases involved in neurofilament phosphorylation, but Cdk5 is so far the only one that has been described to induce the electrophoretic shift of NF-H by phosphorylation of KSP sites of the tail domain (Guidato et al., 1996; Pant et al., 1997; Veeranna et al., 1998; Bajaj et al., 1999; Shea et al., 2004). Cdk5 kinase was shown to be regulated by MAG and other signaling pathways originating from integrin and growth factor receptors (Li et al., 2000; Dashiell et al., 2002). To test whether altered Cdk5 levels are implicated in the pathogenesis of CMT1A, we quantified Cdk5 in sciatic nerve tissue of C22 mice by Western blot analysis loading equal amounts of proteins. At P10, Cdk5 protein expression was reduced in C22 probably indicating delayed myelination. However, at P20 and P60, expression levels were comparable to wild type ones (Figure 5).

For correct interpretation of Cdk5 levels it was necessary to consider the morphological alterations of C22 mice (Figure 1). Therefore, we correlated Cdk5 expression levels to the proportion of axonal area fraction of sciatic nerve cross sections. As the axonal area fraction was only decreased from 31% to 25% (P60), we conclude that at P20 and P60 Cdk5 levels were indeed comparable in C22 and wild type mice.

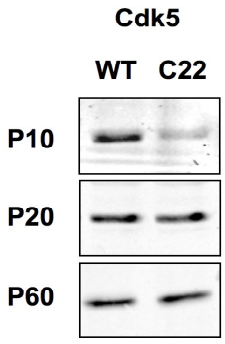

Figure 5 Western blot analysis of Cdk5 in sciatic nerve homogenates from wild type and C22 mice. At P10, levels of Cdk5 were reduced in C22 mice. At P20 and P60, Cdk5 levels were comparable in C22 and wild type mice.

5 Discussion

In this work, we addressed the question of how dysfunctional Schwann cells influence the development and maturation of axons. For this study, we used PMP22 overexpressing mice as an animal model for the CMT1A disease. As previously described, there is a predominance of small caliber axons in PMP22 overexpressing mice (Robaglia-Schlupp et al., 2002). Since axon calibers are mainly determined by the content of neurofilaments, we investigated whether overexpression of PMP22 influences the neurofilament system. We studied the subunit composition and phosphorylation state of neurofilaments during development and in adult C22 and wild type mice.

We analyzed the neurofilament subunit composition as well as the phosphorylation state and distinguished between the stationary (Triton insoluble) and mobile (Triton soluble) pool of neurofilaments. The most prominent pathological alteration in C22 mice is the absence of a mature neurofilament subunit composition and phosphorylation. C22 mice maintain high levels of non-phosphorylated NF-H in their stationary cytoskeleton and mobile neurofilament pool relative to NF-M and NF-L. As these alterations of the neurofilament system occur already during myelination they are reflecting an early abnormal Schwann cell signaling. Recent studies have shown that PMP22 overexpression is associated with a dysmyelinating process and does not just result from demyelination (Robaglia-Schlupp et al., 2002).

The importance of the neurofilament subunit composition and phosphorylation in the regulation of axonal calibers has been well studied. Overexpression of individual neurofilament subunits inhibits radial growth, whereas overexpression of the light chain with either the medium or the heavy chains promotes radial growth (Xu et al., 1996). The absence of the light, medium or heavy chains result in the reduction of axon calibers (Elder et al., 1998a; Elder et al., 1998b). All these studies stress the importance of correct neurofilament subunit stoichiometry for axonal growth. In C22 mice, the relative increase in NF-H levels is significant and this shifts the neurofilament subunit composition.

How altered subunit compositions impair radial growth is not known, however, studies have shown that the relative content of the heavy and medium chains has an impact on axonal transport rates. Overexpression of the neurofilament heavy chain results in selective reduction in the amount and rate of transport of neurofilament subunits which probably hampers the establishment and maintenance of the neurofilament network (Marszalek et al., 1996). The

neurofilament transport is mediated by the anterograde-specific motor protein kinesin, which associates with non-phosphorylated neurofilaments. Phosphorylation of neurofilaments promotes the dissociation from kinesin and the integration into the reticulated neurofilament network (Jung and Shea, 1999; Yabe et al., 2000; Jung et al., 2005). Therefore, in C22 mice, the excess of non-phosphorylated NF-H in the mobile pool of neurofilaments could interfere with the kinesin dependent transport, so that the neurofilament transport itself but also vesicle transport could be impaired.

Phosphorylation does not only regulate neurofilament transport but also the stability of the neurofilament network. *In vitro* studies have clearly demonstrated that dephosphorylation of neurofilaments results in the loss of their capacity to interconnect into a reticulated network (Eyer and Leterrier, 1988). Therefore, high levels of non-phosphorylated NF-H especially in stationary pool of neurofilaments might exert a destabilizing effect on the neurofilament network in CMT1A disease. We found that hypomyelinated axons generally showed an irregular neurofilament distribution compared to axons with a normal myelin sheath in C22 mice. The irregular neurofilament distribution could reflect that the neurofilament network is not properly established and destabilized in those axons. Considering the fact that hypomyelinated axons constitute approximately 65% of the axonal volume in sciatic nerves, we speculate that those fibers are primarily affected by the increase of non-phosphorylated NF-H seen on the Western blots. It is possible that those hypomyelinated fibers correspond to the population from which normally larger myelinated axons evolve.

The precise molecular mechanisms by which Schwann cells modulate the axonal properties during myelination are not known. However, one molecular candidate involved in myelin-axon interactions is MAG, the myelin associated glycoprotein localized at the Schwann cell-axon interface of myelinated fibers (Sternberger et al., 1979). MAG has been suggested to upregulate the activity of the Cdk5 and ERK1/2 kinase system, which is responsible for the phosphorylation of neurofilament tails (Dashiell et al., 2002). Although we found in C22 mice increased proportions of non-phosphorylated NF-H, MAG was upregulated in myelinated fibers in CMT1A patients and mice. This upregulation of MAG detected in myelin membrane preparations may reflect to some extent a general hypomyelination in C22 mice, but could also indicate a compensatory mechanism to induce neurofilament phosphorylation, which may fail due to disrupted downstream signaling. The significance of elevated MAG levels for axons in CMT1A disease remains difficult to assess as many MAG receptors are suggested and downstream signaling cascades are complex and not well defined (Franzen et al., 2001; Vinson et al., 2001b; Venkatesh et al., 2005).

We also directly analyzed the expression of Cdk5, which is the most important kinase for neurofilament tail phosphorylation and has been implicated in the pathomechanisms of neurodegenerative diseases such as ALS and Alzheimer's disease (Nguyen et al., 2001; Noble et al., 2003). Strikingly, Cdk5 expression levels were comparable in C22 and wild type mice. The activity of Cdk5 could also be regulated by its activator p35 (Sun et al., 1996). Therefore we performed Western blot analysis for p35, but we were not able to detect p35 in sciatic nerve preparations of C22 mice as well as wild type (data not shown). To directly investigate whether reduction of Cdk5 activity is responsible for reduced neurofilament phosphorylation in C22 mice, Cdk5 activity could be elevated in C22 mice by crossbreeding them with mice overexpressing Cdk5 activator p35 or p25 (Ahlijanian et al., 2000).

How PMP22 overexpressing Schwann cells induce alterations in neurofilament subunit composition and phosphorylation in CMT1A disease remains unclear. The fact that MAG is overexpressed in periaxonal membranes in C22 mice and CMT1A patients suggests that dysregulations of the neurofilament systems observed in PMP22 overexpressing mice and in MAG knock out mice result from different pathways. It is likely that there are mediators other than MAG involved in Schwann cell-axon communication and that different transduction processes contribute to the regulation of neurofilament subunit composition and phosphorylation.

In summary, we describe a primary effect of abnormal Schwann cells on the determination of the axon caliber in CMT1A disease. We conclude that the signaling between the myelinating cells and the axon is already impaired at the onset of myelination in CMT1A disease leading ultimately to axonal atrophy.

References

Adlkofer K, Martini R, Aguzzi A, Zielasek J, Toyka KV, Suter U (1995) Hypermyelination and demyelinating peripheral neuropathy in Pmp22-deficient mice. Nat Genet 11:274-280.

Agrawal HC, Noronha AB, Agrawal D, Quarles RH (1990) The myelin-associated glycoprotein is phosphorylated in the peripheral nervous system. Biochem Biophys Res Commun 169:953-958.

Ahlijanian MK, Barrezueta NX, Williams RD, Jakowski A, Kowsz KP, McCarthy S, Coskran T, Carlo A, Seymour PA, Burkhardt JE, Nelson RB, McNeish JD (2000) Hyperphosphorylated tau and neurofilament and cytoskeletal disruptions in mice overexpressing human p25, an activator of cdk5. Proc Natl Acad Sci U S A 97:2910-2915.

Almazan G, Tropak M, Roder J (1992) Myelin associated glycoproteins confer heterophilic adhesion properties to an immortalized optic nerve derived cell line. Cell Struct Funct 17:407-415.

Arquint M, Roder J, Chia LS, Down J, Wilkinson D, Bayley H, Braun P, Dunn R (1987) Molecular cloning and primary structure of myelin-associated glycoprotein. Proc Natl Acad Sci U S A 84:600-604.

Attia J, Hicks L, Oikawa K, Kay CM, Dunn RJ (1993) Structural properties of the myelin-associated glycoprotein ectodomain. J Neurochem 61:718-726.

Baechner D, Liehr T, Hameister H, Altenberger H, Grehl H, Suter U, Rautenstrauss B (1995) Widespread expression of the peripheral myelin protein-22 gene (PMP22) in neural and non-neural tissues during murine development. J Neurosci Res 42:733-741.

Bajaj NP, al-Sarraj ST, Leigh PN, Anderson V, Miller CC (1999) Cyclin dependent kinase-5 (CDK-5) phosphorylates neurofilament heavy (NF-H) chain to generate epitopes for antibodies that label neurofilament accumulations in amyotrophic lateral sclerosis (ALS) and is present in affected motor neurones in ALS. Prog Neuropsychopharmacol Biol Psychiatry 23:833-850.

Balice-Gordon RJ, Bone LJ, Scherer SS (1998) Functional gap junctions in the schwann cell myelin sheath. J Cell Biol 142:1095-1104.

Barres BA, Hart IK, Coles HS, Burne JF, Voyvodic JT, Richardson WD, Raff MC (1992) Cell death and control of cell survival in the oligodendrocyte lineage. Cell 70:31-46.

Bartsch S, Montag D, Schachner M, Bartsch U (1997) Increased number of unmyelinated axons in optic nerves of adult mice deficient in the myelin-associated glycoprotein (MAG). Brain Res 762:231-234.

Bartsch U, Kirchhoff F, Schachner M (1989) Immunohistological localization of the adhesion molecules L1, N-CAM, and MAG in the developing and adult optic nerve of mice. J Comp Neurol 284:451-462.

Bartsch U, Montag D, Bartsch S, Schachner M (1995) Multiply myelinated axons in the optic nerve of mice deficient for the myelin-associated glycoprotein. Glia 14:115-122.

Berciano J, Combarros O, Calleja J, Polo JM, Leno C (1989) The application of nerve conduction and clinical studies to genetic counseling in hereditary motor and sensory neuropathy type I. Muscle Nerve 12:302-306.

Berger P, Niemann A, Suter U (2006) Schwann cells and the pathogenesis of inherited motor and sensory neuropathies (Charcot-Marie-Tooth disease). Glia 54:243-257.

Boison D, Bussow H, D'Urso D, Muller HW, Stoffel W (1995) Adhesive properties of proteolipid protein are responsible for the compaction of CNS myelin sheaths. J Neurosci 15:5502-5513.

Bollensen E, Steck AJ, Schachner M (1988) Reactivity with the peripheral myelin glycoprotein P0 in serum from patients with monoclonal IgM gammopathy and polyneuropathy. Neurology 38:1266-1270.

Bouche P, Gherardi R, Cathala HP, Lhermitte F, Castaigne P (1983) Peroneal muscular atrophy. Part 1. Clinical and electrophysiological study. J Neurol Sci 61:389-399.

Bunge RP, Bunge MB, Eldridge CF (1986) Linkage between axonal ensheathment and basal lamina production by Schwann cells. Annu Rev Neurosci 9:305-328.

Burger D, Pidoux L, Steck AJ (1993) Identification of the glycosylated sequons of human myelin-associated glycoprotein. Biochem Biophys Res Commun 197:457-464.

Burger D, Simon M, Perruisseau G, Steck AJ (1990) The epitope(s) recognized by HNK-1 antibody and IgM paraprotein in neuropathy is present on several N-linked oligosaccharide structures on human P0 and myelin-associated glycoprotein. J Neurochem 54:1569-1575.

Carden MJ, Trojanowski JQ, Schlaepfer WW, Lee VM (1987) Two-stage expression of neurofilament polypeptides during rat neurogenesis with early establishment of adult phosphorylation patterns. J Neurosci 7:3489-3504.

Carenini S, Montag D, Schachner M, Martini R (1998) MAG-deficient Schwann cells myelinate dorsal root ganglion neurons in culture. Glia 22:213-220.

Chan JR, Watkins TA, Cosgaya JM, Zhang C, Chen L, Reichardt LF, Shooter EM, Barres BA (2004) NGF controls axonal receptivity to myelination by Schwann cells or oligodendrocytes. Neuron 43:183-191.

Charles P, Tait S, Faivre-Sarrailh C, Barbin G, Gunn-Moore F, Denisenko-Nehrbass N, Guennoc AM, Girault JA, Brophy PJ, Lubetzki C (2002) Neurofascin is a glial receptor for the paranodin/Caspr-contactin axonal complex at the axoglial junction. Curr Biol 12:217-220.

Chomczynski P, Sacchi N (1987) Single-step method of RNA isolation by acid guanidinium thiocyanate-phenol-chloroform extraction. Anal Biochem 162:156-159.

Ciccarelli C, Philipson L, Sorrentino V (1990) Regulation of expression of growth arrest-specific genes in mouse fibroblasts. Mol Cell Biol 10:1525-1529.

Cole JS, Messing A, Trojanowski JQ, Lee VM (1994) Modulation of axon diameter and neurofilaments by hypomyelinating Schwann cells in transgenic mice. J Neurosci 14:6956-6966.

Colman DR, Kreibich G, Frey AB, Sabatini DD (1982) Synthesis and incorporation of myelin polypeptides into CNS myelin. J Cell Biol 95:598-608.

Court FA, Sherman DL, Pratt T, Garry EM, Ribchester RR, Cottrell DF, Fleetwood-Walker SM, Brophy PJ (2004) Restricted growth of Schwann cells lacking Cajal bands slows conduction in myelinated nerves. Nature 431:191-195.

Crocker PR, Clark EA, Filbin M, Gordon S, Jones Y, Kehrl JH, Kelm S, Le Douarin N, Powell L, Roder J, Schnaar RL, Sgroi DC, Stamenkovic K, Schauer R, Schachner M, van den Berg TK, van der Merwe PA, Watt SM, Varki A (1998) Siglecs: a family of sialic-acid binding lectins. Glycobiology 8:v.

D'Urso D, Ehrhardt P, Muller HW (1999) Peripheral myelin protein 22 and protein zero: a novel association in peripheral nervous system myelin. J Neurosci 19:3396-3403.

Dashiell SM, Tanner SL, Pant HC, Quarles RH (2002) Myelin-associated glycoprotein modulates expression and phosphorylation of neuronal cytoskeletal elements and their associated kinases. J Neurochem 81:1263-1272.

De Martino C, Zamboni L (1967) Silver methenamine stain for electron microscopy. J Ultrastruct Res 19:273-282.

de Waegh S, Brady ST (1990) Altered slow axonal transport and regeneration in a myelin-deficient mutant mouse: the trembler as an in vivo model for Schwann cell-axon interactions. J Neurosci 10:1855-1865.

de Waegh SM, Lee VM, Brady ST (1992) Local modulation of neurofilament phosphorylation, axonal caliber, and slow axonal transport by myelinating Schwann cells. Cell 68:451-463.

Delarasse C, Daubas P, Mars LT, Vizler C, Litzenburger T, Iglesias A, Bauer J, Della Gaspera B, Schubart A, Decker L, Dimitri D, Roussel G, Dierich A, Amor S, Dautigny A, Liblau R, Pham-Dinh D (2003) Myelin/oligodendrocyte glycoprotein-deficient (MOG-deficient) mice reveal lack of immune tolerance to MOG in wild-type mice. J Clin Invest 112:544-553.

Desarnaud F, Do Thi AN, Brown AM, Lemke G, Suter U, Baulieu EE, Schumacher M (1998) Progesterone stimulates the activity of the promoters of peripheral myelin protein-22 and protein zero genes in Schwann cells. J Neurochem 71:1765-1768.

Elder GA, Friedrich VL, Jr., Bosco P, Kang C, Gourov A, Tu PH, Lee VM, Lazzarini RA (1998a) Absence of the mid-sized neurofilament subunit decreases axonal calibers, levels of light neurofilament (NF-L), and neurofilament content. J Cell Biol 141:727-739.

Elder GA, Friedrich VL, Jr., Kang C, Bosco P, Gourov A, Tu PH, Zhang B, Lee VM, Lazzarini RA (1998b) Requirement of heavy neurofilament subunit in the development of axons with large calibers. J Cell Biol 143:195-205.

Erb M (2003) Differential Expression and MAL-dependent Targeting of the L-MAG and S-MAG Isoforms to Myelin Membranes. Inauguraldissertation, Universität Basel.

Erb M, Steck AJ, Nave KA, Schaeren-Wiemers N (2003) Differential expression of L- and S-MAG upon cAMP stimulated differentiation in oligodendroglial cells. J Neurosci Res 71:326-337.

Erne B, Sansano S, Frank M, Schaeren-Wiemers N (2002) Rafts in adult peripheral nerve myelin contain major structural myelin proteins and myelin and lymphocyte protein (MAL) and CD59 as specific markers. J Neurochem 82:550-562.

Eyer J, Leterrier JF (1988) Influence of the phosphorylation state of neurofilament proteins on the interactions between purified filaments in vitro. Biochem J 252:655-660.

Fabbretti E, Edomi P, Brancolini C, Schneider C (1995) Apoptotic phenotype induced by overexpression of wild-type gas3/PMP22: its relation to the demyelinating peripheral neuropathy CMT1A. Genes Dev 9:1846-1856.

Fairweather N, Bell C, Cochrane S, Chelly J, Wang S, Mostacciuolo ML, Monaco AP, Haites NE (1994) Mutations in the connexin 32 gene in X-linked dominant Charcot-Marie-Tooth disease (CMTX1). Hum Mol Genet 3:29-34.

Fannon AM, Sherman DL, Ilyina-Gragerova G, Brophy PJ, Friedrich VL, Jr., Colman DR (1995) Novel E-cadherin-mediated adhesion in peripheral nerve: Schwann cell architecture is stabilized by autotypic adherens junctions. J Cell Biol 129:189-202.

Fortun J, Go JC, Li J, Amici SA, Dunn WA, Jr., Notterpek L (2006) Alterations in degradative pathways and protein aggregation in a neuropathy model based on PMP22 overexpression. Neurobiol Dis 22:153-164.

Frank M, van der Haar ME, Schaeren-Wiemers N, Schwab ME (1998) rMAL is a glycosphingolipid-associated protein of myelin and apical membranes of epithelial cells in kidney and stomach. J Neurosci 18:4901-4913.

Franzen R, Tanner SL, Dashiell SM, Rottkamp CA, Hammer JA, Quarles RH (2001) Microtubule-associated protein 1B: a neuronal binding partner for myelin-associated glycoprotein. J Cell Biol 155:893-898.

Fruttiger M, Montag D, Schachner M, Martini R (1995) Crucial role for the myelin-associated glycoprotein in the maintenance of axon-myelin integrity. Eur J Neurosci 7:511-515.

Fujita N, Kemper A, Dupree J, Nakayasu H, Bartsch U, Schachner M, Maeda N, Suzuki K, Popko B (1998) The cytoplasmic domain of the large myelin-associated glycoprotein isoform is needed for proper CNS but not peripheral nervous system myelination. J Neurosci 18:1970-1978.

Gabriel JM, Erne B, Miescher GC, Miller SL, Vital A, Vital C, Steck AJ (1996) Selective loss of myelin-associated glycoprotein from myelin correlates with anti-MAG antibody titre in demyelinating paraproteinaemic polyneuropathy. Brain 119 (Pt 3):775-787.

Garcia A, Combarros O, Calleja J, Berciano J (1998) Charcot-Marie-Tooth disease type 1A with 17p duplication in infancy and early childhood: a longitudinal clinical and electrophysiologic study. Neurology 50:1061-1067.

Guidato S, Tsai LH, Woodgett J, Miller CC (1996) Differential cellular phosphorylation of neurofilament heavy side-arms by glycogen synthase kinase-3 and cyclin-dependent kinase-5. J Neurochem 66:1698-1706.

Haney C, Snipes GJ, Shooter EM, Suter U, Garcia C, Griffin JW, Trapp BD (1996) Ultrastructural distribution of PMP22 in Charcot-Marie-Tooth disease type 1A. J Neuropathol Exp Neurol 55:290-299.

Harauz G, Ishiyama N, Hill CM, Bates IR, Libich DS, Fares C (2004) Myelin basic protein-diverse conformational states of an intrinsically unstructured protein and its roles in myelin assembly and multiple sclerosis. Micron 35:503-542.

Hisanaga S, Gonda Y, Inagaki M, Ikai A, Hirokawa N (1990) Effects of phosphorylation of the neurofilament L protein on filamentous structures. Cell Regul 1:237-248.

Hornig NC, Uhlmann F (2004) Preferential cleavage of chromatin-bound cohesin after targeted phosphorylation by Polo-like kinase. Embo J 23:3144-3153.

Hsieh ST, Kidd GJ, Crawford TO, Xu Z, Lin WM, Trapp BD, Cleveland DW, Griffin JW (1994) Regional modulation of neurofilament organization by myelination in normal axons. J Neurosci 14:6392-6401.

Huxley C, Passage E, Manson A, Putzu G, Figarella-Branger D, Pellissier JF, Fontes M (1996) Construction of a mouse model of Charcot-Marie-Tooth disease type 1A by pronuclear injection of human YAC DNA. Hum Mol Genet 5:563-569.

Huxley C, Passage E, Robertson AM, Youl B, Huston S, Manson A, Saberan-Djoniedi D, Figarella-Branger D, Pellissier JF, Thomas PK, Fontes M (1998) Correlation between varying levels of PMP22 expression and the degree of demyelination and reduction in nerve conduction velocity in transgenic mice. Hum Mol Genet 7:449-458.

Ilyas AA, Chou DK, Jungalwala FB, Costello C, Quarles RH (1990) Variability in the structural requirements for binding of human monoclonal anti-myelin-associated glycoprotein immunoglobulin M antibodies and HNK-1 to sphingoglycolipid antigens. J Neurochem 55:594-601.

Inuzuka T, Fujita N, Sato S, Baba H, Nakano R, Ishiguro H, Miyatake T (1991) Expression of the large myelin-associated glycoprotein isoform during the development in the mouse peripheral nervous system. Brain Res 562:173-175.

Jaramillo ML, Afar DE, Almazan G, Bell JC (1994) Identification of tyrosine 620 as the major phosphorylation site of myelin-associated glycoprotein and its implication in interacting with signaling molecules. J Biol Chem 269:27240-27245.

Jordanova A, De Jonghe P, Boerkoel CF, Takashima H, De Vriendt E, Ceuterick C, Martin JJ, Butler IJ, Mancias P, Papasozomenos S, Terespolsky D, Potocki L, Brown CW, Shy M, Rita DA, Tournev I, Kremensky I, Lupski JR, Timmerman V (2003) Mutations in the neurofilament light chain gene (NEFL) cause early onset severe Charcot-Marie-Tooth disease. Brain 126:590-597.

Jung C, Shea TB (1999) Regulation of neurofilament axonal transport by phosphorylation in optic axons in situ. Cell Motil Cytoskeleton 42:230-240.

Jung C, Yabe JT, Shea TB (2000) C-terminal phosphorylation of the high molecular weight neurofilament subunit correlates with decreased neurofilament axonal transport velocity. Brain Res 856:12-19.

Jung C, Lee S, Ortiz D, Zhu Q, Julien JP, Shea TB (2005) The high and middle molecular weight neurofilament subunits regulate the association of neurofilaments with kinesin: inhibition by phosphorylation of the high molecular weight subunit. Brain Res Mol Brain Res 141:151-155.

Kleitman N, Wood PN, Bunge RP (1998) Tissue culture methods for the study of myelination. In: Culturing Nerve Cells (Banker G, Goslin K, eds), pp 545-594. Cambridge, MA: The MIT Press.

Kleopa KA, Orthmann JL, Enriquez A, Paul DL, Scherer SS (2004) Unique distributions of the gap junction proteins connexin29, connexin32, and connexin47 in oligodendrocytes. Glia 47:346-357.

Krajewski KM, Lewis RA, Fuerst DR, Turansky C, Hinderer SR, Garbern J, Kamholz J, Shy ME (2000) Neurological dysfunction and axonal degeneration in Charcot-Marie-Tooth disease type 1A. Brain 123 (Pt 7):1516-1527.

Kruse J, Mailhammer R, Wernecke H, Faissner A, Sommer I, Goridis C, Schachner M (1984) Neural cell adhesion molecules and myelin-associated glycoprotein share a common carbohydrate moiety recognized by monoclonal antibodies L2 and HNK-1. Nature 311:153-155.

Kursula P, Lehto VP, Heape AM (2001) The small myelin-associated glycoprotein binds to tubulin and microtubules. Brain Res Mol Brain Res 87:22-30.

Kursula P, Tikkanen G, Lehto VP, Nishikimi M, Heape AM (1999) Calcium-dependent interaction between the large myelin-associated glycoprotein and S100beta. J Neurochem 73:1724-1732.

Laemmli UK (1970) Cleavage of structural proteins during the assembly of the head of bacteriophage T4. Nature 227:680-685.

Lai C, Brow MA, Nave KA, Noronha AB, Quarles RH, Bloom FE, Milner RJ, Sutcliffe JG (1987) Two forms of 1B236/myelin-associated glycoprotein, a cell adhesion molecule for postnatal neural development, are produced by alternative splicing. Proc Natl Acad Sci U S A 84:4337-4341.

Lassmann H, Bartsch U, Montag D, Schachner M (1997) Dying-back oligodendrogliopathy: a late sequel of myelin-associated glycoprotein deficiency. Glia 19:104-110.

Lauren J, Airaksinen MS, Saarma M, Timmusk T (2003) Two novel mammalian Nogo receptor homologs differentially expressed in the central and peripheral nervous systems. Mol Cell Neurosci 24:581-594.

Lazzarini R. A. GJW, Lassman H. , Nave K.-A. , Miller Robert H., Trapp B. D. (2004) Myelin Biology and Disorders 1.

Lemke G, Axel R (1985) Isolation and sequence of a cDNA encoding the major structural protein of peripheral myelin. Cell 40:501-508.

Li BS, Zhang L, Gu J, Amin ND, Pant HC (2000) Integrin alpha(1) beta(1)-mediated activation of cyclin-dependent kinase 5 activity is involved in neurite outgrowth and human neurofilament protein H Lys-Ser-Pro tail domain phosphorylation. J Neurosci 20:6055-6062.

Li X, Lynn BD, Olson C, Meier C, Davidson KG, Yasumura T, Rash JE, Nagy JI (2002) Connexin29 expression, immunocytochemistry and freeze-fracture replica immunogold labelling (FRIL) in sciatic nerve. Eur J Neurosci 16:795-806.

Liu BP, Fournier A, GrandPre T, Strittmatter SM (2002) Myelin-associated glycoprotein as a functional ligand for the Nogo-66 receptor. Science 297:1190-1193.

Magyar JP, Martini R, Ruelicke T, Aguzzi A, Adlkofer K, Dembic Z, Zielasek J, Toyka KV, Suter U (1996) Impaired differentiation of Schwann cells in transgenic mice with increased PMP22 gene dosage. J Neurosci 16:5351-5360.

Marcus J, Dupree JL, Popko B (2002) Myelin-associated glycoprotein and myelin galactolipids stabilize developing axo-glial interactions. J Cell Biol 156:567-577.

Marszalek JR, Williamson TL, Lee MK, Xu Z, Hoffman PN, Becher MW, Crawford TO, Cleveland DW (1996) Neurofilament subunit NF-H modulates axonal diameter by selectively slowing neurofilament transport. J Cell Biol 135:711-724.

Martini R, Schachner M (1988) Immunoelectron microscopic localization of neural cell adhesion molecules (L1, N-CAM, and myelin-associated glycoprotein) in regenerating adult mouse sciatic nerve. J Cell Biol 106:1735-1746.

Martini R, Mohajeri MH, Kasper S, Giese KP, Schachner M (1995) Mice doubly deficient in the genes for P0 and myelin basic protein show that both proteins contribute to the formation of the major dense line in peripheral nerve myelin. J Neurosci 15:4488-4495.

Mata M, Kupina N, Fink DJ (1992) Phosphorylation-dependent neurofilament epitopes are reduced at the node of Ranvier. J Neurocytol 21:199-210.

Meier C, Dermietzel R, Davidson KG, Yasumura T, Rash JE (2004) Connexin32-containing gap junctions in Schwann cells at the internodal zone of partial myelin compaction and in Schmidt-Lanterman incisures. J Neurosci 24:3186-3198.

Messier AM, Bizzozero OA (2000) Conserved fatty acid composition of proteolipid protein during brain development and in myelin subfractions. Neurochem Res 25:449-455.

Michailov GV, Sereda MW, Brinkmann BG, Fischer TM, Haug B, Birchmeier C, Role L, Lai C, Schwab MH, Nave KA (2004) Axonal neuregulin-1 regulates myelin sheath thickness. Science 304:700-703.

Miescher GC, Lutzelschwab R, Erne B, Ferracin F, Huber S, Steck AJ (1997) Reciprocal expression of myelin-associated glycoprotein splice variants in the adult human peripheral and central nervous systems. Brain Res Mol Brain Res 52:299-306.

Miller SL, Pleasure D, Herlyn M, Atkinson B, Ernst C, Tachovsky TG, Baird L (1984) Production and characterization of monoclonal antibodies to peripheral and central nervous system myelin. J Neurochem 43:394-400.

Moller JR (1996) Rapid conversion of myelin-associated glycoprotein to a soluble derivative in primates. Brain Res 741:27-31.

Montag D, Giese KP, Bartsch U, Martini R, Lang Y, Bluthmann H, Karthigasan J, Kirschner DA, Wintergerst ES, Nave KA, et al. (1994) Mice deficient for the myelin-associated glycoprotein show subtle abnormalities in myelin. Neuron 13:229-246.

Nagarajan R, Svaren J, Le N, Araki T, Watson M, Milbrandt J (2001) EGR2 mutations in inherited neuropathies dominant-negatively inhibit myelin gene expression. Neuron 30:355-368.

Nave KA, Bloom FE, Milner RJ (1987) A single nucleotide difference in the gene for myelin proteolipid protein defines the jimpy mutation in mouse. J Neurochem 49:1873-1877.

Nguyen MD, Lariviere RC, Julien JP (2001) Deregulation of Cdk5 in a mouse model of ALS: toxicity alleviated by perikaryal neurofilament inclusions. Neuron 30:135-147.

Nicholson GA (1991) Penetrance of the hereditary motor and sensory neuropathy Ia mutation: assessment by nerve conduction studies. Neurology 41:547-552.

Niemann S, Sereda MW, Suter U, Griffiths IR, Nave KA (2000) Uncoupling of myelin assembly and schwann cell differentiation by transgenic overexpression of peripheral myelin protein 22. J Neurosci 20:4120-4128.

Nishiyama A, Lin XH, Giese N, Heldin CH, Stallcup WB (1996) Interaction between NG2 proteoglycan and PDGF alpha-receptor on O2A progenitor cells is required for optimal response to PDGF. J Neurosci Res 43:315-330.

Noble W, Olm V, Takata K, Casey E, Mary O, Meyerson J, Gaynor K, LaFrancois J, Wang L, Kondo T, Davies P, Burns M, Veeranna, Nixon R, Dickson D, Matsuoka Y, Ahlijanian M, Lau LF, Duff K (2003) Cdk5 is a key factor in tau aggregation and tangle formation in vivo. Neuron 38:555-565.

Noronha AB, Hammer JA, Lai C, Kiel M, Milner RJ, Sutcliffe JG, Quarles RH (1989) Myelin-associated glycoprotein (MAG) and rat brain-specific 1B236 protein: mapping of epitopes and demonstration of immunological identity. J Mol Neurosci 1:159-170.

Notterpek L, Ryan MC, Tobler AR, Shooter EM (1999) PMP22 accumulation in aggresomes: implications for CMT1A pathology. Neurobiol Dis 6:450-460.

Ohara O, Gahara Y, Miyake T, Teraoka H, Kitamura T (1993) Neurofilament deficiency in quail caused by nonsense mutation in neurofilament-L gene. J Cell Biol 121:387-395.

Owens GC, Bunge RP (1989) Evidence for an early role for myelin-associated glycoprotein in the process of myelination. Glia 2:119-128.

Owens GC, Bunge RP (1991) Schwann cells infected with a recombinant retrovirus expressing myelin-associated glycoprotein antisense RNA do not form myelin. Neuron 7:565-575.

Owens GC, Boyd CJ, Bunge RP, Salzer JL (1990a) Expression of recombinant myelin-associated glycoprotein in primary Schwann cells promotes the initial investment of axons by myelinating Schwann cells. J Cell Biol 111:1171-1182.

Paivalainen S, Suokas M, Lahti O, Heape AM (2003) Degraded myelin-associated glycoprotein (dMAG) formation from pure human brain myelin-associated glycoprotein (MAG) is not mediated by calpain or cathepsin L-like activities. J Neurochem 84:533-545.

Pant AC, Veeranna, Pant HC, Amin N (1997) Phosphorylation of human high molecular weight neurofilament protein (hNF-H) by neuronal cyclin-dependent kinase 5 (cdk5). Brain Res 765:259-266.

Pareek S, Suter U, Snipes GJ, Welcher AA, Shooter EM, Murphy RA (1993) Detection and processing of peripheral myelin protein PMP22 in cultured Schwann cells. J Biol Chem 268:10372-10379.

Passage E, Norreel JC, Noack-Fraissignes P, Sanguedolce V, Pizant J, Thirion X, Robaglia-Schlupp A, Pellissier JF, Fontes M (2004) Ascorbic acid treatment corrects the phenotype of a mouse model of Charcot-Marie-Tooth disease. Nat Med 10:396-401.

Patel PI, Roa BB, Welcher AA, Schoener-Scott R, Trask BJ, Pentao L, Snipes GJ, Garcia CA, Francke U, Shooter EM, Lupski JR, Suter U (1992) The gene for the peripheral myelin protein PMP-22 is a candidate for Charcot-Marie-Tooth disease type 1A. Nat Genet 1:159-165.

Petzold A (2005) Neurofilament phosphoforms: surrogate markers for axonal injury, degeneration and loss. J Neurol Sci 233:183-198.

Poliak S, Matlis S, Ullmer C, Scherer SS, Peles E (2002) Distinct claudins and associated PDZ proteins form different autotypic tight junctions in myelinating Schwann cells. J Cell Biol 159:361-372.

Poltorak M, Sadoul R, Keilhauer G, Landa C, Fahrig T, Schachner M (1987) Myelin-associated glycoprotein, a member of the L2/HNK-1 family of neural cell adhesion molecules, is involved in neuron-oligodendrocyte and oligodendrocyte-oligodendrocyte interaction. J Cell Biol 105:1893-1899.

Pringle NP, Mudhar HS, Collarini EJ, Richardson WD (1992) PDGF receptors in the rat CNS: during late neurogenesis, PDGF alpha-receptor expression appears to be restricted to glial cells of the oligodendrocyte lineage. Development 115:535-551.

Probstmeier R, Fahrig T, Spiess E, Schachner M (1992) Interactions of the neural cell adhesion molecule and the myelin-associated glycoprotein with collagen type I: involvement in fibrillogenesis. J Cell Biol 116:1063-1070.

Quarles RH (2002) Myelin sheaths: glycoproteins involved in their formation, maintenance and degeneration. Cell Mol Life Sci 59:1851-1871.

Rao MV, Houseweart MK, Williamson TL, Crawford TO, Folmer J, Cleveland DW (1998) Neurofilament-dependent radial growth of motor axons and axonal organization of

neurofilaments does not require the neurofilament heavy subunit (NF-H) or its phosphorylation. J Cell Biol 143:171-181.

Rao MV, Campbell J, Yuan A, Kumar A, Gotow T, Uchiyama Y, Nixon RA (2003) The neurofilament middle molecular mass subunit carboxyl-terminal tail domains is essential for the radial growth and cytoskeletal architecture of axons but not for regulating neurofilament transport rate. J Cell Biol 163:1021-1031.

Roa BB, Garcia CA, Lupski JR (1991) Charcot-Marie-Tooth disease type 1A: molecular mechanisms of gene dosage and point mutation underlying a common inherited peripheral neuropathy. Int J Neurol 25-26:97-107.

Roach A, Takahashi N, Pravtcheva D, Ruddle F, Hood L (1985) Chromosomal mapping of mouse myelin basic protein gene and structure and transcription of the partially deleted gene in shiverer mutant mice. Cell 42:149-155.

Robaglia-Schlupp A, Pizant J, Norreel JC, Passage E, Saberan-Djoneidi D, Ansaldi JL, Vinay L, Figarella-Branger D, Levy N, Clarac F, Cau P, Pellissier JF, Fontes M (2002) PMP22 overexpression causes dysmyelination in mice. Brain 125:2213-2221.

Robertson AM, Huxley C, King RH, Thomas PK (1999) Development of early postnatal peripheral nerve abnormalities in Trembler-J and PMP22 transgenic mice. J Anat 195 (Pt 3):331-339.

Robertson AM, Perea J, McGuigan A, King RH, Muddle JR, Gabreels-Festen AA, Thomas PK, Huxley C (2002) Comparison of a new pmp22 transgenic mouse line with other mouse models and human patients with CMT1A. J Anat 200:377-390.

Robertson JD (1958) The ultrastructure of Schmidt-Lanterman clefts and related shearing defects of the myelin sheath. J Biophysic and Biochem Cytol 4:39-44.

Rosenbluth J (1980) Peripheral myelin in the mouse mutant Shiverer. J Comp Neurol 193:729-739.

Schaeren-Wiemers N, Bonnet A, Erb M, Erne B, Bartsch U, Kern F, Mantei N, Sherman D, Suter U (2004) The raft-associated protein MAL is required for maintenance of proper axon--glia interactions in the central nervous system. J Cell Biol 166:731-742.

Schnaar RL, Collins BE, Wright LP, Kiso M, Tropak MB, Roder JC, Crocker PR (1998) Myelin-associated glycoprotein binding to gangliosides. Structural specificity and functional implications. Ann N Y Acad Sci 845:92-105.

Seilheimer B, Persohn E, Schachner M (1989) Antibodies to the L1 adhesion molecule inhibit Schwann cell ensheathment of neurons in vitro. J Cell Biol 109:3095-3103.

Sereda M, Griffiths I, Puhlhofer A, Stewart H, Rossner MJ, Zimmerman F, Magyar JP, Schneider A, Hund E, Meinck HM, Suter U, Nave KA (1996) A transgenic rat model of Charcot-Marie-Tooth disease. Neuron 16:1049-1060.

Sereda MW, Meyer zu Horste G, Suter U, Uzma N, Nave KA (2003) Therapeutic administration of progesterone antagonist in a model of Charcot-Marie-Tooth disease (CMT-1A). Nat Med 9:1533-1537.

Shea TB, Sihag RK, Nixon RA (1990) Dynamics of phosphorylation and assembly of the high molecular weight neurofilament subunit in NB2a/d1 neuroblastoma. J Neurochem 55:1784-1792.

Shea TB, Dahl DC, Nixon RA, Fischer I (1997) Triton-soluble phosphovariants of the heavy neurofilament subunit in developing and mature mouse central nervous system. J Neurosci Res 48:515-523.

Shea TB, Yabe JT, Ortiz D, Pimenta A, Loomis P, Goldman RD, Amin N, Pant HC (2004) Cdk5 regulates axonal transport and phosphorylation of neurofilaments in cultured neurons. J Cell Sci 117:933-941.

Sheikh KA, Sun J, Liu Y, Kawai H, Crawford TO, Proia RL, Griffin JW, Schnaar RL (1999) Mice lacking complex gangliosides develop Wallerian degeneration and myelination defects. Proc Natl Acad Sci U S A 96:7532-7537.

Skre H (1974) Genetic and clinical aspects of Charcot-Marie-Tooth's disease. Clin Genet 6:98-118.

Snipes GJ, Suter U, Welcher AA, Shooter EM (1992) Characterization of a novel peripheral nervous system myelin protein (PMP-22/SR13). J Cell Biol 117:225-238.

Starr R, Attema B, DeVries GH, Monteiro MJ (1996) Neurofilament phosphorylation is modulated by myelination. J Neurosci Res 44:328-337.

Staugaitis SM, Colman DR, Pedraza L (1996) Membrane adhesion and other functions for the myelin basic proteins. Bioessays 18:13-18.

Stebbins JW, Jaffe H, Moller JR (1998) Characterization of myelin-associated glycoprotein (MAG) proteolysis in the human central nervous system. Neurochem Res 23:1005-1010.

Sternberger NH, Quarles RH, Itoyama Y, Webster HD (1979) Myelin-associated glycoprotein demonstrated immunocytochemically in myelin and myelin-forming cells of developing rat. Proc Natl Acad Sci U S A 76:1510-1514.

Sun D, Leung CL, Liem RK (1996) Phosphorylation of the high molecular weight neurofilament protein (NF-H) by Cdk5 and p35. J Biol Chem 271:14245-14251.

Suter U, Welcher AA, Ozcelik T, Snipes GJ, Kosaras B, Francke U, Billings-Gagliardi S, Sidman RL, Shooter EM (1992) Trembler mouse carries a point mutation in a myelin gene. Nature 356:241-244.

Suter U, Snipes GJ, Schoener-Scott R, Welcher AA, Pareek S, Lupski JR, Murphy RA, Shooter EM, Patel PI (1994) Regulation of tissue-specific expression of alternative peripheral myelin protein-22 (PMP22) gene transcripts by two promoters. J Biol Chem 269:25795-25808.

Taveggia C, Zanazzi G, Petrylak A, Yano H, Rosenbluth J, Einheber S, Xu X, Esper RM, Loeb JA, Shrager P, Chao MV, Falls DL, Role L, Salzer JL (2005) Neuregulin-1 type III determines the ensheathment fate of axons. Neuron 47:681-694.

Topilko P, Schneider-Maunoury S, Levi G, Baron-Van Evercooren A, Chennoufi AB, Seitanidou T, Babinet C, Charnay P (1994) Krox-20 controls myelination in the peripheral nervous system. Nature 371:796-799.

Trapp BD (1988) Distribution of the myelin-associated glycoprotein and P0 protein during myelin compaction in Quaking mouse peripheral nerve. J Cell Biol 107:675-685.

Trapp BD, Quarles RH (1982) Presence of the myelin-associated glycoprotein correlates with alterations in the periodicity of peripheral myelin. J Cell Biol 92:877-882.

Trapp BD, Andrews SB, Cootauco C, Quarles R (1989) The myelin-associated glycoprotein is enriched in multivesicular bodies and periaxonal membranes of actively myelinating oligodendrocytes. J Cell Biol 109:2417-2426.

Tropak MB, Johnson PW, Dunn RJ, Roder JC (1988) Differential splicing of MAG transcripts during CNS and PNS development. Mol Brain Res 4:143-155.

Umemori H, Sato S, Yagi T, Aizawa S, Yamamoto T (1994) Initial events of myelination involve Fyn tyrosine kinase signalling. Nature 367:572-576.

Veeranna, Amin ND, Ahn NG, Jaffe H, Winters CA, Grant P, Pant HC (1998) Mitogen-activated protein kinases (Erk1,2) phosphorylate Lys-Ser-Pro (KSP) repeats in neurofilament proteins NF-H and NF-M. J Neurosci 18:4008-4021.

Venkatesh K, Chivatakarn O, Lee H, Joshi PS, Kantor DB, Newman BA, Mage R, Rader C, Giger RJ (2005) The Nogo-66 receptor homolog NgR2 is a sialic acid-dependent receptor selective for myelin-associated glycoprotein. J Neurosci 25:808-822.

Vinson M, Strijbos PJ, Rowles A, Facci L, Moore SE, Simmons DL, Walsh FS (2001a) Myelin-associated glycoprotein interacts with ganglioside GT1b. A mechanism for neurite outgrowth inhibition. J Biol Chem 276:20280-20285. Epub 22001 Mar 20286.

Vinson M, Strijbos PJ, Rowles A, Facci L, Moore SE, Simmons DL, Walsh FS (2001b) Myelin-associated glycoprotein interacts with ganglioside GT1b. A mechanism for neurite outgrowth inhibition. J Biol Chem 276:20280-20285.

Vyas AA, Schnaar RL (2001) Brain gangliosides: functional ligands for myelin stability and the control of nerve regeneration. Biochimie 83:677-682.

Vyas AA, Patel HV, Fromholt SE, Heffer-Lauc M, Vyas KA, Dang J, Schachner M, Schnaar RL (2002) Gangliosides are functional nerve cell ligands for myelin-associated glycoprotein (MAG), an inhibitor of nerve regeneration. Proc Natl Acad Sci U S A 99:8412-8417.

Wang KC, Kim JA, Sivasankaran R, Segal R, He Z (2002a) P75 interacts with the Nogo receptor as a co-receptor for Nogo, MAG and OMgp. Nature 420:74-78.

Wanner IB, Wood PM (2002) N-cadherin mediates axon-aligned process growth and cell-cell interaction in rat Schwann cells. J Neurosci 22:4066-4079.

Weinstein DE, Burrola PG, Lemke G (1995) Premature Schwann cell differentiation and hypermyelination in mice expressing a targeted antagonist of the POU transcription factor SCIP. Mol Cell Neurosci 6:212-229.

Williamson AJ, Dibling BC, Boyne JR, Selby P, Burchill SA (2004) Basic fibroblast growth factor-induced cell death is effected through sustained activation of p38MAPK and up-regulation of the death receptor p75NTR. J Biol Chem 279:47912-47928.

Wong ST, Henley JR, Kanning KC, Huang KH, Bothwell M, Poo MM (2002) A p75(NTR) and Nogo receptor complex mediates repulsive signaling by myelin-associated glycoprotein. Nat Neurosci 5:1302-1308.

Wu JI, Reed RB, Grabowski PJ, Artzt K (2002) Function of quaking in myelination: regulation of alternative splicing. Proc Natl Acad Sci U S A 99:4233-4238.

Xu Z, Marszalek JR, Lee MK, Wong PC, Folmer J, Crawford TO, Hsieh ST, Griffin JW, Cleveland DW (1996) Subunit composition of neurofilaments specifies axonal diameter. J Cell Biol 133:1061-1069.

Yabe JT, Jung C, Chan WK, Shea TB (2000) Phospho-dependent association of neurofilament proteins with kinesin in situ. Cell Motil Cytoskeleton 45:249-262.

Yamasaki H, Itakura C, Mizutani M (1991) Hereditary hypotrophic axonopathy with neurofilament deficiency in a mutant strain of the Japanese quail. Acta Neuropathol (Berl) 82:427-434.

Yamashita T, Higuchi H, Tohyama M (2002a) The p75 receptor transduces the signal from myelin-associated glycoprotein to Rho. J Cell Biol 157:565-570. Epub 2002 May 2013.

Yang H, Xiao ZC, Becker B, Hillenbrand R, Rougon G, Schachner M (1999) Role for myelin-associated glycoprotein as a functional tenascin-R receptor. J Neurosci Res 55:687-701.

Yang LJ, Zeller CB, Shaper NL, Kiso M, Hasegawa A, Shapiro RE, Schnaar RL (1996a) Gangliosides are neuronal ligands for myelin-associated glycoprotein. Proc Natl Acad Sci U S A 93:814-818.

Yin X, Crawford TO, Griffin JW, Tu P, Lee VM, Li C, Roder J, Trapp BD (1998) Myelin-associated glycoprotein is a myelin signal that modulates the caliber of myelinated axons. J Neurosci 18:1953-1962.

Zhao C, Takita J, Tanaka Y, Setou M, Nakagawa T, Takeda S, Yang HW, Terada S, Nakata T, Takei Y, Saito M, Tsuji S, Hayashi Y, Hirokawa N (2001) Charcot-Marie-Tooth disease type 2A caused by mutation in a microtubule motor KIF1Bbeta. Cell 105:587-597.

Acknowledgements

The presented work was performed in the laboratory of Neurobiology at the Department of Research at the University Hospital Basel under the supervision of Prof. Dr. Nicole Schaeren-Wiemers and Prof. Dr. Andreas Steck.

I would like to thank:

Prof. Dr. Nicole Schaeren-Wiemers and **Prof. Dr. Andreas Steck** for giving me the opportunity to do my PhD thesis in their laboratory.

Dr. Anna Stalder, Dr. Michael Erb, Dr. Jochen Kinter and **Beat Erne** for their continuous support during the thesis and for their contributions to the publications.

Frances Kern, Thomas Zeis, Ralf Brunner, Cyril Reber, Andres Buser, Marie-Francoise Ritz, Chantal Urdieux and Daniela Schmid for their support and for creating a pleasant atmosphere in the lab.